INVESTIGATION OF A LOW HEAT LOSS HIGH
TEMPERATURE THERMAL ENERGY STORAGE SYSTEM

BY

NORMAN ALAN COPE

A DISSERTATION PRESENTED TO THE GRADUATE COUNCIL
OF THE UNIVERSITY OF FLORIDA IN PARTIAL
FULFILLMENT OF THE REQUIREMENTS FOR THE DEGREE
OF DOCTOR OF PHILOSOPHY

UNIVERSITY OF FLORIDA

1981

## ACKNOWLEDGEMENTS

I would like to express my deepest gratitude to Dr. Erich A. Farber, for his inspiring guidance and encouragement during my course of this research. I would also like to express my thanks to the other members of my committee for their constructive criticism and advice during the course of this work.

I would like to acknowledge the helpful assistance of the Shop personnel ably led by Mr. Richard Tomlinson.

I would like to acknowledge the patience and encouragement of my wife, Elizabeth, without whose help this work would not have been possible.

Finally, I would like to thank my typist, Denise Jobb, for her excellent typing and assistance in preparing this dissertation and John Murdoch for his assistance in preparing some of the drawings of this text.

iii

TABLE OF CONTENTS

iv

LIST OF TABLES

LIST OF FIGURES

LIST OF SYMBOLS

| | |
|---|---|
| $A$ | area, $ft^2$ |
| $A_a$ | aperture area, $ft^2$ |
| $A_{gc}$ | gas conduction area, $ft^2$ |
| $A_s$ | solid conduction area, $ft^2$ |
| $A_T$ | total area, $ft^2$ |
| $A_n$ | Avogadro's number |
| $a$ | accommodation coefficient (dimensionless) |
| $\bar{a}$ | average accommodation coefficient (dimensionless) |
| $B$ | variable, $lb_f/ft$ |
| $b$ | length, ft |
| Btu | British Thermal Unit |
| $C$ | correction factor (dimensionless) |
| $\bar{C}$ | average molecular velocity, ft/sec. |
| $C'$ | correction factor, contact points/particle |
| $C_p$ | specific heat at constant pressure, $Btu/lb_m\,°F$ |
| $C_v$ | specific heat at constant volume, $Btu/lb_m\,°F$ |
| $D$ | diameter, ft |
| $\bar{d}$ | mean void diameter, ft |
| $D_c$ | equivalent contact diameter, ft |
| $D_n$ | nominal particle diameter, ft |
| $dx$ | differential length, ft |
| $e$ | correction factor, dimensionless |
| $E$ | Young's modulus, psi |
| $F$ | force, $lb_f$ |
| $°F$ | degree Fahrenheit |
| ft | feet |
| $ft^2$ | square feet |
| $ft^3$ | cubic feet |
| $G$ | constant, dimensionless |

| | |
|---|---|
| h | convective heat transfer coefficient, $Btu/hrft^2°F$ |
| $H_{in}$ | rate of energy input, Btu/hr |
| hr | hour |
| $H_{sto}$ | rate of energy storage, Btu/hr |
| I | current, A |
| $I_s$ | insolation, $Btu/hrft^2$ |
| in. | inch |
| K | thermal conductivity, Btu/hrft°F |
| $K_a$ | apparent thermal conductivity, Btu/hrft°F |
| $k_f$ | thermal conductivity of a fluid, Btu/hrft°F |
| $K_g$ | thermal conductivity coefficient of a gas for continuum, Btu/hrft°F |
| $\overline{K}_g$ | thermal conductivity coefficient of a gas for continuum, transition, and non-continuum, Btu/hrft°F |
| Kn | Knudsen number, $\lambda/\overline{d}$, dimensionless |
| $K_r$ | radiative conductivity coefficient, Btu/hrft°F |
| $k_{rv}$ | radiative transfer through particle voids, Btu/hrft°F |
| $K_s$ | thermal conductivity coefficient through a particle bed, Btu/hrft°F |
| $\overline{K}_s$ | modified thermal conductivity coefficient through a particle bed, Btu/hrft°F |
| $k_s$ | thermal conductivity of a particle, Btu/hrft°F |
| L | modified mean free path or length, ft |
| $lb_m$ | pounds mass |
| $lb_f$ | pounds force |
| M | molecular weight, $lb_m/lb_m$-mole |
| mm Hg | millimeters of mercury |
| min | minute |
| n | contact regions per particle |
| $N_A$ | particles per unit area |
| $N_h$ | particles per unit length |
| Nu | Nusselt number, dimensionless |

| | |
|---|---|
| OD | outside diameter, ft |
| P | pressure, $lb_f/ft^2$ |
| psi | pressure difference, $lb_f/in^2$ |
| psig | gauge pressure, $lb_f/in^2$ |
| Q | heat transfer, Btu/hr |
| Q''' | energy generated per unit volume, $Btu/hrft^3$ |
| $q_c$ | heat transfer by convection, $Btu/hrft^2$ |
| $Q_{elec}$ | electrical energy dissipation, Btu/hr |
| $q_{gc}$ | heat transfer by gas conduction, $Btu/hrft^2$ |
| $q_h$ | heat transfer by convection, $Btu/hrft^2$ |
| $Q_{loss}$ | heat loss, Btu/hr |
| $q_r$ | radiation transfer, $Btu/hrft^2$ |
| $q_s$ | heat transfer through solids, $Btu/hrft^2$ |
| $Q_T$ | heat transfer, Btu/hr |
| $q_T$ | heat flux, $Btu/hrft^2$ |
| $R_e$ | resistance to heat flow, $hrft°F/Btu$ |
| R | particle radius, ft |
| °R | degree Rankine |
| r | radial coordinate, ft |
| $r_i$ | inner tank radius, ft |
| $r_o$ | outer tank radius, ft |
| $R_u$ | universal gas constant, 1.986 $Btu/lb_m$-mole °R |
| S | average stress, $lb_f/in^2$ |
| T | temperature, °F, °R |
| $T_b$ | average or bulk powder temperature, °F, °R |
| $T_C$ | average temperature of hot boundary surface, °F |
| $T_H$ | average temperature of cold boundary surface, °F |
| $T_o$ | average surface temperature, °F, °R |
| V | volume, $ft^3$ |
| wt | weight, $lb_f$ |
| x | length or X-axis coordinate |
| y | particle contact radius, ft |
| z | coordinate direction, ft |

# GREEK SYMBOLS

| | |
|---|---|
| $\alpha$ | thermal diffusivity, $ft^2/hr$ |
| $\beta$ | constant, dimensionless |
| $\gamma$ | specific heat ratio, dimensionless |
| $\delta$ | void fraction, dimensionless |
| $\Delta$ | finite change of variable |
| $\varepsilon$ | emissivity, dimensionless |
| $\xi$ | Stephan-Boltzmann constant, $0.1714 \times 10^{-8}$ Btu/hr $ft^2\,{}^\circ R^4$ |
| $\eta_\tau$ | thermal efficiency, dimensionless |
| $\theta$ | coordinate direction, degrees |
| $\lambda$ | mean free path in a continuum, ft |
| $\mu$ | Poisson ratio, dimensionless |
| $\mu_f$ | viscosity, lbm/hrft |
| $\mu m$ Hg | micrometers of mercury |
| $\rho$ | density $lb_m/ft^3$ |
| $\sigma$ | collision diameter, ft |
| $\tau$ | time, hours |
| $\phi$ | phase angle |

Abstract of Dissertation Presented to the Graduate
Council of the University of Florida in Partial
Fulfillment of the Requirements for the Degree
of Doctor of Philosophy

INVESTIGATION OF A LOW HEAT LOSS HIGH
TEMPERATURE THERMAL ENERGY STORAGE VESSEL

By

Norman Alan Cope

May 1982

Chairman:  Erich A. Farber
Major Department:  Mechanical Engineering

A low heat loss thermal energy storage system capable

of storage in a range of 250-1000°F is described in this

dissertation.  The design criteria called for a storage

system that would be simple to construct, use inexpensive

and readily available materials, utilize an insulating

material with a thermal conductivity between 0.003 - 0.015

Btu/hrft°F for temperatures ranging between 250-1000°F, and

be suitable for residential or commercial applications.

A design selected to fulfill the above criteria consists

of a double tank wherein the annular space between the tanks

is filled with a porous powder (silica) and then evacuated

to a pressure of approximately 1 mm Hg.  Thermal conductivity

values of 0.0029 - 0.110 Btu/hrft°F were achieved experi-

mentally for vacuum levels ranging from 0.5 - 3.0 mm Hg and

hot surface temperatures ranging from 340 - 711°F.

The results of an analysis of the modes of heat transfer through the porous powder under vacuum indicate several means of potential improvement in the conductivity of an insulating powder. Based on theoretical considerations, the means for reducing the conductivity include

1.  selecting powder materials with a low thermal conductivity, such as quartz particles,

2.  selecting a particle size where an average void dimension is obtained that is less than or equal to the mean free path of the gas molecules at a selected operating condition,

3.  selecting gases whose properties inhibit free-molecular energy transport, such as gases with high molecular weights, high specific heat ratios and large molecular cross-sections; several of the more practical gases being air, argon and carbon dioxide.

The results of this study indicate for the temperature range investigated, 250-1000°F, thermal energy storage is technically and economically feasible. The availability of inexpensive thermal energy storage will make it possible to use current energy resources more effectively, particularly those that occur on an intermittent basis, such as direct solar (thermal). The concept of thermal energy storage in the temperature range indicated suggests the possibility of an independent energy system, particularly for residential and commercial applications.

# CHAPTER I

## INTRODUCTION

The more successful techniques used to store energy,
electrical or thermal, involve chemical or mechanical tech-
niques such as lead-acid batteries and thermal energy stor-
age, respectively.  There has been little practical advance-
ment in energy storage technology over the techniques
just mentioned.  With the current emphasis on energy
efficiency, there is a need to examine the benefits of
developing and using energy storage devices.  In many appli-
cations the need for thermal energy is greater than the
need for electrical energy.  For example, in a household,
about 85% of the energy needs can be provided by thermal
energy.  This quantity of thermal energy is needed for
house heating, house cooling by absorption air-conditioning,*
domestic water heating, and cooking.  The remaining 15% of
the energy requirements, for current lifestyles, is needed
in the form of electricity for lighting, refrigeration
and powering communications systems, fans and pumps.

---

\* It should be noted that a gas-fired or hot water driven
absorption air conditioner generally requires electricity
to run pumps and controls.

It should be recognized in the above example that energy, in the form of either heat or work, is most effective when used in a direct manner. For example, when thermal energy is converted into electrical energy (work), there follows a substantial loss as a result of the second law of thermodynamics in the form of the Carnot principle. And while electric energy (work) can be converted into thermal energy with no loss, the Carnot loss suffered in creating work from heat can be substantial. However, from a systems point of view, one may wish to convert from one form of energy to another for convenience, to enhance the system usefulness, or to enhance the life-cycle cost of the system.

Research and development of materials for storing thermal energy indicate that energy storage on a residential, commercial and industrial scale is feasible. Phase change materials, such as nitrate salts, can store large quantities of latent thermal energy associated with its phase change and organic oils, such as cottonseed oil, can be used to store large quantities of sensible thermal energy.

A primary difficulty of storing thermal energy at temperatures of 250-1000°F is that one must find an economical means of constructing a storage system with low heat loss characteristics. Very little literature exists in this area. Most of the research efforts in the past have been limited to developing insulation and insulating techniques in the cryogenic field.

Many of the problems encountered in insulating a cryogenic vessel are also encountered in insulating a high temperature system. Therefore, the cryogenic area seems to be a good starting point for developing a high temperature thermal energy storage system. Shared problems in the development of high temperature or cryogenic storage container are

1) heat leaks due to supports and tank penetrations,

2) insulation and tank materials,

3) outgassing of materials in the evacuated space,

4) inner tank support structure,

5) leak-free penetration ports for piping and electrical wiring,

6) improved evacuating techniques when fine powders are used as the insulating material, and

7) reasonable material and system cost.

The solutions to the above problems are different for cryogenic than for high temperature. For example, in cryogenic vessels, some plastics can be utilized as a spacing material; whereas, this same material in moderate or high temperature environments would cause problems like loss of structural integrity or outgassing.

In constructing a high temperature storage vessel there are different concepts that one may employ to achieve the same results. For example, one could build a storage vessel using a fibrous insulating material under a vacuum

but, obviously, this material would not support the inner vessel. A porous powder under vacuum could be used to support the inner vessel and to insulate the inner tank as well. Both insulating materials may result in a similar heat loss characteristic; however, there may be advantages and disadvantages with using one material in place of the other.

This study investigated the use of powder insulation at a typical pressure level of 1 mm Hg for insulating a high temperature thermal energy storage system. This technique of insulating was chosen over multi-layer insulation because

1) powder insulation works well at pressures of 1-10 mm Hg and this level is easier to maintain than a pressure level of 1 μm Hg or less, as required by multi-layer insulation,

2) suitable powders for withstanding high temperatures are readily available,

3) a need exists for many uses in high temperature technology,

4) it may be possible to form a load bearing member of powder to support the inner vessel and this would avoid the structural complexities of building thick walled vessels.

Powder insulations suitable for high temperatures are readily available and can be anything from wood ash to sand. The particular material used in this study was diatomaceous earth, a material readily available, inexpensive, and suitable for high temperature use because of low

particle thermal conductivity and a softening point[*] of
1600°F.

Projected applications of high temperature storage systems.
The intention of developing a high temperature thermal
energy storage system was to provide this component in a
self-contained cooking system for residential use [1]. This
system utilizes a concentrating collector with an automatic
solar powered tracking mechanism [2], a heat storage vessel,
and a cooking range. The concentrating collector coolant
and the heat storage media are organic oil.

Four organic oils (cottonseed, peanut, corn and soy-
bean oil) were evaluated for the above use [3]. In opera-
tion, the organic oil was heated as it circulated through
a heat exchanger located in the focal point of the collector.
With a minimum temperature of 400°F, the heated fluid
contained in the storage vessel would circulate through
the heating coils of the cooking range. The main advantage
of this system is that thermal energy is accumulated and
stored for use at a later time, eliminating the disadvantage
of having to wait for direct radiation and the necessity
to cook outdoors.

The system can also be used as the basis for an integra-
ted, residential power system as shown in Figure 1. For

---

[*] A softening point represents a temperature beyond which
the yield stress of a material drops off rapidly with
increasing temperature.
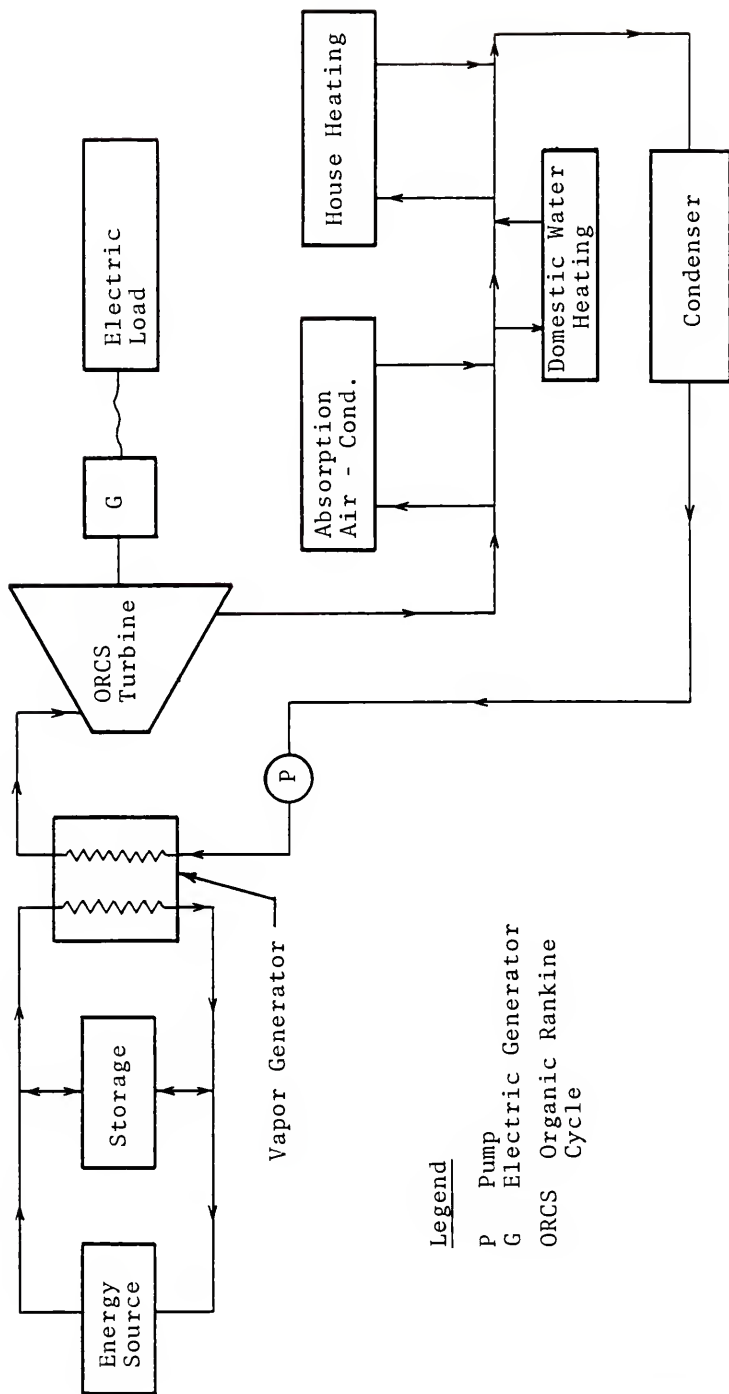
Figure 1

Schematic of a Residential Energy System
Using High Temperature Thermal Energy Storage

Legend

P   Pump
G   Electric Generator

ORCS   Organic Rankine
       Cycle

example, energy accumulated in the storage vessel can be used to drive a heat engine to produce electricity. The energy rejected from the continuously operating heat engine can be used to drive either an absorption air conditioner or heater, domestic water heater, or similar low temperature devices. The high temperature storage medium, such as organic oil, can be used to power a cooking range.

Energy for the above system may be collected from available energy resources. Some of these possible resources are

1) direct solar, thermal conversion,

2) fossil or nuclear fuel in the form of off-peak electricity,

3) direct solar, electrical to thermal energy conversion (photovoltaic cells),

4) wind energy (mechanical to thermal energy conversion).

As emphasized earlier energy is best used in a direct manner; that is, work is best used as work and thermal energy as thermal energy. Processes that convert thermal energy to work, as in the conversion of solar energy to electric in a photovoltaic cell (3) or to wind (4), processes that transform work into thermal energy, such as in statements 3 and 4 above will have irreversible losses associated with them and these losses will be substantial. This concept is embodied in the second law of thermodynamics and may be reviewed in elementary texts on thermodynamics [4]. However, it could nevertheless be economically practical to convert work

into thermal energy. For example, if an industrial process
requires high temperature fluids, it might prove advantageous
to purchase electrical energy at reduced rates from a utility
company during periods of low demand and to convert that
power into thermal energy to be stored for later use.

As apparent from the above paragraphs, the listed
energy resources occur on an intermittent basis and may
not coincide with the energy use pattern for which they
were intended. Storing energy for later use transforms an
intermittent source of energy into a potentially continuous
commodity.

In addition to residential applications an efficient
cost effective insulating technique is needed for high
temperature batteries [5]. For example, a lithium-sulfur
battery operates between 707 - 797°F and a sodium-sulfur
battery operates between 446 - 572°F. A particular problem
associated with operating these batteries is that energy
must be supplied to bring them to operating temperature
and to maintain stand-by losses. This energy is not avail-
able for work and must be viewed as lost work. If an
efficient and cost effective insulating jacket reduced
these losses, then high temperature batteries would be one
step closer to reality.

Scope of investigation. The goal of this research was to
develop a thermal energy storage system suitable for storing
latent or sensible thermal energy between temperatures of
250 to 1000°F. The particular objectives required to ob-
tain this goal were to

1)  find a practical insulating technique capable
    of reducing the thermal conductivity to less
    than 0.015 Btu/hrft°F @ 1000°F,

2)  identify and experimentally determine the
    necessary thermo-physical properties of the
    insulating material,

3)  construct a high temperature thermal energy
    storage system to verify the thermodynamic
    analysis and results of the insulating material
    and to verify the system design.

CHAPTER II

LITERATURE REVIEW

One of the more important facts to emerge from the
literature review was that no significant references were
found concerning efficient, high temperature insulation
suitable for residential or commercial sized thermal
energy storage systems.  This search included a manual
search of the library at the University of Florida
and a computer search that included the National Aeronautics
and Space Administration (NASA) and the National Technical
Information Service (NTIS) engineering files.

In view of the above, the goal of this research was
to develop a thermal energy storage system suitable for
storing latent or sensible thermal energy between tempera-
tures 250 - 1000°F.  The successful development of a
thermal energy storage system depends upon the type and
quality of the insulation used in constructing the system.
The initial literature review shows that there are basically
three types of insulation suitable for the indicated
temperature range.  Based on physical structure they can
be described as

    1)   fibrous insulation,

    2)   laminated insulation,

    3)   granular insulation.

10

Fibrous insulation includes such materials as fiberboard and rockwool, which are suitable for low and moderate temperature applications. Laminated insulation consists of alternating layers of low density insulation such as ceramic paper and low emittance radiation shields. Granular insulation includes such materials as sand, microsheres of glass, and diatomaceous earth. Laminated and granular insulation are suitable for use from cryogenic to high temperature applications.

As described by Jakob [6] , some of the earliest work on conduction through porous material was done by such men as Maxwell, Nusselt and Eucker. These investigators included gross simplifications of the heat transfer mechanisms in their analyses. Their aim was to make it possible to obtain reasonable answers to a very complex problem with a minimum of data. It seems that little advancement has been made in the area of heat transfer through porous materials since these early studies.

The basic ideas presented by Reference 6 concerning Maxwell's, Nusselt's, and Eucker's analyses indicate that all three viewed a porous body as either a base material with small particles of another substance distributed throughout that material, or as alternating layers of solids and gases with heat flow perpendicular to the layers.

One of the classic works on thermal conductivity of fine powders at reduced pressures, as described by Jakob [6], was that of Smoluchowski. The essence of Smoluchowski's

work was that at reduced pressures, gas molecules would experience slip flow in the vicinity of a solid surface. This causes a discernible temperature discontinuity to exist between the solid surface and the gas. When this theory is applied to fine powders, one correctly concludes that many temperature discontinuities are created. These added resistnaces in turn reduce the transfer of heat through porous powder.

Most of the early works of heat flow through porous material were developed considering ambient or lower temperatures. Few studies were found concerning the flow of heat from one particle to another. One study, by Strong et al. [7], analyzed heat flow through glass fibers at a pressure of 10 μm Hg. Even though this investigation worked with materials with smooth surface geometry, its experimental particle-to-particle conductivity was off by an order of magnitude when compared with theoretical values of heat flow perpendicular to the fiberglas rods.

In the first part of the twentieth century, two facts important in insulation were discovered and then investigated. First, it was noted by Smoluchowski [8] that soot had a lower conductance than air. At that time it was thought that the conductivity of air established a minimum value for thermal insulation. However, Kistler and Caldwell [9] in 1934 found that silica aerogel had a thermal conductivity less than air and reasoned that the lower conduc-

tivity resulted from the fact that the pore size of the material was less than the mean free path of molecules of air.

The second important fact, noted by Kistler and described by Wilkes [10], was that when commercial cork was placed in an evacuated chamber, thermal conduction and radiant transfer, through the material, at low temperature, was found to be a small part of the overall heat transfer. This indicated that air was responsible for the majority of the energy transport through the material.

In a more recent study, Peterson [1] showed that successive thin foil radiation shields of low emissivity wound with fine steel wool spacers were exceptionally good insulators, especially when used under vacuum conditions.

Based upon the three developments mentioned above, it was possible to construct super-insulated vessels, at least for cryogenic purposes. The requirements for space age technology placed a premium on lightweight, high efficiency insulation, and, consequently, great interest was shown in cellular and laminated or multi-layer insulation [12, 13]. Most of the development work on multi-layer insulation was done for cryogenic vessels, but some work was performed for high temperature applications. For example, the early design of a thermoelectric nuclear power system for spacecrafts used multi-layer insulation operating at a hot surface temperature of 1285°F [14]. The multi-layer consisted of alternating layers of copper foil with

quartz paper separators, and had an upper temperature limit
of 1400°F. The vacuum space was designed and built to
hold a pressure of less than 10 μm Hg for at least five
years.

As evident from much of the literature, multi-layer
insulation for spacecraft and for cryogenic work was
expensive. Prior to the need for super-insulators for
spacecraft use, evacuated powders were sufficient for most
low temperature pruposes. As pointed out by Black et al.
[15], although powder insulation does not have as low a
thermal conductivity as multi-layer insulation, its advantages
are

    1)   it can operate effectively at a few millimeters
          of mercury or less, thus eliminating the need
          for high vacuum,

    2)   it can be used in vessels of intricate design, and
          this eliminates the wrapping and bonding of each
          component in a vessel, as is necessary with multi-
          layer insulation,

    3)   it costs less than multi-layer insulation.

In view of this, it seemed that porous powder under partial
vacuum should be suitable for terrestrial high temperature
insulation applications where weight is not a serious dis-
advantage.

There is a growing need for efficient high temperature
insulation. The present technique used to insulate large,
high temperature (200-1000°F) storage vessels is to use
thick layers of granular insulation at atmospheric pressure

[16,17]. This approach seems reasonable for large thermal
energy storage systems in view of the quantity of energy
stored relative to the amount of energy lost. In smaller
systems, such as a residential sized thermal energy
storage vessel capable of storing $10^6$ Btu with minimal
losses, the storage efficiency is more closely tied to the
overall system size and shape. This results from a smaller
volume-to-surface ratio. No references were found con-
cerning high efficiency insulation suited to small systems.
Available literature indicates that little consideration
has been given to high temperature thermal energy storage
systems. It seems that more attention has been directed
into developing heat storage media than in developing the
heat storage media containment system.

Table 1 has been compiled to illustrate the types of
materials, and their associated thermal conductivities,
that are available as high temperature insulators. Note
that most high temperature insulating materials listed in
Table 1 have similar thermal conductivities. This result
is not unexpected since these materials are composed of
similar materials which is basically $SiO_2$. All of the
above materials are at atmospheric pressure, with the excep-
tion of the diatomaceous earth which is at 1 mm Hg. The
reduced pressure results in a thermal conductivity value
that is approximately one order of magnitude lower than
similar material at atmospheric pressure. Lower thermal
conductivities can be obtained as will be explained in the
next chapter.

TABLE 1

High Temperature Insulators

| Material | Bulk Density ($lb_m/ft^3$) | Max Temperature (°F) | Thermal Conductivity Btu/hrft°F Mean Temperature | |
|---|---|---|---|---|
| | | | @ 500°F | @ 1000°F |
| Diatomaceous earth, asbestos and bonding material [18] | 18 | 1600 | 0.053 | 0.065 |
| Glass blocks, average values [18] | 14-24 | 1600 | 0.053 | 0.074 |
| Micro-quartz fiber, blanket [18] | 3 | 3000 | 0.042 | 0.075 |
| Rock wool [18] | 8-12 | — | 0.049 | 0.078 |
| Sil-O-Cel [19] Insulating brick | 40 | 2500 | 0.142 | 0.163 |
| Diatomaceous earth, @ 1 mm Hg pressure in air. Nominal particle size 50 µm. | 20 | 1600 | 0.004 | 0.010 (est.) |

CHAPTER III

THEORETICAL CONSIDERATIONS OF POWDER INSULATION

## Introduction

It is relatively easy to measure the overall apparent
conductivity[*] of a powder insulation.  However, if one
wishes to alter and optimize apparent conductivity other
than by increasing thickness, it is necessary to have
an acceptable theory with which to proceed.  If one ideal-
izes the properties of the media which form the powder and
spaces, then one can model its apparent conductivity.
Unfortunately, the true geometry is not well modeled by
a simple approximation, nor are the properties adequately
approximated as ideal.  As a result, it is very difficult,
perhaps impossible to evolve an analytically tractable
model that also accurately describes the phenomena as
they occur in the powder.  This seems to be the case with
modeling of energy transport through porous powder insula-
ting material.

In this study diatomaceous earth (98% $SiO_2$) was used
as the insulating powder.  In view of the above discussion
the major questions encountered in modeling the irregularly

--------

[*] Apparent conductivity is heat flow from conduction, con-
vection, and radiation combined and used in equations as
if it were conduction alone.

shaped particles were how to describe factors that enhance or impede heat flow through this material. These factors are

    1)   gaseous thermal conduction, as limited by the molecular mean free path and influenced by gas pocket geometry and boundary conditions,

    2)   conduction through solids, limited especially by particle geometry and boundary conditions,

    3)   radiation resistance determined by particle-void space geometry, particle surface properties and boundary conditions.

The best understood of the processes applicable to heat transfer through powders seems to be gaseous conduction, followed by radiation and particle-to-particle conduction. The relative importance of each process is discussed later. The remainder of this chapter is devoted to developing a model for heat flow through porous powder insulation which addresses the above questions.

## Theoretical Model

    A mechanistic model for heat flow through a porous powder is shown in Figure 2. The total energy flow through the gas-powder mixture is a combination of conductive, convective, and radiant interaction between the solid and gaseous materials present. Symbolically, the total heat flow through the gas powder mixture can be written in functional form as

$$q_T = q_T(q_c, q_r, q_h) \qquad (1)$$

For powders with particle size less than 0.2 inches, investigators such as Hill and Wilhelm [20] found no evidence of convection in quiescent, gas-solid beds for conditions of interest to this study. Also, in this work, the powder material was studied at pressures ranging from atmospheric to less than 1 mm Hg. Consequently, convection heat transfer was eliminated from further consideration.
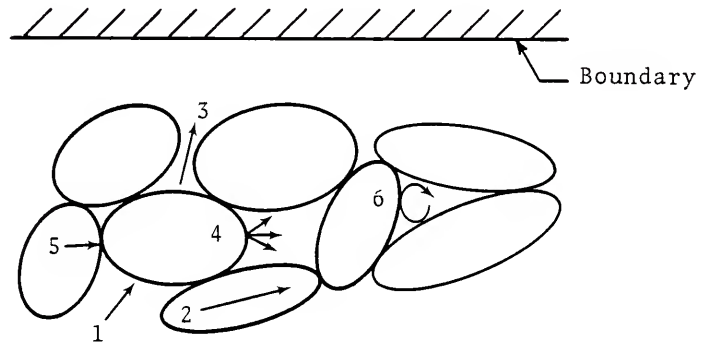


Figure 2

Mechanistic Description of Heat Transfer Through Porous Powder

(1) Gaseous conduction, (2) solid conduction,
(3) radiant heat transfer through voids, (4) radiant
heat transfer, solid-to-solid, (5) conduction,
point contact, (6) convection.

The justification for eliminating convection heat transfer under the conditions discussed above can be shown by estimating the convective heat transfer coefficient, h, between particles. This analysis is given in Appendix B. The results of this analysis reveal that the Nusselt number,

$$Nu = \frac{hb}{k} \tag{2}$$

is of order unity at atmospheric pressure and at temperatures between 250 - 1000°F, then the convective heat transfer coefficient reduces by two orders of magnitude. Hence, convection heat transfer at high temperature and low pressure can be eliminated from further consideration. In view of Equation 2, energy transport through a gas-solid mixture in which convection has been eliminated reduces to primarily a function of conduction. It will be shown later that net radiant transfer contributes only a small fraction of energy transfer under conditions encountered in this work. Thus, Equation 1 is rewritten as

$$q_T = q_T(q_c) \tag{3}$$

The remainder of this chapter is devoted to examining in detail conduction through both gas and solids and the small contribution of radiant transfer through porous powders (silica) under partial vacuum.

Thermal Conductivity of a Perfect Gas

Introduction. This section examines the thermal
conductivity of a perfect gas. It is implicit in the use
of the property thermal conductivity that a continuum
exists. A continuum is assumed to exist as long as the
mean free path of a molecule is comparable to the smallest
significant dimension of its surroundings. The ratio of
the mean free path, $\lambda$, of a gas molecule to the average
dimension of its boundaries, $\overline{d}$, is referred to as the
Knudsen number. That is,

$$Kn = \lambda/\overline{d}. \tag{4}$$

This number is useful in identifying the conditions under
which continuum assumptions apply. The need for identify-
ing whether a continuum exists is important in determin-
ing the proper relationship required for calculating the
thermal conductivity of a gas. As will be shown in the
following sections, the thermal conductivity of a gas in a
gas-powder mixture is influenced by the magnitude of the
Knudsen number.

Conductivity in a perfect gas. This section examines
thermal conductivity of a continuum. A continuum is said
to exist when the mean free path of a gas molecule is small
($Kn << 1$) compared to the dimensions of its boundaries.
For energy transport in a continuum, the gaseous thermal
conductivity is given by

$$q_{gc} = - K_g \nabla T \tag{5}$$

The conductivity coefficient, $K_g$, is given by [21]

$$K_g = \tfrac{1}{4}(9\gamma - 5)(\tfrac{1}{2}\rho \overline{C} C_v \lambda) \tag{6}$$

Density, $\rho$, is given by

$$\rho = \frac{PM}{R_u T} \tag{7}$$

where P is the pressure, M is the molecular weight of the gas, $R_u$ is the universal gas constant, and T is the temperature of the gas (absolute temperature). The average gaseous molecular velocity, $\overline{C}$, is given by

$$\overline{C} = (\frac{8 R_u T}{\pi M})^{\tfrac{1}{2}} \tag{8}$$

The mean free path, $\lambda$, for a perfect gas is given by

$$\lambda = \frac{R_u T}{\sqrt{2}\pi \sigma^2 A_n P} \tag{9}$$

where $\sigma$ is the collision diameter of the gaseous molecule, P is pressure and $A_n$ is Avogadro's number.

Specific heat at constant volume, $C_v$, is given by

$$C_v = R_u/M(\gamma-1) \tag{10}$$

where $\gamma$ is the specific heat ratio.

Combining Equations 7, 8, 9, and 10 into Equation 6 yields

$$K_g = \frac{(9\gamma-5)}{4(\gamma-1)} \left(\frac{R_u T}{\pi M}\right)^{\frac{1}{2}} \frac{R_u}{\pi \sigma^2 A_n} \tag{11}$$

Equation 11 indicates that gaseous conductivity is a function of temperature and that it should rise with an increase in temperature according to $T^{\frac{1}{2}}$. With an increase in temperature over the range of 250 - 1000°F, and taking into account the temperature variation of $C_v$ and $\gamma$, experimental values of thermal conductivity of air at atmospheric pressure change from 0.0192 to 0.0337 Btu/hrft°F.

From Equation 11 one can identify the gaseous molecular properties that will cause the conductivity coefficient to be small. For example, one would choose a gas with high molecular weight, large collision diameter, and a high specific heat ratio. Table 2 lists some values of M, $\sigma$ and $\gamma$ for several of the more common gases.

It is interesting to note in Equation 11 that the thermal conductivity of a perfect gas is independent of pressure. Mathematically, the reason for this result is that the direct proportionality of pressure in the density term, $\rho$, cancels with the inverse proportionality of pressure in the mean free path, $\lambda$, expression. Physically, this means that if the density, or number of gas molecules in a given space is decreased, the mean free path or distance between collisions of gas molecules increases so that the transport of energy is unchanged.

TABLE 2

Molecular Weight, Collision Diameter, and Specific
Heat Ratio of Selected Gases

| Molecule | M ($lb_m/lb_m$-mole) | $\sigma$ [22] (ft x $10^{-9}$) | $\gamma$ [23] * (dimensionless) |
|----------|----------------------|--------------------------------|---------------------------------|
| A        | 39.948               | 0.125                          | 1.667                           |
| Air      | 28.97                | 1.1975                         | 1.40                            |
| CO       | 28.011               | 1.05                           | 1.40                            |
| $CO_2$   | 44.011               | 1.10                           | 1.285                           |
| $H_2$    | 2.015                | .886                           | 1.40                            |
| He       | 4.003                | .689                           | 1.667                           |
| $N_2$    | 28.013               | 1.23                           | 1.40                            |
| $O_2$    | 31.999               | 1.94+                          | 1.40                            |
| Ne       | 20.183               | 1.61                           | 1.667                           |

*Specific heat ratios for gases at low pressure at 80°F.

+Corrected value [24].

The calculation of the thermal conductivity of a gas, as calculated with the perfect gas continuum assumptions, yields results that are adequate for describing real gases in many situations. However, once the variables of temperature, pressure, and boundary conditions are such that a continuum no longer exists, that is Kn > 1, then Equation 6 must be modified. This is the topic of the following section.

## Thermal Conductivity of a Non-Continuum Gas

As mentioned in the previous section, the conductivity of gases is theoretically independent of pressure in a continuum. However, both Knudsen [25] and Smoluchowski [8] developed theories concerning gaseous thermal conduction for non-continuum. Non-continuum and in the limit free-molecular energy transfer occurs when the confining boundaries of a gas molecule become smaller than the mean free path of the gas molecule. For this condition another phenomenon occurs that limits the energy transfer between a gas molecule and a solid boundary. Knudsen found that when a gas molecule strikes a solid surface that the gas molecule does not necessarily come into thermal equilibrium with the surface. That is, a temperature discontinuity was found between the temperature of the surface and the temperature of the gas molecule leaving the surface. Thus, Knudsen introduced a constant surface property, called the thermal accommodation coefficient, a,

which is a measure of the degree of energy exchange between a gas molecule and a solid surface. The maximum value of the accommodation coefficient is unity. This value is approached by surfaces that are roughened.

The energy transfer between parallel plates a distance x apart and at moderately low pressure is given by [26]

$$q = \frac{K_g (T_H - T_C)}{x + 2\beta\lambda} \tag{12}$$

where $\beta$ is

$$\beta = \frac{2-a}{a} \frac{2e}{\gamma+1} \tag{13}$$

and

$$e = \frac{1}{4} (9\gamma - 5) \tag{14}$$

At very low pressures, in the range of molecular conduction, it was found that energy transfer becomes independent of the plate spacing, and proportional to the pressure, P. Rewriting Equation 9 for the mean free path of a gas molecule as

$$\lambda = B/P \tag{15}$$

where

$$B = \frac{R_u T}{\sqrt{2}\pi\sigma^2 A_n} \tag{16}$$

and rewriting Equation 12 in view of Equation 15 for conditions where energy transfer is independent of x yields,

$$q = \frac{K_g (T_H - T_C) P}{2 \beta B} \tag{17}$$

Hence, molecular heat conduction is proportional to pressure at very low pressures, $(Kn > 1)$.

Equation 17 did not appear suitable for the present investigation for the following reasons:

1.  an equation was needed that would be suitable for energy transfer for continuum, transitional, and non-continuum conditions, and not just the latter,

2.  the use of Equation 17 requires a knowledge of accommodation coefficients and these values are generally not available,

3.  Equation 17 was derived on the basis of parallel plates and the material under investigation is powder material with particles and cavities that are irregular in size and shape and oriented at random; that is, the boundary dimensions must be taken into account.

Strong et al. [7] have found that Equation 6, when modified for non-continuum conditions, gave experimental results that were in good agreement with theoretical predictions

over the range of continuum, transitional, and non-continuum
conditions. The material investigated by Strong et al.
[7] was fiberglass rods which formed small cavities, as does
the powder material of this investigation. The basic
assumptions in using Equation 6 were

1. the accommodation coefficient could be approxi-
   mated as unity, and

2. that by modifying the definition of the mean free
   path, the equation would be suitable over the
   range of pressure from continuum to non-continuum
   conditions.

Since the accommodation coefficient is a measure of the
degree of energy transfer between a gas molecule and a
solid surface, then it seemed reasonable to conclude
that for a material with cavities on the order of the mean
free path of the gas, that an effective accommodation
coefficient near unit will result. That is, a gas mole-
cule will interact with the boundaries of a given cavity
a sufficient number of times to reach equilibrium before
escaping to another cavity.

In a non-continuum gas there are two space dimensions
that must be taken into account — the mean free path, $\lambda$,
of the gas molecule and the average space or void dimension
of its confining boundaries, $\bar{d}$. When the mean free path
is less than the space dimension, $\bar{d}$, Kn < 1, perfect gas

conductivity is independent of pressure, as expressed
by Equation 6. When the mean free path of the gas molecule
is close to or greater than the space dimension, Kn > 1,
then the conduction equation must be modified to take this
into account. A modified mean free path of a gas molecule,
L, is related to the continuum mean free path, $\lambda$, and
the gas space dimension, $\overline{d}$, by Strong et al. [7] as

$$L = (\frac{1}{\lambda} + \frac{1}{\overline{d}})^{-1} \tag{18}$$

In the continuum region where $\lambda << \overline{d}$, then

$$L \sim \lambda$$

In the non-continuum region where $\lambda >> \overline{d}$, then

$$L \sim \overline{d}$$

To relate the modified mean free path, L, to gaseous con-
ductivity, recall that

$$K_g = \frac{1}{4}(9\gamma-5)(\frac{1}{2}\rho\overline{C}C_V\lambda) \tag{6}$$

Substituting Equation 12 into Equation 6 yields

$$\overline{K}_g = \frac{1}{4}(9\gamma-5) \frac{1}{2}\rho\overline{C}C_V (1/\lambda + 1/\overline{d})^{-1} \tag{19}$$

where $\overline{K}_g$ is the modified gaseous thermal conductivity coef-
ficient. Equation 19 can now be used to calculate the
thermal conductivity of a gas for continuum, transitional,
and non-continuum conditions.

Finally, to show that gaseous thermal conductivity, $K_g$, is related to pressure, recall Equations 15 and 16 and with the appropriate substitution, Equation 19 becomes

$$\overline{K}_g = \frac{(9\gamma-5)}{4(\gamma-1)} \left(\frac{2R_u}{\pi MT}\right)^{\frac{1}{2}} (1/P\overline{d} + 1/B)^{-1} \tag{20}$$

Thus, as the pressure is lowered, at a fixed void geometry and temperature, the gaseous thermal conductivity decreases monotonically. Note that as the product of $P\overline{d}$ becomes smaller than B, the former value dominates, and it can be concluded that $\overline{K}_g$ varies essentially linearly with pressure. Conversely, as the product of $P\overline{d}$ becomes large relative to B, $\overline{K}_g$ is seen to be essentially independent of pressure.

Equation 20 also suggests that the gaseous conductivity will remain the same if, at a given temperature, the modified mean free path, L, is held at a constant value, that is,

$$L = (1/P\overline{d} + 1/B)^{-1} = \text{constant} \tag{18}$$

This means that a given value of $\overline{K}_g$ can be maintained by either decreasing $\overline{d}$ and increasing P, or by increasing $\overline{d}$ and decreasing P. This suggests that by decreasing the particle size, which will lower the average void dimension, $\overline{d}$, a higher gas pressure will be acceptable. For example, by selecting particles such that the pressure level is raised from 0.10 mm Hg to 5 mm Hg, while maintaining a constant value of $\overline{K}_g$, many of the problems associated with

low pressure, such as the need for diffusion pumps, out-
gassing of surfaces, and long term leakage, can be avoided
or minimized.  It is the control over the particle size,
and consequently the gas space dimension, that makes a
gas-powder mixture attractive for high temperature insula-
tion.  Both Equations 17 and 20 indicate that molecular
energy transport can be reduced by selecting gases with
high molecular weights and high specific heat ratios.
This same trend is also exhibited for conduction of heat
by gases in a continuum.  Equations 17 and 20 do not show
a dependency on the collision cross-section in the regime
of molecular conduction ($P\overline{d} < < B$) since the mean free
path has been superseded by the confining boundaries of
the gas molecule.  Also, for non-continuum or molecular
conduction, $K_g$ is found to vary with temperature by $T^{-\frac{1}{2}}$.
Hence, molecular conductivity decreases as the temperature
is elevated.

When the thermal conductivity of a gas has been reduced
below the particle-to-particle thermal conductivity in a
gas powder bed, little will be gained by further reducing
conduction through the gas.  Under these circumstances,
the particle-to-particle thermal conductivity sets the lower
limit of the apparent thermal conductivity through a porous
powder under vacuum.  (It will be shown later that net
radiant transfer appears negligible for the conditions
encountered in this study).

The following section examines the contribution of particle-to-particle thermal conductivity to the apparent thermal conductivity of a powder under vacuum.

## Particle-to-Particle Conductivity of a Porous Powder

Introduction.  Conduction through a region of contact between particles is not easily analyzed except for ideal geometries.  For an idealized geometry one may express energy transfer between particles of given size, mathematically define the contact area, and express the proper number of contact points.  In most real powders, for example, see Figure 8, page 68, the particles are both irregular in shape and size and oriented at random.  These factors make it difficult to determine the parameters necessary to express energy transport by conduction through the powder.

Even with the difficulties of analyzing particle-to-particle conductivity mentioned above, and the fact that there is little in the literature analyzing this topic, it is useful to develop an approximate mathematical expression to describe particle-to-particle conductivity.  With a mathemathical expression one may readily identify those variables that control the behavior of the material under study.

Theoretical Model.  For particle-to-particle conductivity to exist there must be an unbroken path connecting the particles and continuing through them.  It is through this path that energy is transferred by solid conduction.  A particular problem in analyzing heat transfer through a powder that

consists of irregularly shaped material, such as the material under consideration in this study, is the difficulty of mathematically defining the path through which energy flows. For example, in Figures 8, 9, and 10 (pages 68 and 69) one sees a variety of shapes ranging from per-forated, hollow and solid cylinders to perforated plates, and irregularly shaped solid pieces. With the variety of shapes shown, following the path of heat transfer from particle-to-particle appears to be virtually an impossible task, thus the need for a simplifying model.

In following the path of energy transfer from one particle to the next, one finds that the region of greatest resistance occurs at the smallest area, that is, in a region of contact. If the dimensions of the contact region are small relative to the bulk particle size, then one may approximate particle-to-particle energy transfer in a powder by analyzing the resistance due to the contact region only. This concept is best illustrated by an example.

Consider a cylinder as a particle body as shown in Figure 3. Beside this cylinder is a smaller cylinder which represents the contact region. The two cylinders are in intimate contact and they are aligned on the same axis. Each cylinder has a length to diameter ratio of 10:1 and the size of the two cylinders relative to each other is 100:1. Assuming the conductivity coefficient to be the same

(a)
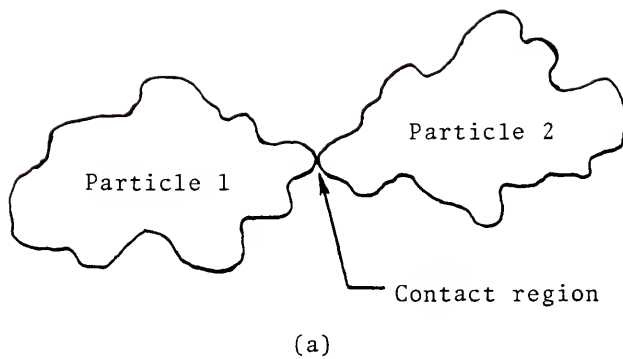
General Particle Shapes In Contact



(b)
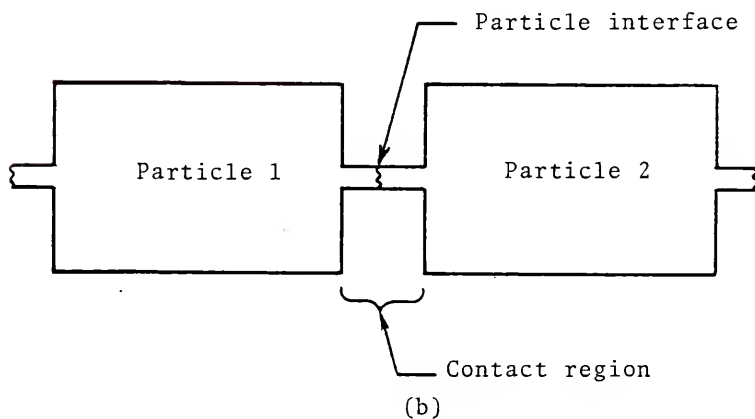
Idealization Of Particles In Contact

Figure 3

Idealization Of A Contact Region

for both cylinders, one can easily demonstrate that the resistance to heat flow in the smaller cylinder is 100 times that of the larger cylinder. This indicates that the contact resistance, as represented by the smaller cylinder, predominates and that the body resistance of the particles, as represented by the larger cylinder, is negligible. In Chapter V it will also be demonstrated that the relative dimensions of the particle body and contact region are such that a resistance ratio greater than 100:1 is not unusual.

Note carefully that a distinction is made between a contact area and a region of contact. A contact area is the physical area or interface between two particles. A contact region is defined to be the contact area along with the particle materials adjacent to the contact area that restrict energy transfer between two particles forming the contact area. See Figure 3. The contact region is viewed as a continuous path of solid material through which conduction heat transfer occurs even though an interface exist between two particles. This assumption is based upon the existence of sufficient stresses to maintain the two particles in intimate contact. That is,

$$S = F/A \tag{21}$$

where S is the average stress between the particle, F is the force or weight supported by a particle, and A is the contact area between two particles. It will

be demonstrated in Chapter 5 that sufficient stress exists at a contact region to assume intimate, solid contact between particles.

The contact region of a solid particle can be analyzed by any suitable coordinate system. For simplicity, cylindrical coordinates will be used. Assuming constant conductivity, one can express energy conservation in conduction by

$$\frac{\partial^2 T}{\partial r^2} + \frac{\partial T}{r \partial r} + \frac{\partial^2 T}{r^2 \partial \theta^2} + \frac{\partial^2 T}{\partial x^2} + \frac{q'''}{k_s} = \frac{1 \partial T}{\alpha \partial \tau} \tag{22}$$

Since the contact region is small relative to the particle body dimensions, with the latter varying from 1 μm to 100μm in diameter, the particle material conductivity coefficient, $k_s$, is assumed to be homogeneous and isotropic. The following assumptions are also made on Equation 22.

1.  steady-state,

2.  no internal heat generator, and

3.  the temperature variations in the r and θ directions are negligible.

A steady-state assumption is made since the material under investigation is intended for use as an insulator operating under steady-state conditions.

The temperature variations in the r and θ directions are considered negligible since the contact region is small relative to the particle body.

With the above assumptions, Equation 22 reduces to a one-dimensional equation and heat flow through a contact region is viewed as quasi-one-dimensional. Thus,

$$\frac{d^2T}{dx^2} = 0 \qquad (23)$$

A method of solution for one-dimensional problems in which $q$ = constant at every cross-section is [27]

$$d[q_xA(x)] = 0 \qquad (24)$$

which gives

$$Q_T = q_xA(x) = \text{constant} \qquad (25)$$

The x denotes heat transfer in the x-direction and

$$q_x = - k \frac{dT}{dx} \qquad (26)$$

Introducing Equation 26 into Equation 25, rearranging and integrating between limits gives

$$Q = \frac{T_H-T_L}{(1/k_s) \int_{x_1}^{x_2} dx/A(x)} = \frac{T_H-T_L}{R_e} \qquad (27)$$

where

$$R_e = (1/k_s) \int_{x_1}^{x_2} dx/A(x) \qquad (28)$$

and represents the conductive resistance through a contact region. Equation 28 shows that conductive resistance to heat flow is directly proportional to the path length, dx, and inversely proportional to the area, A(x).

An electron microscope photograph of a diatomaceous earth particle, Figures 14 and 15, page 92, shows that the surface of these particles, where contact occurs, has

rounded or smooth geometric features as shown in Figure 4(a). It would appear that the regions of contact could be viewed as hemispherical, cylindrical, conical and so forth. For the purpose of illustration, a hemispherical contact region will be assumed.

A contact region formed by two hemispherical protrusions is shown in Figure 4(a). Note that the area of contact of the hemispherical protrusions has been flattened, as illustrated by the solid line, due to forces imposed on the particles. An equivalent cylindrical heat flow path has been superimposed on the hemispherical contacts. This is to illustrate that the hemispherical contact region is still considered quasi-one-dimensional. The use of a hemispherical contact region serves these two purposes

1. it closely resembles the actual contact region of a particle, and

2. it facilitates the calculations of the contact area with the use of the Hertz formula [28].

The symbols used in analyzing the resistance to heat flow through a contact region are shown in Figure 4(b). Equation 28, written in terms shown in Figure 4(b) is,

$$Re = \frac{1}{k_s} \int_{x_1}^{x_2} \frac{1}{\pi y^2(x)} \, dx \qquad (28)$$

The following variable transformations are made.

$y = R \sin \theta$

$x = R \cos \theta$

$dx = R \sin \theta \, d\theta$

Equivalent cylindrical heat flow path

$y$

$x$

$D_c$

$Q$

particle body

Contact Region

(a)
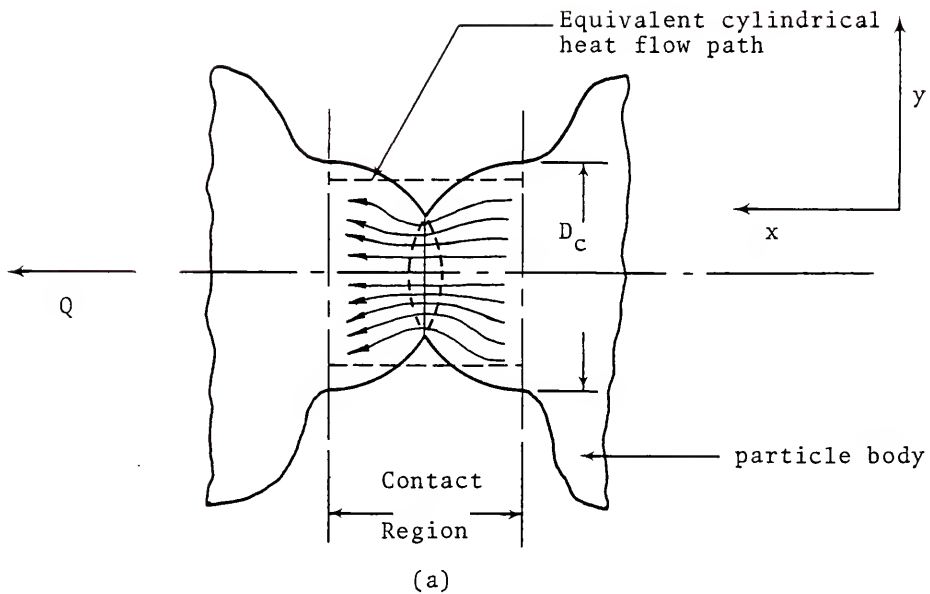
Parameters Used in Analyzing Heat Flow Through A Hemispheric Contact Region



$R$

$y$

$y^*$

$\theta^*$

$\theta$

$R-h$

$h$

$y$

$x$

(b)
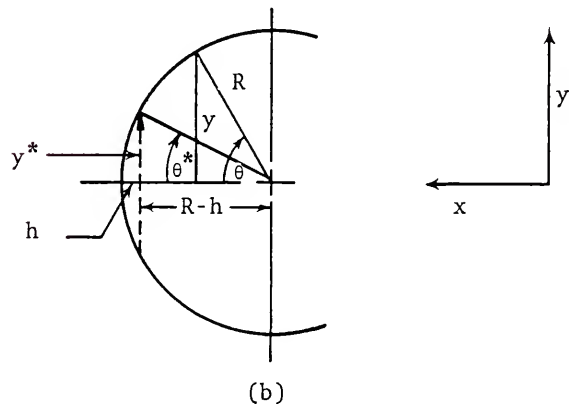
Two Hemispherical Projections Forming A Contact Region

Figure 4

Two Particles Forming A Contact Region

Substituting into Equation 28 and simplifying,

$$Re = \frac{1}{k_s \pi R} \int_{\theta_1}^{\theta_2} \frac{1}{\sin\theta} \, d\theta \tag{29}$$

Evaluating,

$$Re = \frac{1}{k_s \pi R} \ln \tan \frac{\theta}{2} \Big|_{\theta^*}^{\pi/2} \tag{30}$$

and

$$Re = - \frac{1}{k_s \pi R} \ln \tan \frac{\theta^*}{2} \tag{31}$$

The term $\theta^*$ represents the angle at which a mimimum contact radius, $y^*$, occurs for a given particle. The contact radius $y^*$ is defined below. Since the contact angle $\theta^*$ is less than one degree as calculated using the Hertz formula (see Equation 35), then $\tan \theta^*/2$ can be approximated as

$$\tan \frac{\theta^*}{2} \sim \frac{\theta^*}{2} \sim y^*/2(R-h) \tag{32}$$

Now, Equation 31 is

$$Re = - \frac{1}{k_s \pi R} \ln \frac{y^*}{2(R-h)} \tag{33}$$

Since R >> h, the conductive resistance can be written as

$$Re = \frac{1}{k_s \pi R} \ln \frac{2R}{y^*} \tag{34}$$

The value of $y^*$ represents the radius of the contact area between two hemispheres in contact and it is calculated from the Hertz formula [28] by

$$y^* = \{ \frac{3F}{8} [\frac{(1-\mu_1^2)/E_1 + (1 - \mu_2^2)/E_2}{\frac{1}{D_1} + \frac{1}{D_2}}]\}^{1/3} \tag{35}$$

where

F = load per contact

$D_1$ = diameter of particle one

$D_2$ = diameter of particle two

μ = Poisson's ratio

E = Young's modulus

In Equation 35, $D_1$ and $D_2$ are diameters of spheres. In this text, the values of $D_1$ and $D_2$ represent the diameters of two hemispherical protrusions that form a contact point. Hence, the parameters $D_1$ and $D_2$ will be redefined as $D_{c_1}$ and $D_{c_2}$, respectively. Generally, these two diameters are not equal but throughout this text the values of $D_{c_1}$ and $D_{c_2}$ are assumed to be equal and will therefore be written as $D_c$.

Equation 34 represents the conductive resistance to heat flow through one contact region. Combining Equation 34 with Equation 27 and rearranging results in an equation for heat flow through one contact region. If there are $N_h$ particles in series and $N_A$ particles in parallel, then the rate of heat flow through one foot cube of material can be written

$$Q_T = \frac{n\pi \ k_s \ D_c \ N_A (T_H - T_C)}{2N_h \ \ln(D_c/y^*)} \qquad (36)$$

where

    n   = number of contact points per particle
         (heat flow in) for particle in series

    $D_c$  = estimated contact region diameter

    $N_A$  = number of particles per unit of area
         (parallel heat flow)

    $N_h$  = number of particles in a unit of
         height (series heat flow)

The equivalent contact region diameter, $D_c$, is the estimated diameter of a hemispherical protrusion on a particle. This was shown earlier in Figure 4(a). Also note in Equation 36 that radius, R, has been converted into terms of diameter, $D_c$.

For a unit temperature difference across a given depth of insulating material, Equation 36 allows one to define an effective coefficient of particle-to-particle thermal conductivity as

$$K_s = \frac{n\pi\, k_s\, D_c\, N_A}{2N_h\, \ln(D_c/y^*)} \tag{37}$$

The above equations were devised on the basis of an array of uniform particles. However, a material such as diatomaceous earth consists of particles that are non-uniform in size and shape and are oriented at random. Therefore, an empirically determined correction factor, C, must be incorporated into Equation 37. The correction factor will take into account

    1.  bridging of particle columns,

    2.  discontinuities in the heat flow path, such
        as terminated columns,

3.  non-uniformity of particle size and shape, and

4.  changes in material properties, such as the addition of a foreign substance in a pure base material.

In view of the above, Equation 37 is now

$$\overline{K}_s = \frac{C \pi k_s n D_c N_A}{2N_h \ln(D_c/y^*)} \tag{37}$$

A sample evaluation of the above equation will be discussed in Chapter V.

Equation 37 was derived for application in the contact region connecting two irregularly shaped particles. As a material more closely approximates a sphere, $D_c$ approaches the diameter of the sphere. In this case, $N_A \simeq 1/D_c^2$ and $N_h \simeq 1/D_c$. Equation 37 can then be written as

$$\overline{K}_s = \frac{C'k_s}{\ln(D_c/y^*)} \tag{38}$$

where

$$C' = C\pi n/2$$

The particle-to-particle conductivity, $\overline{K}_s$, is seen to depend primarily on the particle conductivity, $k_s$. The natural log term is essentially a constant for typical variations of the material parameters encountered in this study; that is, for a given powder sample.

The value of C' is a constant for a given material. Incorporated into C' is the value of n, the number of

contact regions leading into a particle.[*]   The value
of $\bar{K}_s$ is seen to vary directly with n.   Thus, one should
choose an insulating powder so that n is minimized.

## Radiant Transfer in a Porous Medium

   Introduction.   The ratio of radiant-to-total heat
transfer in a porous medium has been modeled extensively.
However, there is little explicit experimental data,
identifying radiation separately, with which to judge
the effectiveness of these models.   In a porous medium
in which the particles are opaque and small ($<10^{-2}$ ft)
and in which the temperatures are less than 2700°F, there
is agreement in the literature that radiant compared to
total heat flow is negligible [29,30].

   Radiant heat transfer in a porous powder.   In view of
the above paragraph, net radiant transfer through powders
for conditions encountered in this study was considered
to be negligible.   The powders used were on the order of
$10^{-4}$ ft in diameter and upper temperature limit was 1000°F.
As will be demonstrated in Chapter V, net radiant transfer
through diatomaceous earth powder under typical operating
conditions accounted for approximately 1%, on a theoretical
basis, of total energy transfer.   Even though this is

---

[*]   Contact regions for energy transport out of a particle are
     considered as a contact region leading into an adjacent
     particle.

considered to be negligible, a theoretical analysis of radiant heat transfer through powders will be presented for completeness.

The theoretical model presented is similar to those of Argo and Smith [29] and Schotte [30]. To model radiant transport the above authors assumed spherical particles and considered radiant transfer through parallel planes located on each side of a particle. See Figure 5.
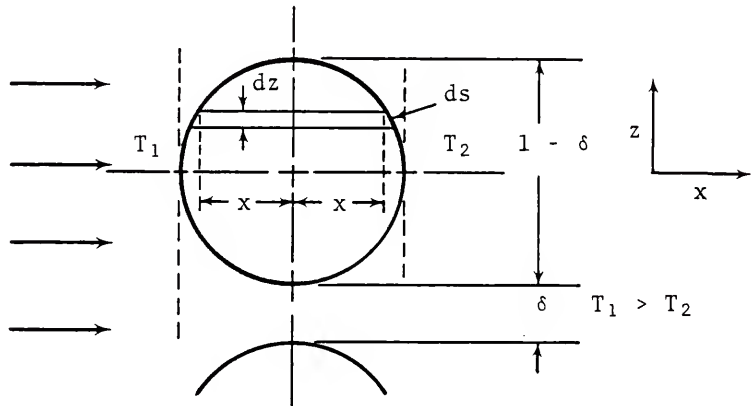


Figure 5

Model for Derivation of Radiant Contribution to
Thermal Conductivity through a Porous Medium

The model considers radiant transfer through the voids between particles and radiant transfer from surface to surface in series with the solid particle conduction.

The model also assumes that the particles were opaque
and that the particle size was large compared to the
wavelength of radiation. Considering the last restriction,
the particle size used in this study was 15 - 125 μm.
For a temperature range of 250 - 1000°F, Wien's displace-
ment law gives an average wavelength of 7.35 - 3.57 μm,
respectively. Thus, the condition is well satisfied
with large particles at all conditions, reasonably
well satisfied with medium size particles at higher
temperatures or small particles at lower temperatures,
but is doubtful for the smallest particles at the lowest
temperatures.

One may view radiant energy as a packet of energy,
or photon, instead of a wave. Of the many photons that
participate in radiation passing through a porous powder
most will strike the surfaces that form a void many times
before they could escape. As a result the probability of
absorption is very high compared to the probability of
escape. Hence, the effective absorptivity and emmissivity
may be approximated as unity. By viewing radiant transfer
in terms of photons, it is easy to visualize radiant energy
transfer as meeting great resistance in flowing through a
porous powder, especially for conditions previously
described.

The results of the analysis by Schotte [30] give an
overall radiative conductivity coefficient of

$$K_r = \frac{1 - \delta}{\frac{1}{k_s} + \frac{1}{k_{rv}}} + \delta k_{rv} \qquad (29)$$

where $\delta$ is the void fraction, $k_s$ is the solid particle conductivity, and $k_{rv}$ is a particle radiation conductivity coefficient. The latter variable represents radiant heat transfer between a particle and its neighbor. This value will be defined shortly.

The right-hand side of Equation 39 consists of two terms. The first term represents radiant heat transfer to a particle in series with conduction through the particle. The second term accounts for radiation through the void space adjacent to the particle.

The radiative coefficient, $k_{rv}$, which represents radiative transfer between a particle and its neighbor, is given by Schotte [30] as,[+]

$$k_{rv} = 4\epsilon \bar{d} \xi T^3 \qquad (40)$$

where $\epsilon$ is the emissivity of the particles, $\bar{d}$ is the average void dimension, $\xi$ is the Stefan-Boltzmann constant, and $T$ is absolute temperature. The temperature used in this equation, $T$, is the average temperature of the particles. Argo and Smith [29] have pointed out that

---

[+] This equation is presented by Schotte [30] as $k_{rv} = 0.692\bar{d}$ $T^3/10^8$. This equation and the one used above are the same.

one investigator [31] used a bulk mean temperature in
evaluating Equation 36 and found it in agreement with more
elaborate methods for determining radiative transfer
through powders.

In summary, the above paragraphs illustrate the
role of radiant to total energy transport through a porous
powder. The parameters that apparently control radiant
heat flow through powders are the particle size, opacity
of the material, particle conductivity, void dimension,
and boundary temperatures.

CHAPTER IV

EQUIPMENT DESIGN
AND MATERIAL PREPARATION

## Introduction

The intent of the experimental procedure was two-fold.  First, apparent thermal conductivities for various particle sizes were needed to establish the required insulation thicknesses for a high temperature storage system.  This required the design and construction of a conductivity test apparatus capable of measuring conductivity of a powder material with a hot face temperature up to 1000°F and for vacuum levels down to 100 μm Hg.

The second objective of the experimental procedure was to design a prototype high temperature thermal energy storage system using a porous powder under a moderate vacuum (P ~ 1 mm Hg) as the insulating material.  The thermal energy storage vessel was designed to use an organic oil (corn, cottonseed, peanut, or soybean) as the storage medium.

## Conductivity Test Apparatus

The conductivity test apparatus is shown in Figures 6(a) and 6(b).  The central core of the test cell consists

electrical wiring port
wax cup
thermocouple port
$\frac{1}{2}$" OD pipe
vacuum port
centering plate
$2\frac{1}{8}$ OD copper sleeve
vacuum gauge port
$1\frac{7}{8}$" aluminum plug, four threads per inch
$4\frac{1}{8}$" OD copper cylinder
centering plate
vacuum port
steel wool (grade 000)
$2\frac{9}{16}$
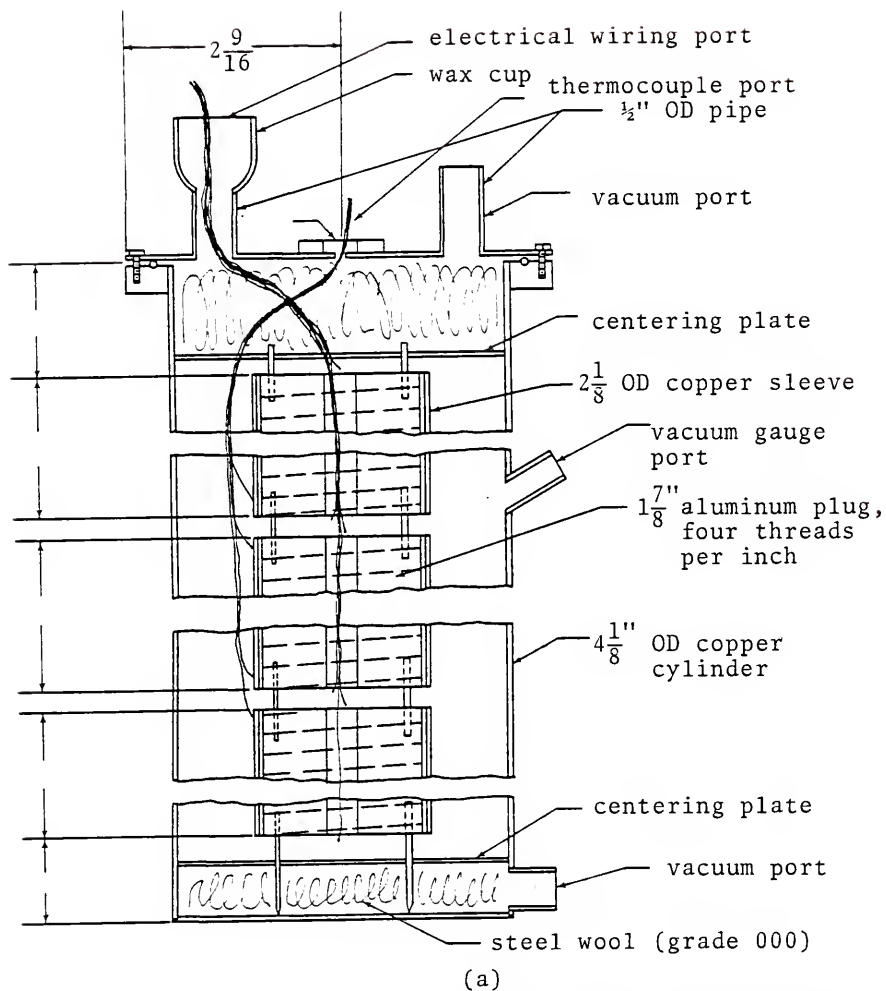
(a)
Sectional View Of Conductivity Test Apparatus

Figure 6
Conductivity Test Apparatus
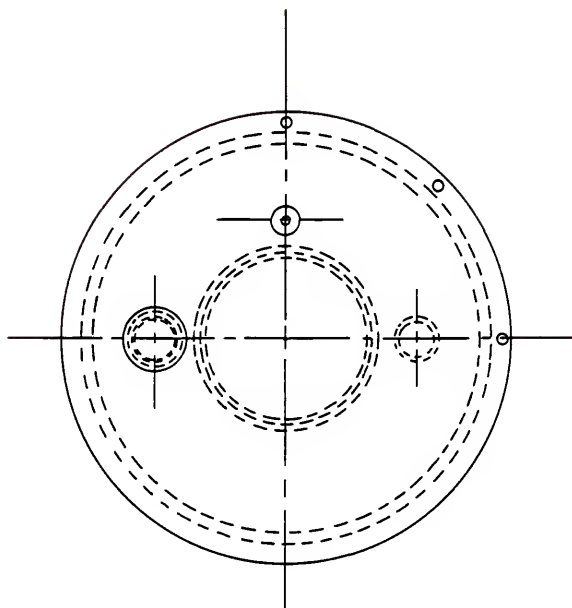
Top View
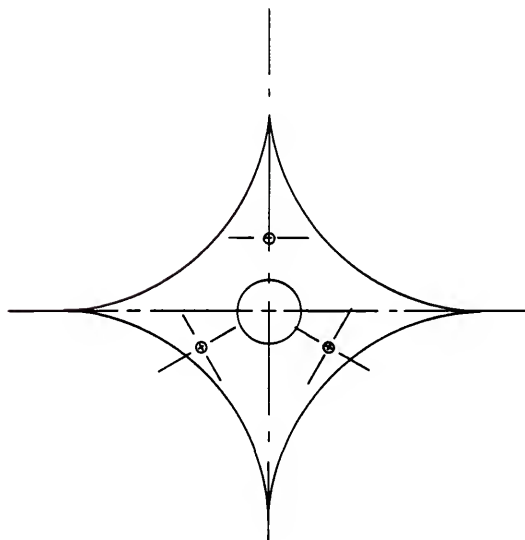


Centering Plate

Figure 6(a) (Cont'd.)

(b)

Figure 6

Photograph of Conductivity Test Apparatus

of two guard heaters and a center test section heater. The nichrome heater wires were wound on a threaded aluminum core which served to thermally dampen small devia- tions in the power supply. The aluminum core was wrapped with a ceramic paper and inserted into a copper sleeve. The copper sleeve helped to insure a uniformly heated surface. Chromel-alumel thermocouples were welded to the copper sleeve so that a temperature difference between the guard heaters and the center test section heater could be read. In this manner, the guard heaters could be adjusted to the same temperature ($\pm$ 1/2°F) as the center test section heater, insuring radial heat flow in that section. By measuring the electrical energy dissi- pated in the central test section, and by measuring the surface temperatures at the boundaries of the powder insulation, the apparent thermal conductivity was calcula- ted. For a cylindrical geometry,

$$Q_{elec} = \frac{2\pi K_a (T_H - T_C) L}{\ln(r_o/r_i)} \tag{41}$$

Solving for conductivity,

$$K_a = \frac{Q_{elec} \ln(r_o/r_i)}{2\pi (T_H - T_C) L} \tag{42}$$

For this apparatus,

$Q_{elec}$ = rate of electrical energy dissipation

L = 1 ft test section length

$r_o$ = 0.163 ft outside radius of insulating material

$r_i$ = 0.089 ft inside radius of insulating material

$T_C$ = average cold surface temperature of insulation at boundary

$T_H$ = average hot surface temperature of insulation at boundary

The electrical energy dissipated was calculated by measuring the voltage and current of the center test section heater wires. Thus,

$$Q_{elec} = EI \cos \phi \qquad (43)$$

where,

$\cos \phi \approx 1$ (assuming the power factor to be unity for resistance heating)

E = potential

I = current

The value of $T_C$, the cold wall temperature, was measured on the outside surface of the conductivity test cell. The calculated estimate of the temperature drop across the copper wall was negligible (< 0.002°F). The heat losses through the wires, thermocouples, and electrical conductors had a negligible effect on the test section energy balance, since the temperature difference between

that section and the guard heaters was held to $\pm$ 1/2°F
of each other.

Pads of fine steel wool were placed at the top and
bottom of the conductivity test cell to facilitate evacua-
ting the fine powder without entrainment. The vacuum
ports at the top and bottom of the test cell permitted
a faster evacuation time than a single port.

A vacuum port was placed above the upper guard
heater and below the lower guard heater so that its
presence would not interfere with the center test section.
Several different types of vacuum gauges were used during
the course of testing.

The first was a thermocouple gauge with a range of one
atmosphere to 1 μm Hg. However, it was difficult to
maintain calibration due to powders infiltrating its
sensing element and, consequently, this gauge was not used.
A swivel type McLeod gauge with a range of 1 μm - 5 mm Hg
was the second type used. The gauge worked well after a
small piece of fine steel wool (0000) was put in line with
it to prevent powders from reaching the mercury.

Alignment of the central core of the test apparatus
was maintained by a centering plate as shown in Figure 6(a).

Wire feeds were created by packing asbestos string
around the wires. The wires were sealed as they passed
into the test apparatus by melting high temperature wax
around them. The wax had to be re-heated periodically

due to differential expansion between the wire and wax.

## The Design of a High Temperature Thermal Energy Storage System

A high temperature thermal energy storage system was designed according to the following criteria.

1.  Heat loss per day not to exceel 10 Btu/hrft$^2$.

2.  The inner tank has a minimum high pressure rating of 150 psi at 700°F.

3.  Both the inner and outer tank have low pressure rating at $1.32 \times 10^{-5}$ psi (100 μm Hg).

4.  The inner tank is capable of holding organic oils.

5.  The vessel construction is simple and durable.

6.  The vessel requires little maintenance.

7.  The inner storage vessel is sized to be compatible with a 6' x 8' concentrating collector.

8.  The design potential is intended for mass production at an acceptable cost.

The tank design is shown in Figure 7.

The inner tank was made from a 14 gauge galvanized steel, 42 gallon water tank. Note that one end of the water tank was changed from concave to convex to insure stability at elevated pressures.

The outer tank was constructed from a 14 gauge galvanized steel 200 gallon water tank. The cylindrical

inlet port
½" iron pipe

heater port
3/4" iron pipe

inlet port
½" iron pipe

½" iron water pipe

steel cable
and turnbuckle

2" flange

50"

16"

58"

Section View of High Temperature Storage
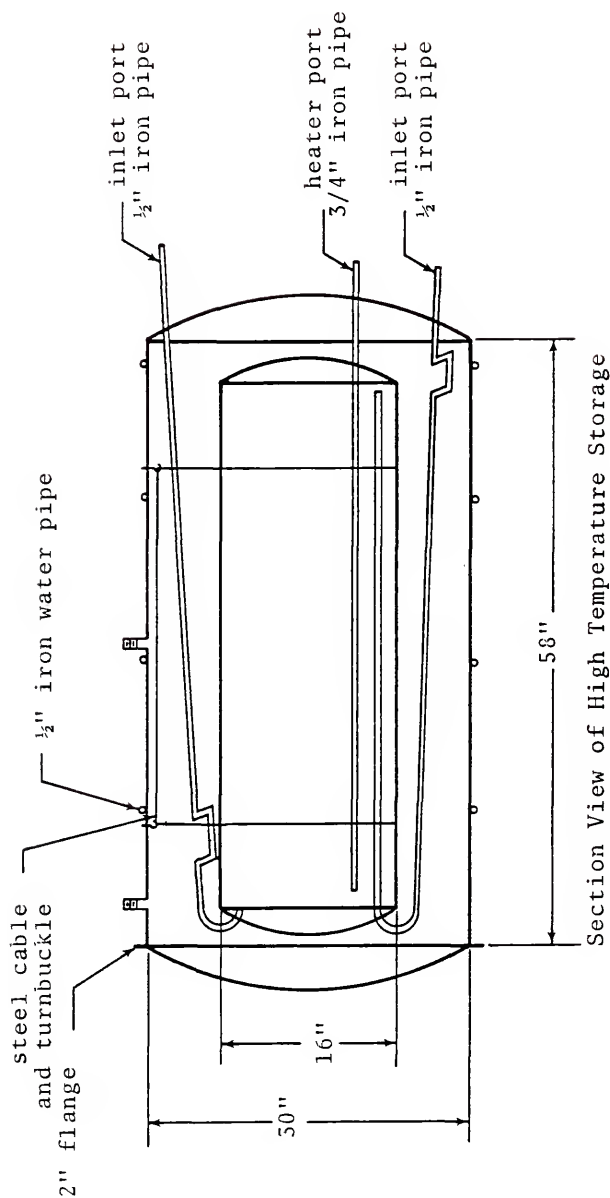
Figure 7

Prototype High Temperature Thermal Energy Storage System

5/16" bolts, typical
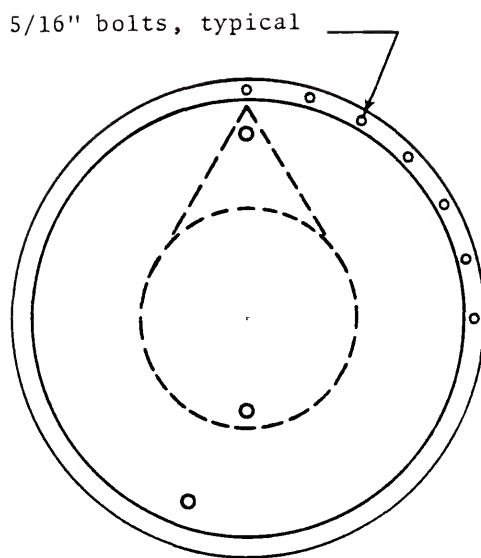


Figure 7(b) (Cont'd)

End View of Tank Showing Internal
Cable Support and Flange Bolt Pattern

$\frac{1''}{16}$ x 2" x 2" angle iron

$\frac{1''}{8}$ x 1" x 1" angle iron
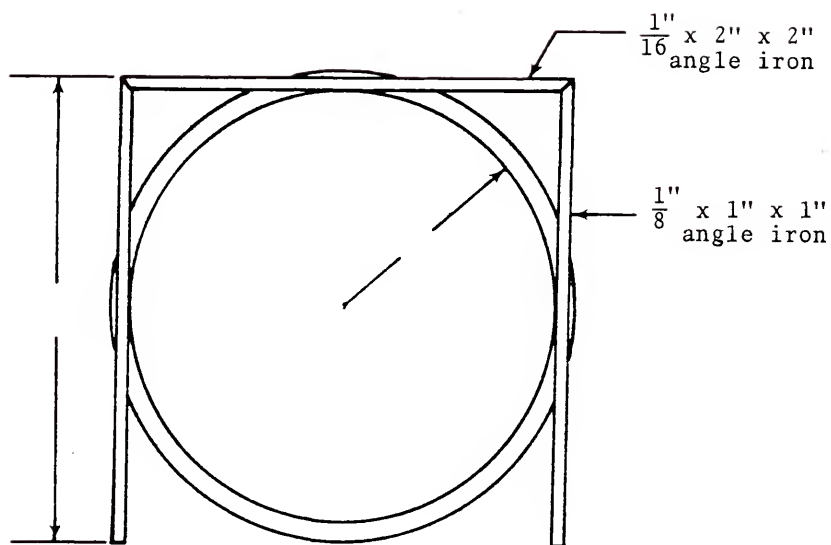
Figure 7(c) (Cont'd)

External Support for Inner Tank

(d)

Figure 7

Photograph of Prototype High Temperature
Thermal Energy Storage System

portion of the tank was shortened and the concave end was changed to convex so that the insulation thickness at the ends of the tanks would be equal to the thickness between the cylindrical portions of the tank.

The inner tank was suspended by two 1/16" diameter stainless steel cables. These cables were selected for their high breaking strength (500 lb. at room temperature) and low thermal conductivity (10 Btu/hrft°F at room temperature). The two cables had sufficient strength at elevated temperatures (1000°F) to afford a safety factor of two (2).

The inlet and outlet pipes were designed with a U-shaped trap which served as an expansion loop and a heat trap. The inlet pipe at the top had the loop placed close to the inner tank so that it would prevent volatile vapors from the organic oil from entering the outlet pipe when the pipe was not in use. The loop on the botton outlet pipe was placed at the opposite end of its point of attachment and the outlet pipe was sloped downward so that heat conducted through the metal would induce convective flow in the opposite direction, thereby helping to minimize heat flow out of the inner tank.

The rings on the outer tank were needed to meet safety recommendations on externally pressurized tank design [32].

The inner tank was designed to contain organic oils. Copper metal cannot be used with organic oils since these

oils are acidic in nature and react chemically with copper.
The long term effect of high temperature organic oils on
steel is presently unknown. At low temperatures, steel
containers have been used successfully to contain organic
oils.

The minimum storage vessel size was estimated for
a 6 ft x 8 ft (aperture area) concentrating collector
as follows.

$$\begin{matrix} \text{Heat delivered to} \\ \text{storage system} \end{matrix} = \begin{matrix} \text{Heat stored in oil} \\ \text{and its container} \end{matrix} + \begin{matrix} \text{Heat losses} \\ \text{from piping} \end{matrix} \qquad (44)$$

Assuming the pipe losses equal 10% of the energy stored
in the oil and its container, then

$$H_{in} = 1.10\ H_{sto} \qquad (45)$$

and

$$I_s A_a \eta_t \tau = 1.1 \rho V C_p \Delta T \qquad (46)$$

where $I_s$ is solar insolation, $A_a$ is the collector aperture
area, $\eta_\tau$ is the collector average thermal efficiency, $\rho$ is
density of organic oil (cottonseed), V is the oil tank
volume, $C_p$ is the average specific heat of the oil, and
$\Delta T$ is the temperature rise of the oil.
Solving for volume

$$V = \frac{I_s A_a \eta_t \tau}{1.1\ C_p \Delta T} \qquad (47)$$

Assuming the following values,

$n_\tau$ = 50%

$I_s$ = 300 Btu/hrft$^2$

$\tau$ = 8 hr/day

$\rho$ = 46.5 lbm/ft$^3$ @ 600°F (estimated)*

$C_p$ = 0.66 Btu/lbm°F @ 600°F (estimated)*

$\Delta T$ = 400°F (200 - 600°F)

$A_a$ = 48 ft$^2$

and solving for V in Equation 47 yields

$V$ = 4.27 ft$^3$ (maximum)

A 42 gallon tank holds 5.62 ft$^3$ and afforded an excess capacity to serve as an expansion chamber.

The outer tank size was chosen from commercially available tanks. The most convenient size was a 220 gallon galvanized water tank. The outer tank diameter was 2.5 ft and the inner tank outside diameter was 1.33 ft. Thus, there was a 0.585 ft space for insulation. The ends of the tank were designed to leave an equivalent 0.585 ft space.

A preliminary test on diatomaceous earth powder indicated that an apparent conductivity value of $K_a$ = 0.01

---

* Cottonseed oil data [3]

Btu/hrft°F could be obtained at a hot surface temperature
of 600°F, a cold surface temperature of 70°F, and at 1 mm
Hg pressure.  A 0.585 ft thick layer of insulating powder
for these conditions would hold the daily energy loss
of the storage tank to approximately 9% per day of the
initial energy stored.  This approximation is based on
changes in temperature and average values of $C_v$ over the
interval of temperature change.

## Diatomaceous Earth Properties

Diatomaceous earth is the fossilized remains of micro-
scopic marine algae.  It consists of approximately 98%
$SiO_2$ (silica).  The diatomaceous earth used in this study
was purchased commercially.  Its intended purpose was for
use in swimming pool filters.  This material has been
used industrially as high temperature, loose fill, insula-
tion and in compressed brick form as a furnace lining.
The loose fill material has an upper temperature limit of
1600°F  and the brick has an upper limit of 2500°F [19].
The apparent reason for the limitation of the loose fill
material is that the powder particles begin to soften
at that temperature.  This would increase the point-to-
point solid conductivity and also cause loss of volume of
the material due to settling.

In fine powder insulation it is useful to determine
the effect of particle size on apparent thermal conductivity.

One difficulty of determining particle size is that fine powders tend to clump. An explanation for this phenomenon will be discussed later. However, this made it difficult to separate these particles in a sieve and shaker. Grinding these particles in a ball and mill reduced their size but did not make it easier to separate them into various particle sizes.

It was found that the addition of small amount of fine carbon black to the diatomaceous earth, either during the separation process or the grinding process, permitted the powder to separate quickly in a sieve and shaker. The reason for this is that the fine carbon particles act like a lubricant. Carbon particles are shown in Figure 11. Note the puffy appearance of the agglomerated carbon particles. This suggests that the large particles may be comprised of many smaller carbon particles.

A possible explanation of how carbon acts as a lubricant may derive from the fact that carbon is electrically conductive. When the diatomaceous earth particles are vibrated, the particles become charged with static electricity. Hence, if particles have opposing charges, they attract each other. This prevents the particles from passing through the sieve and, consequently, no separation of particles occur. When carbon powder is added to diatomaceous earth, it short circuits the static charge between the particles and this permits the particles to pass through the sieve.

After the diatomaceous earth was separated into its various particle sizes, its geometry remained essentially the same. Figure 8 shows particles trapped in Tyler Sieve #500. Figure 9 shows particles trapped by Tyler Sieve #170. Both of these photographs vividly display the irregular characteristics of these powders.

The various particle size distributions obtained in a sieve and shaker are given in Table 3. The Tyler sieve number corresponds to screen weaves of the following opening size

| Tyler Sieve No. | 120 | 170 | 200 | 270 | 325 | 500 | <500 |
|---|---|---|---|---|---|---|---|
| Opening (microns) | 125 | 90 | 75 | 53 | 45 | 25 | < 25 |

The last category, <500, was simply a catch pan for particles falling through the #500 screen.

The values shown in Table 3 are representative only of the particle sizes in the original diatomaceous earth. These values changed somewhat with each test.

The purpose of generating data for Table 3 was to find the various nominal particle sizes with their corresponding quantities. The variables influencing the separation process were the length of time the shaker was operated and the amount of carbon present. The objective was to use as little carbon as possible. The general results of Table 3 follow.

TABLE 3

Diatomaceous Earth Particle Size and Distribution
Typical Results

| Run # | Shaker time (min.) | Diatom. earth (grams) | Carbon (grams) | Tyler Sieve Number | | | | | | |
|---|---|---|---|---|---|---|---|---|---|---|
| | | | | 120 | 170 | 200 | 270 | 325 | 500 | <500 |
| 1 | 30 | 174.50 | 0 | 62.25 | 81.75 | 28.25 | -* | 2.00 | 0.25 | 0 |
| 2 | 10 | 175.70 | 1.0 | 31.55 | 73.00 | 45.00 | 15.25 | 8.25 | 2.75 | 0.90 |
| 3 | 15 | 190.50 | 1.0 | 35.50 | 11.25 | 42.00 | -* | 35.50 | 49.50 | 17.75 |
| 4 | 10 | 188.75 | 1.5 | 40.25 | 12.50 | 24.50 | 40.00 | 32.00 | 34.50 | 6.50 |
| 5 | 10 | 172.00 | 1.5 | 25.00 | 13.75 | 29.50 | 47.50 | 26.50 | 30.25 | 1.00 |
| 6 | 10 | 177.75 | 2.0 | 30.75 | 11.25 | 23.50 | 47.25 | 34.75 | 29.50 | 2.75 |
| 7 | 10 | 179.50 | 2.0 | 31.50 | 10.00 | 19.50 | 41.50 | 38.50 | 33.75 | 6.75 |
| 8 | 10 | 172.75 | 3.0 | 29.50 | 10.75 | 18.50 | 37.50 | 40.75 | 33.00 | 5.25 |
| 9 | 8 | 179.00 | 4.0 | 35.50 | 38.75 | 63.25 | -* | 36.50 | 9.00 | 0 |
| 10 | 16 | 178.50 | 4.0 | 31.75 | 10.50 | 38.00 | -* | 52.75 | 49.50 | 0 |
| 11 | 24 | 171.75 | 4.0 | 32.75 | 9.25 | 31.00 | -* | 27.25 | 49.75 | 25.75 |
| 12 | 60 | 200.25 | 4.0 | 32.25 | 11.00 | 25.50 | -* | 29.25 | 35.25 | 69.00 |
| 13+ | 10 | 326.00 | 5.0 | 0 | 0 | 21.00 | 148.00 | 76.00 | 81.00 | 5.00 |
| 14• | 10 | 334.50 | 5.0 | 18.00 | 52.00 | 133.00 | 111.50 | 20.00 | 5.00 | 0 |

*This size sieve not used during this test.
+In ball mill for 30 minutes, carbon added at beginning.
•Carbon added after powder pulverized for 1 hour.

Figure 8

Electron Microscope Photograph of Diatomaceous
Earth-Carbon (1% wt) Mixture, Particles from
Tyler Sieve #500 (x 1,000)
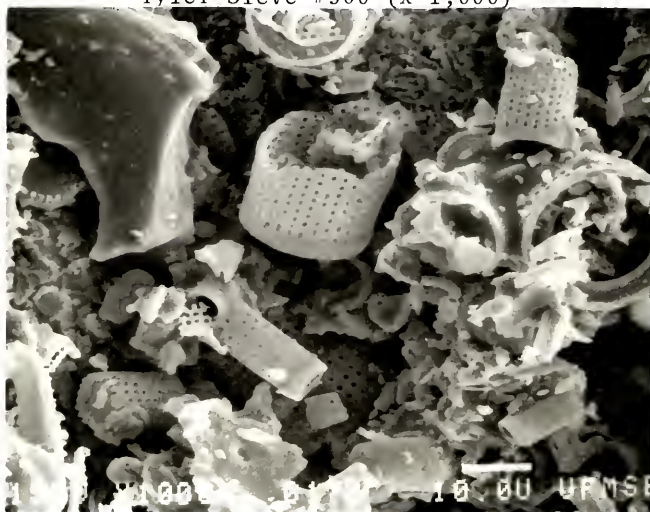


Figure 9

Electron Microscope Photograph of Diatomaceous
Earth-Carbon (1% wt) Mixture, Particles from
Tyler Sieve #170 (x 1,000)
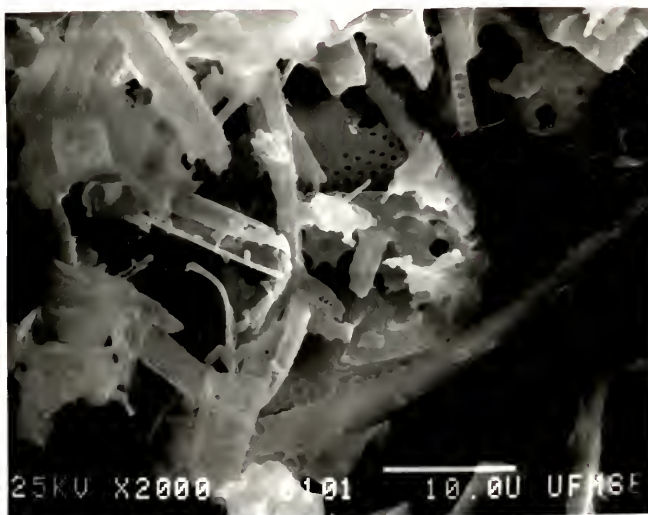
Figure 10

Electron Microscope Photograph of Diatomaceous Earth
(as purchased), x 2,000
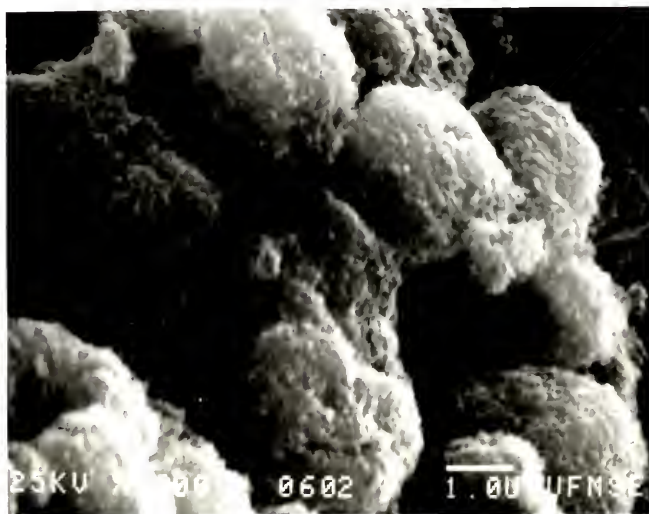


Figure 11

Electron Microscope Photograph of Carbon Black,
Monarch 500 (x 10,000)

1. Run #1 illustrates the difficulty of separating raw* diatomaceous earth. Even after 30 minutes, very few particles were separated.

2. Run #2 illustrates that a large percentage of the particles in the powder are indeed small.

3. The general trend is that as the amount of carbon increased, the greater the percentage of small particles and the faster they separated.

4. A given type of powder with the same amount of carbon and the same shake time shows a general consistency in particle distribution, but some particles of a given size may vary appreciably. Compare Run #4 and Run #5.

5. Carbon added prior to pulverzing diatomaceous earth permits the separation of fine particles in less time than when it was added after pulverizing.

Representative data on density of the various particle sizes are given in Table 4. Note the discrepancy between the measured void fractions[†] and the calculated void fractions. This could be due to air being trapped in and among the particles and not being displaced during the void measurement process. Another explanation, in view of Figures 8 and 9, is that the particles do not separate well and that the mixture of large and small particles causes the void fraction to remain relatively constant.

---

\* Raw diatomaceous earth refers to the material as purchased.

[†] Void fraction is the ratio of the void space in a container to the total volume of the container.

TABLE 4

Particle Density and Void Fraction of Diatomaceous Earth

| Particle Size | Density (lbm/ft$^3$)$^†$ (measured) | Void Fraction (measured) | Void Fraction (calculated) |
|---|---|---|---|
| Tyler Sieve #120 | 15.53 | - | 0.89 |
| "    "  #170 | 17.57 | 0.71 | 0.88 |
| "    "  #200 | 18.98 | 0.76 | 0.87 |
| "    "  #270 | 19.70 | 0.71 | 0.86 |
| "    "  #325 | 19.92 | 0.77 | 0.86 |
| "    "  #500 | 20.08 | 0.76 | 0.86 |
| less than #500 (catch pan) | 22.67 | 0.75 | 0.84 |
| raw diatomaceous earth | 17.35 | 0.83 | 0.88 |
| carbon black | 11.77 | - | - |
| powder for prototype tank | 32.84 | 0.70 | 0.77 |
| solid diatomaceous* earth (SiO$_2$) | 145.0 | | |

* Calculated from molecular weight of $S_iO_2$.
$^†$ 1% carbon black in powders.

The method used to measure the void fraction and density was to fill carefully a graduated cylinder of known weight with the powder and gently tap the cylinder to settle the particles. The cylinder with the particles was then weighted. The cylinder with the powder was then filled with water to the original level of the powders, and it was then weighed again. With a knowledge of the volume and weight of the powders, a density was then calculated. The void fraction was found by deducing the volume of water required to fill the graduated cylinder to the original volume of powder. The ratio of the latter two quantities is the void fraction.

CHAPTER V

EXPERIMENTAL PROCEDURE AND RESULTS

## Conductivity Test Equipment

The conductivity test equipment arrangement is shown
in Figures 12 and 13.  Power was supplied through rheostats
connected to a standard 120 volt AC outlet.  Variations in
the AC outlet due to daytime peaks were overcome by obtain-
ing a long-term average for the data over a period of
several days to more than a week for each datum point.
These data were recorded manually.

The test section heaters were monitored for current
and voltage.  This was accomplished by placing an ammeter on
one lead of the heater wire.  Voltage was measured on the
heater side of the power supply.  The guard heater power
was monitored only for interest in their power levels
relative to the central heater.  The guard heater power
levels were adjusted to give a temperature within $\pm 0.5°F$
of the central heater.  This power level was usually slightly
more than the power level of the central heater.

The temperature of the four thermocouples inside the
test cell were measured with a digital volt-ohm meter.
An ice bath was used as a temperature reference for the
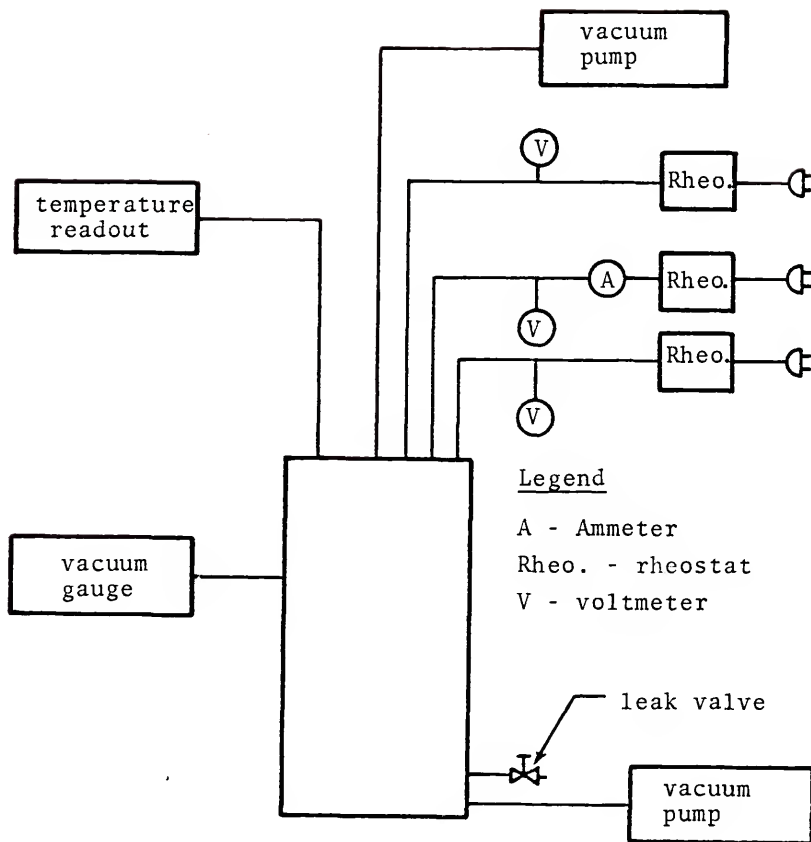
Figure 12

Conductivity Test Equipment Arrangement

Figure 13

Conductivity Test Equipment

chromel-alumel (Type K) thermocouples.  The temperature
levels were recorded manually.

A mercury-filled McLeod gauge with a range of 1 μm - 5
mm Hg was used to measure the vacuum level in the conducti-
vity test cell for data presented in this study.  For the
preliminary testing period a thermocouple vacuum gauge
was used.  It was found to lose calibration often and a
standard gauge was needed for recalibration.  It was found
easier to use the standard gauge (McLeod) directly in the
experiment.

A common vacuum pump with a blank-off pressure of 15
μm Hg was used for evacuating the system.  A variable
leak valve was placed at the bottom of the test cell to
regulate pressure.

The objective of this experiment was to find the
change in thermal conductivity due to changes in

    1.   particle size,

    2.   vacuum level, and

    3.   temperature levels.

## Thermal Conductivity of Powder Insulation Under Vacuum

For the determination of the thermal conductivity of
a powder, the thermal conductivity apparatus, as shown in
Figure 6, was filled with the powder to be tested.  The
powders were heated prior to evacuation so that the elevated
temperatures would aid moisture removal from the powder
particles.

Once the system was thoroughly heated, it was sealed and evacuation was initiated. The heater elements were adjusted so that the main heater and guard heater thermo-couples read within 1/2°F of each other. This process usually required several days. After a uniform temperature was reached, the system was generally operated under this condition for at least one day to insure that steady-state had been achieved. This additional time was necessary to minimize the effect of the daily changes in the AC power supply and the daily temperature swing of the test room.

During the testing procedure, data were taken manually, usually on hourly intervals, for the three heater tempera-tures (6 points), outside surface of test apparatus, test heater potential and current, and room temperature.

## Data and Results from Thermal Conductivity Test

The experimental values obtained from the thermal conductivity apparatus are shown in Table 5. The four measurements were

1. pressure level, measured in $\mu m$ Hg,

2. the hot surface temperature, $T_H$, bounding the powder material adjacent to the main heater,

3. the cold surface temperature, $T_C$, taken on the outside surface of the test apparatus,

4. power dissipated from the central test section heater (potential x current).

From the measured data the apparent thermal conductivity coefficient, $K_a$, was calculated with the use of Equation 42.

## Discussion of Results of Apparent Conductivity Test

Range of values. The range of apparent conductivity values, as seen in Table 5, vary as follows

Highest value:    $K_a$ = 0.0648 Btu/hrft°F

@ $T_H$ = 631°F, P = 760 mm Hg

Lowest value:    $K_a$ = 0.0029 Btu/hrft°F

@ $T_H$ = 340°F, P = 0.6 mm Hg

To put these values in perspective, air has the following experimental conductivity values [33]

Air at 631°F:    K = 0.0272 Btu/hrft°F

@ P = 760 mm Hg

Air at 340°F:    K = 0.0212 Btu/hr ft°F

@ P = 760 mm Hg

From this, the highest test data value, taken at 760 mm Hg pressure, is 2.4 times higher than the conductivity of air, but the lowest value, with a pressure of 0.6 mm Hg, is 7.3 times less than air at 760 mm Hg. This is significant since the conductivity of air is essentially independent of pressure except under the low pressure conditions (Kn > 1)

TABLE 5

Average Thermal Conductivity Values
For Evacuated Diatomaceous Earth[*]

Powder in Tyler Sieve #500 (loose powder)

|  | Pressure (μm Hg) | $T_H$ (°F) | $T_C$ (°F) | $K_a$ (Btu/hrft°F) |
|---|---|---|---|---|
| 1 | 500 | 405 | 90 | .00364 |
| 2 | 600 | 733 | 101 | .00648 |
| 3 | 800 | 700 | 93 | .00750 |
| 4 | 850 | 330 | 89 | .00483 |
| 5 | 1000 | 730 | 104 | .00722 |
| 6 | 1000 | 660 | 85 | .00790 |
| 7 | 1000 | 558 | 97 | .00444 |
| 8 | 1000 | 452 | 87 | .00407 |
| 9 | 1000 | 443 | 84 | .00417 |
| 10 | 760,000 | 631 | 192 | .06480 |
| 11 | 760,000 | 432 | 154 | .04600 |

Powder in Tyler Sieve #500 (powders physically compressed to 45 psi)

| 12 | 600 | 340 | 97 | .00290 |
|---|---|---|---|---|
| 13 | 725 | 472 | 85 | .00380 |
| 14 | 650 | 498 | 100 | .00540 |
| 15 | 725 | 691 | 100 | .00910 |
| 16 | 775 | 295 | 86 | .00338 |
| 17 | 800 | 300 | 84 | .00327 |
| 18 | 850 | 685 | 103 | .00910 |
| 19 | 900 | 677 | 102 | .00930 |
| 20 | 1000 | 694 | 108 | .01230 |
| 21 | 1000 | 746 | 111 | .01130 |

[*] Powders contain approximately 1% carbon by weight.

TABLE 5, Continued

Powder in #325 pan (loose powder)

|    | Pressure ($\mu$m Hg) | $T_H$ ($^\circ$F) | $T_C$ ($^\circ$F) | $K_a$ (Btu/hrft F) |
|----|----------|-------|-------|-------------|
| 22 | 1400 | 740 | 100 | .00580 |
| 23 | 1800 | 462 | 90 | .00475 |

Powder in #170 pan (loose powder)

| 24 | 175 | 456 | 81 | .00635 |
| 25 | 200 | 699 | 88 | .00656 |
| 26 | 300 | 588 | 108 | .00590 |
| 27 | 800 | 647 | 110 | .00723 |
| 28 | 1000 | 344 | 80 | .00972 |
| 29 | 1000 | 531 | 85 | .01198 |
| 30 | 1000 | 710 | 98 | .01343 |
| 31 | 3800 | 557 | 95 | .01714 |

Raw Diatomaceous Earth (No carbon added to loose powder)

| 32 | 600 | 441 | 93 | .00920 |
| 33 | 1000 | 725 | 110 | .01200 |
| 34 | 2000 | 545 | 96 | .00980 |
| 35 | 8000 | 386 | 110 | .02900 |
| 36 | 8000 | 583 | 117 | .02740 |

Pulverized Diatomaceous Earth (loose powder)

| 37 | 1000 | 446 | 99 | .00960 |
| 38 | 8000 | 511 | 101 | .01560 |
| 39 | 8000 | 715 | 116 | .01448 |

Air Only

| 40 | 760,000 | 603 | 235 | .07800 |

Fiberglass Cloth and Aluminum Foil - 5 layers

| 41 | 400 | 720 | 110 | .01440 |

discussed earlier. This indicates that a powder under
vacuum is effective insulation at elevated temperatures.

The particular area of interest in this study was the
conductivity values of the powders near 1 mm Hg, since
this vacuum level was within the range of common mechanical
vacuum pumps. The conductivities of several of the more
thoroughly investigated powders are shown in Figure 16
(page 96). This graph shows the approximate limits and
the general trend of the apparent conductivities associated
with the large and small grain powders tested.

Radiative transfer. The net contribution due to
radiation through a powder insulation, in the temperature
range of interest in this study, appears to be negligible.
Recall Equations 39 and 40,

$$K_r = \frac{1 - \delta}{1/k_s + 1/k_{rv}} + \delta \; k_{rv} \tag{39}$$

$$k_{rv} = 4\epsilon \; \overline{d} \; \xi \; T^3 \tag{40}$$

Using typical values in these equations, the resulting
coefficient of radiative conductivity is small compared
to other modes of energy transfer. For example, using the
following values for particles in Tyler sieve #500

$$\delta \quad = 0.76 \text{ (Table 4)}$$

$$\epsilon \quad = 1.0 \text{ (assumed value)}$$

$$\bar{d} \quad = 0.5D = 5.75 \times 10^{-5} \text{ ft.}$$

$$k_s \quad = 0.76 \text{ Btu/hrft°F (pyrex glass)}$$

and calculating for radiant transfer for powder in a plane adjacent to a hot surface boundary of 1000°F (1460°R) and for a plane at 250°R gives a range of

$$K_r = 0.001 \text{ to } 0.0001 \text{ Btu/hrft°F}$$

Comparing the above values to a typical apparent conductivities of $K_a = 0.015$ and 0.005 Btu/hrft°F, shows that radiation accounts for 7% and 2% of the totals, respectively. These values represent a worst case for both temperatures since they were calculated for radiant transfer near the hot surface boundary. For powder near a cold face boundary at $T_C = 90°F$ (550°R), then $K_r$ represents about 1% compared to an average value of $K_a = 0.01$ Btu/hrft°F. Thus, the net contribution of radiant transfer through a powder for the temperature limits of this study appears to be negligible.

Effective gas conductivity. Note that Equation 20, when rearranged gives

$$\overline{K}_g = \frac{(9\gamma - 5)}{4(\gamma - 1)} \; (\frac{2R_u}{\pi MT})^{\frac{1}{2}} \; (\frac{1}{P\overline{d}} \; + \; \frac{\sqrt{2} \; \pi \; \sigma^2 \; A_N}{R_u T})^{-1}$$

Evaluating with the following parameters for air alone in a container of one foot cubed,

$$P \;\; = \;\; 760,000 \text{ m Hg}$$

$$T \;\; = \;\; 492°R \; (32°F)$$

$$M \;\; = \;\; 28.97 \text{ lb}_m/\text{lb}_m\text{-mole}$$

$$\sigma \;\; = \;\; 1.1975 \times 10^{-9} \text{ ft}$$

$$\overline{d} \;\; = \;\; 1.0 \text{ ft (since } \overline{d} \gg \lambda)$$

$$\gamma \;\; = \;\; 1.39$$

$$C_v \;\; = \;\; 0.18 \text{ Btu/lb}_m °F$$

gives a value of $\overline{K}_g$ of

$$\overline{K}_g \;\; = \;\; 0.014 \text{ Btu/hrft°F}$$

and this is in close agreement with published experimental data [34]. However, if Equation 12 is evaluated at higher temperatures, around 600°F, its theoretical values are about 18% below the above cited experimental value. This discrepancy arises because of the departure of real gases from the assumptions used in deriving Equation 6.

Table 6 has been prepared to show a relative comparison for air and argon when used under non-continuum conditions and at typical mean temperatures encountered in this study. Table 6 suggests that the smaller particle size inhibits gaseous conductivity and that at higher tempera-

TABLE 6

Theoretical Thermal Conductivity of Air and Argon
For Non-Continuum Conditions at $T_b$ = 860°R

| Particle Size | Tyler Sieve #170 | Tyler Sieve #170 | Tyler Sieve #500 | Tyler Sieve #500 |
|---|---|---|---|---|
| Gas | Air | Argon | Air | Argon |
| d = 0.5 D (ft) | $1.625 \times 10^{-4}$ | $1.625 \times 10^{-4}$ | $5.75 \times 10^{-5}$ | $5.75 \times 10^{-5}$ |
| M ($lb_m/lb_m$-mole) | 28.85 | 39.95 | 28.85 | 39.95 |
| $\sigma$ (ft) | $1.1975 \times 10^{-9}$ | $1.25 \times 10^{-9}$ | $1.1975 \times 10^{-9}$ | $1.25 \times 10^{-9}$ |
| $C_v$ ($Btu/lb_m$°R) | 0.18 | 0.0748 | 0.18 | 0.0748 |

| Pressure (μm Hg) | $K_a$ (Btu/hrft°F) | $K_a$ (Btu/hrft°F) | $K_a$ (Btu/hrft°F) | $K_a$ (Btu/hrft°F) |
|---|---|---|---|---|
| 10 | .00012 | .0000753 | .000042 | .0000268 |
| 100 | .00111 | .000712 | .00041 | .000262 |
| 200 | .00211 | .00134 | .00080 | .000513 |
| 400 | .00381 | .00241 | .00154 | .000983 |
| 600 | .00522 | .00328 | .00222 | .143 |
| 800 | .00640 | .00399 | .00286 | .00181 |
| 1,000 | .00740 | .00460 | .00345 | .00218 |
| 2,000 | .01078 | .00661 | .00588 | .00368 |
| 4,000 | .01398 | .00846 | .00907 | .00561 |
| 8,000 | .01642 | .00983 | .01246 | .00759 |
| 10,000 | .01701 | .01016 | .01346 | .00816 |
| 50,000 | .01923 | .01138 | .01815 | .01080 |
| 100,000 | .01955 | .01156 | .01897 | .01124 |
| 380,000 | .01979 | .01169 | .01963 | .01167 |
| 760,000 | .01983 | .01171 | .01975 | .01167 |

tures, argon performs significantly better than air, especially in the pressure range of interest (0.50 μm to 10 mm Hg). Carbon dioxide has a lower thermal conductivity than air, but its values are not as low as those of argon. In checking these values with Equation 12, keep in mind that the theoretical conductivites at ambient pressures tend to fall as much as 20% below experimental values, as the temperature is raised from 32 to 600°F. It is not apparent if this deviation continues at reduced pressures.

This nominal diameters used in evaluating the powder particles were taken as the average of the screen openings below and above the trapped powder. For example, if powders were trapped between Tyler Sieve #500, screen opening 25 μm, but passed through Tyler Sieve #325, screen opening 45 μm, then the nominal particle size was taken as the average of the two values, or 35 μm. It is well to point out that the nominal diameter is used for convenience in discussing the particles.

Average void diameters of 50% of the nominal diameter were assumed in view of Figures 8 and 9 and from observation of diatomaceous earth particles under an optical microscope. At the onset of this study it was assumed that powders separated by sieves would be of fairly uniform size. However, Figures 8 and 9 indicate that the nominal size, as defined above, is larger than many particles found in the powders.

Particle-to-particle conductivity. Table 4 (page 80) shows a variety of vacuum levels, hot face temperatures, and apparent thermal conductivity values for powder insulation under vacuum. These values were obtained from typical operating conditions of a high temperature thermal energy storage system. With the experimental data of Table 5, and by recalling that energy transport through powders under vacuum occurs principally by conduction, one may use the developed theoretical equations to proportion heat flow through gas and particle-to-particle conduction. This will be done in the following paragraphs by evaluating the conductivity coefficients, $\overline{K}_g$ and $\overline{K}_s$.

Table 7 illustrates the proportioning of apparent conductivity into gaseous and particle-to-particle conductivity. The gaseous conductivity, $\overline{K}_g$, was calculated from Equation 12 and the apparent conductivity values, $K_a$, were taken from Table 5. The particle-to-particle conductivity was then calculated from these values using the estimated area ratios. As a result of viewing the diatomaceous earth powders under an optical microscope, a parallel heat flow model, in the low pressure range, was selected. The gas and solid materials were viewed as parallel tubes. Heat flows through the separate tubes composed of different materials, in parallel. This can be expressed as

TABLE 7

Proportioning of Thermal Conductivity
Into Gaseous and Solid-to-Solid Conductivity

Small Grain Particles

| Line* | $T_b$ (°F) | P (μm Hg) | $K_a$* (Btu/hrft°F) | $\overline{K}_g$ (Btu/hrft°F) | $\overline{K}_s$ (Btu/hrft°F) |
|---|---|---|---|---|---|
| 1 | 247.5 | 500 | 0.00364 | 0.00204 | 0.0316 |
| 2 | 417.0 | 600 | 0.00648 | 0.00239 | 0.0319 |
| 3 | 396.5 | 800 | 0.00750 | 0.00286 | 0.0364 |
| 4 | 209.5 | 850 | 0.00483 | 0.00327 | 0.0145 |
| 5 | 417.0 | 1000 | 0.00722 | 0.00343 | 0.0308 |
| 6 | 372.0 | 1000 | 0.00790 | 0.00348 | 0.0357 |
| 7 | 327.5 | 1000 | 0.00444 | 0.00355 | 0.0103 |
| 8 | 269.5 | 1000 | 0.00407 | 0.00363 | 0.0068 |
| 9 | 263.5 | 1000 | 0.00417 | 0.00364 | 0.0075 |
| 10 | 411.5 | 760,000+ | 0.0648 | 0.01988 | 0.3445 |
| 11 | 293.0 | 760,000 | 0.0460 | 0.01850 | 0.2172 |

Large Grain Particles

| Line* | $T_b$ (°F) | P (μm Hg) | $K_a$* (Btu/hrft°F) | $\overline{K}_g$ (Btu/hrft°F) | $\overline{K}_s$ (Btu/hrft°F) |
|---|---|---|---|---|---|
| 24 | 268.5 | 175 | 0.00635 | 0.00202 | 0.0378 |
| 25 | 393.5 | 200 | 0.00656 | 0.00211 | 0.0388 |
| 26 | 348.0 | 300 | 0.00590 | 0.00307 | 0.0264 |
| 27 | 378.5 | 800 | 0.00723 | 0.00642 | 0.0131 |
| 28 | 212.0 | 1000 | 0.00972 | 0.00758 | 0.0252 |
| 29 | 308.0 | 1000 | 0.01198 | 0.00750 | 0.0445 |
| 30 | 404.0 | 3800 | 0.01343 | 0.00739 | 0.0572 |
| 31 | 326.0 | 600 | 0.01714 | 0.01352 | 0.0434 |

*From Table 5.

+760,000 μm Hg equals one standard atmosphere.

$$q_T = q_{gc} + q_s \tag{48}$$

This results in,

$$K_a = \frac{A_{gc}}{A_T} \overline{K}_g + \frac{A_s}{A_T} \overline{K}_s \tag{49}$$

The area fractions of the above equation would be a difficult parameter to measure for a loose powder. These values can be estimated under the assumption that the area ratios can be deduced from the void ratio. For example, if all of the loose powder material in a unit cube were separated into a uniform solid in the bottom of the cube, with the void volume (residual gas space) above it, then the ratio of the void volume to total volume equals the void ratio. Since the cube is of unit width, the void will equal the area ratio as given in the first term on the right-hand side of Equation 49. The same reasoning will also apply to the solid ratio which is the ratio of the solid volume to total volume or the solid area to the total area, as seen from the edge of the unit cube. Hence, for a differential thickness of powder, the projected solid and void areas will, on the average, be equal to the solid ratio and the void ratio, respectively.

In reviewing Table 5, one would generally expect a relationship between particle-to-particle conductivity and

temperature. This relationship certainly exists, but is not readily apparent as it is masked by the pressure sensitive gaseous conductivity. This is evident in Lines 4-5 of Table 5. These values suggest the need for more detailed information -- particle sizes, void dimensions, and so forth. Also, the temperature gradient, particularly near the hot face boundary, influences the overall apparent conductivity. [Typical temperature profiles are shown in Figure 22.] For amorphous powder particles with an increasing value of particle conductivity, $k_s$, the conductance next to the hot face boundary will be signifiantly more than throughout the remainder of the material.

One particular difficulty in working with powders is that the value of its solid particle conductivity, $k_s$, is not available. An obvious choice as a substitute for $k_s$ of diatomaceous earth would be to use the conductivity coefficient for another amorphous material, such as that of pyrex or quartz glass. The reason for selecting these materials is that the electron microscope photographs reveal particles that show cleavage planes characteristic of an amorphous material. Evidence of crystallinity was not apparent. Also, the data reported herein indicate that point-to-point solid conductivity increases with temperature, and this is consistent with amorphous material such as pyrex or quartz glass.

Equation 37 can now be evaluated for particle-to-particle conductivity.  Recall Equation 37,

$$\overline{K}_s = \frac{C\, k_s\, n\pi\, D_c\, N_A}{2N_h\, \ln(D_c/y^*)}$$
(37)

where,

$$y^* = \{\frac{3}{8}\, F[\frac{(1 - \mu_1^2)E_1 + (1 - \mu_2^2)/E_2}{1/D_1 + 1/D_2}]\}^{1/3}$$
(38)

The above equations will be evaluated based on the following assumed values for a one foot cube sample of Tyler Sieve #500 particle (nominal diameter $D_n = 1.5 \times 10^{-5}$ ft) at a mean temperature of 400°F.

$k_s = 0.76$ Btu/hrft°F (pyrex glass)

$n = 1$ contact point per particle (heat flow in)

$N_h = 1/\frac{1}{2}\, D_n \sim 1.33 \times 10^5$ particles/ft

$N_A = (1/\frac{1}{2}\, D_n^2)^2 \sim 1.78 \times 10^{10}$ particles/ft$^2$

$F = (2/3)(20.0\ \text{lbf/ft}^2)/1.78 \times 10^{10}$ particles/ft$^2$

$\quad = 7.5 \times 10^{-10}\ \text{lb}_f$

$\mu_1 = \mu_2 = 0.25$

$E_1 = E_2 = 10 \times 10^6\ \text{lb}_f/\text{in}^2$

$D_c = D_1 = D_2 = 3.3 \times 10^{-6}$ ft (estimated equivalent diameter of contact region.)

Note in the above values that the particle size has been estimated as 1/2 the nominal particle size.  The weight of force, F, is taken at 2/3 the depth of the powder

bed, and the force is divided by the number of points of
contact that support it.  In this case a value of unity
has been assumed.  This will be explained later.  The
value of $D_c$ was estimated from Figure 14 and for this
example all particle contact points are assumed to have
the same value.

With the above values, Equation 37 gives

$$K_s = C(0.09) \text{ Btu/hrft}^2{}^\circ F$$

The correction factor required is on the order of unity.
This is consistent with values of solid conductivity shown
in Table 6 for particle-to-particle conductivity values
obtained at low pressure.

The average stress holding two particles in contact
for the conditions listed above is found with the use
of Equations 21 and 35, to be

$$S = 2.1 \times 10^4 \text{ lb}_f/\text{in}^2$$

This value appears to be more than sufficient to maintain
two particles in intimate, solid contact.  It is on this
basis that the contact area resistance was replaced with
a contact region conductive resistance.

The two values at atmospheric pressure suggest that
other factors affect heat transfer at that pressure level.
One avenue that may be explored is that at conditions where
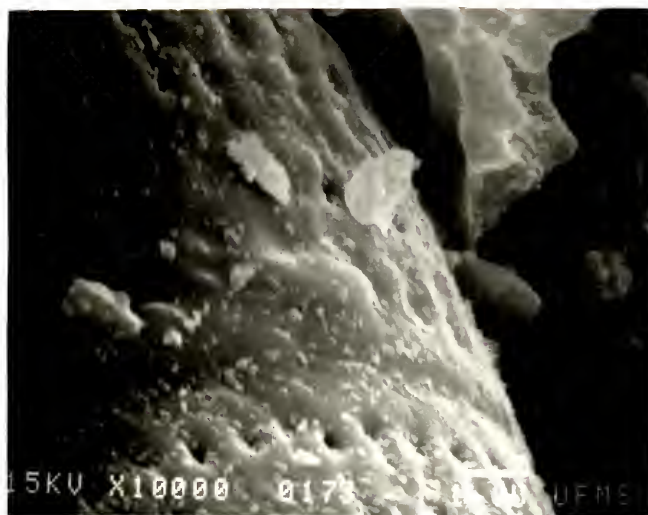
Figure 14

Electron Microscope Photograph of Surface
of Diatomaceous Earth Particle, Tyler Sieve #500
(x 10,000)
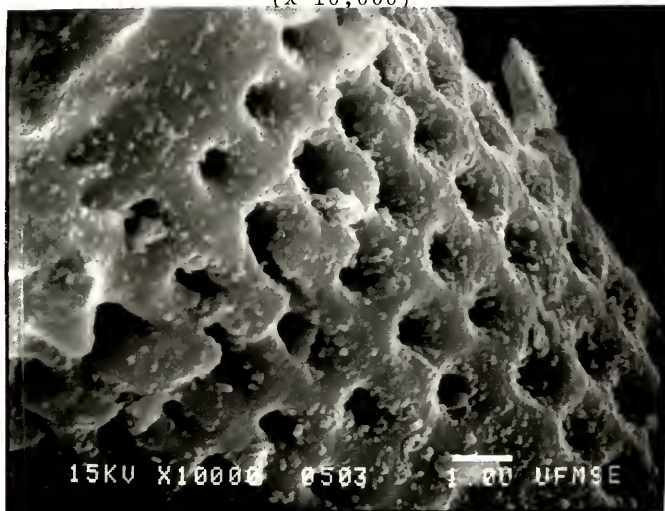


Figure 15

Electron Microscope Photograph of Surface
of Diatomaceous Earth Particle, Tyler Sieve #170
(x 10,000)

continuum assumptions apply, Kn << 1, a series-parallel
model may be more applicable.  Since the analysis of energy
transport through powders at atmospheric pressure was
beyond the scope of this study, this topic was not pursued.

In the sample calculation, the number of contact
regions, n, was assumed to be unity.  This value was selected
after inspecting the particles in an optical microscope which
gives a three as opposed to a two-dimensional view as seen
in the electron microscope photographs.  In three dimensions
the diatomaceous earth particles look much like an assembly
of tinker toys.  The particles adhere in groups and these
groups are separated with thin columns of particles.  These
columns appear like small magnets clinging together.  Within
the groups, it appears as though the individual particles
are repelling each other.  This separation of particles
reduces the number of contacts between particles.  For
example, small pebbles form piles in which each higher
pebble is supported by several lower pebbles with several
points of contact.  Because of the formation of groups,
separated by strands, diatomaceous earth particles seem
to minimize the number of contact regions without breaking
apart.  In the following paragraphs, the cause of this
arrangement is discussed.

The force of attraction between particles is thought
to be electrostatic in origin.  In that sense, it is
similar to polished metals which adhere to each other.
The diatomaceous earth particles do not appear to interlock

as do pebbles (uncharged particles). It was thought that water surface tension would be a factor in particle adhesion. However, heating the particles, to drive off moisture, did not appear to alter their attraction, at least at atmospheric pressure.

When the diatomaceous earth particles were viewed under an optical microscope and the glass support was vibrated by tapping, the individual particles did not vibrate. This is in contrast to similar observations of aluminum powder particles, which have no electrostatic forces. The absence of induced vibrations implies a force of attraction between the particles.

One can see from Equation 35 that the effect of a force or weight on porous powders is two fold. First, it increases the contact diameter. This effect is small as evidenced by the log term in the denominator. Second, and more significantly, increased force presses more particles together and as a result a larger number of contact regions form. This net effect of weight on $\bar{K}_a$, as shown in Figure 16, contrasts the curves for Tyler Sieve #500 powders for compressed and uncompressed material. Note that the effect of compressing the powder at lower temperatures is to decrease its thermal conductivity as compared to uncompressed particles. Presumably, this occurs because of a decrease in the thermal conductivity of the gas that results from a reduced void dimension in the non-continuum regime.

At higher temperatures, on the other hand, the apparent
conductivity of the compressed powders increases rather
sharply.  Nevertheless, Figure 16 suggests that compressed
powders may be used to support a storage tank weight without
a large penalty in insulation performance.  Specifically,
fine compressed powders can be placed under a container for
support and loose, uncompressed powders can be placed
in the remaining volume.  In this manner only limited supports
or no supports at all are needed to separate the internal
and external tank.  This eliminates the need for large
internal or external supports through which heat may be
lost.

The apparent thermal conductivity values of Table 5
have been reviewed except for the last four categories:
raw diatomaceous earth, pulverized diatomaceous earth, air
only, and fiberglass cloth and aluminum foil.  The raw
diatomaceous earth appears to perform similar to the powder
in the #170 pan.  That is, the powder particles and the
average void dimensions are large.  Pulverizing the raw
diatomaceous earth and using it without separating it into
different particle sizes will be of some advantage.

The air-only condition was measured to demonstrate
the effect of using air alone without convection suppression
or radiation shielding.

The fiberglass cloth and aluminum foil demonstrate a
value that one might expect from this material.  The one
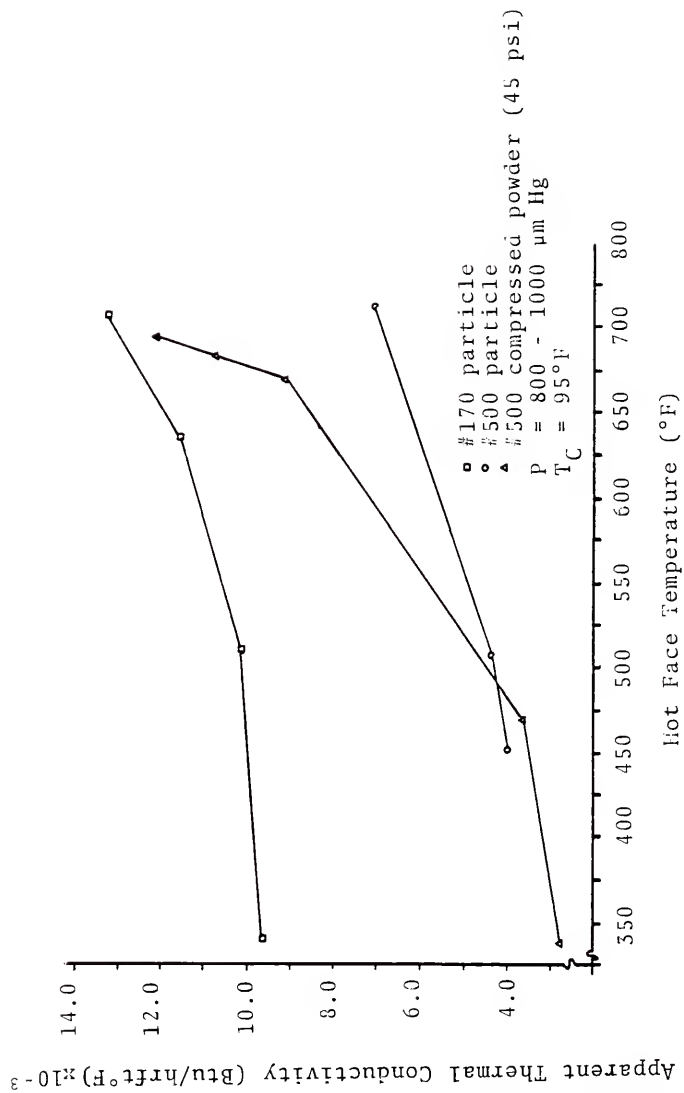
Figure 16

Apparent Thermal Conductivity of Selected
Diatomaceous Earth - Carbon (1% wt.) Particles

value given in Table 4 is relatively high, but it can be made some-what lower by using more layers of fiberglass cloth and aluminum foil. However, note that this multilayer material is at a pressure of 0.40 mm Hg. To produce a significant drop in $K_a$ for this material, the pressure must be reduced to a level of 0.10 mm Hg or less. See Table 5, page 79.

The fiberglass cloth and aluminum foil were difficult to put together since the multi-foil layers were individually wrapped. Some of the probles with wrapping the insulation were

1. the need for securing the layers so that they did not unravel,

2. a support system was required to separate the inner and outer tank, and

3. the supports and piping to and from the inner tank had to be carefully wrapped to prevent heat loss.

It is well to point out that multi-foil insulation at low pressure works well. But, its complexity and expense make it an unlikely candidate for routine high temperature use.

Effect of particle size in a non-continuum. Figure 16 (page 96) illustrates the trend of particle size versus conductivity. The larger particles, in the case from Tyler Sieve #170, pass heat about three times more readily than the particles of Tyler Sieve #500. This trend is also seen in the cryogenic region [10]. The apparent reason for this

is that small powders suppress gaseous conductivity more effectively and they create a greater resistance to heat flow due to contact region resistance as explained in Chapter 3. It is interesting to note the behavior of the compressed powder (Tyler Sieve #500) in Figure 16. At the low temperature end of the graph the compressed powders have a high resistance to heat flow due to non-continuum conditions created by the fine particles. However, at higher temperature, the conductivity increases rapidly. It is assumed that this is due to the presence of additional solid material through which heat may pass. This powder was compressed to about one half of its original volume. The above observation is consistent with Equation 37 in which heat flow is directly proportional to the number of particles, $N_A$.

Effect of vacuum level. The vacuum level has a major impact on the heat loss characteristic of the powder insulation under vacuum. Figure 17 is a theoretical curve showing the characteristic decline of gaseous conductivity for air and argon. The decline is seen to be linear at points less than 1000 μm Hg. The gaseous conductivity below this pressure varies asymptotically with pressure. Note the relatively flat response at pressures near 10,000 μm Hg (10 mm Hg) in Figure 17. This indicates the importance of operating evacuated insulation at less than 10 mm Hg.

Figure 17 illustrates the trend in the gaseous conductivity for air and argon at pressures below 10 mm Hg
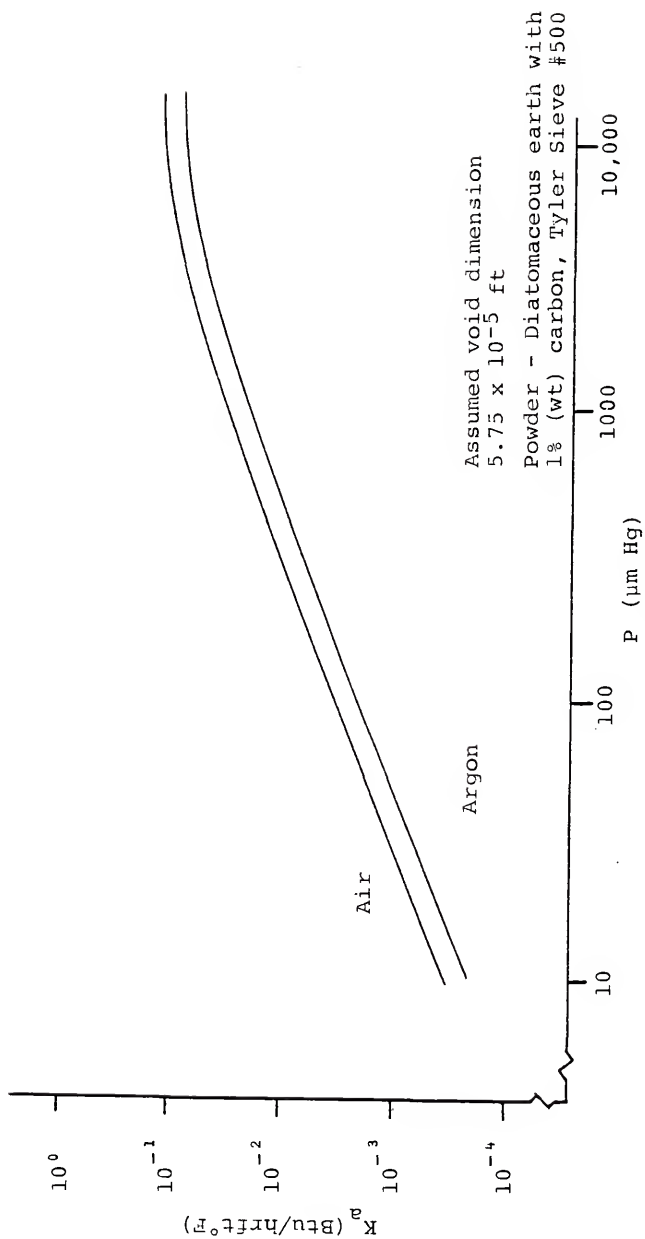
Figure 17

Gas Conduction vs Gas Pressure in Powders
Under Vacuum (Theoretical)

where a rapid declind in conductivity occurs. On this scale, a recommended operating range falls between 0.5 mm Hg to 3 mm Hg since these values are easily obtained with common mechanical vacuum pumps.

Selection of a particular operating pressure will depend upon the particle size, particle material, residual gas present, temperature level, cost of stored energy and so forth. A pressure much lower than 0.5 mm Hg can be used but at the expense of more complex vacuum pumps (diffusion or molecular pumps), longer pumping times, and potential problems of outgassing. From theoretical considerations a point will be reached in which further reductions in heat loss through gas conduction becomes negligible compared to solid particle conduction losses. This investigation did not experimentally identify this pressure region due to equipment limitations. However, part of the goal of this work was to identify a practical upper limit for pressure commensurate with a low coefficient of thermal conductivity (K < 0.015 Btu/hrft°F (@ 1000°F). The pressure range of 0.5 mm Hg to 3.0 mm Hg is designated as an upper pressure range for accomplishing this goal.

Effect of carbon and iron in diatomaceous earth. Carbon was added to the diatomaceous earth, at about 1% by weight, to enhance pouring and separating characteristics of the latter. Very small amounts of steel powder found its way into the material that was pulverized in a ball mill. [The

ball mill container and rollers were made of steel.] From
the limited data of Table 5, it appears that neither
the carbon nor fine steel had a significant measurable
effect on the thermal conductivity of diatomaceous earth.

## Thermal Energy Storage System

The thermal energy storage system was filled with
approximately 500 pounds of diatomaceous earth that had
been pulverized in a ball mill for 30 minutes. Approxi-
mately 1% by weight of carbon black was added prior to
pulverizing since the carbon was found to give the dia-
tomaceous earth better pouring characteristics. A small
amount of raw diatomaceous earth, 50 pounds, had to be used
to completely fill the tank. This material was located in
the top back section of the tank and no observable tempera-
ture difference in this area was noticed during the test.

The tank was filled by first evacuating the insula-
tion space and then letting the powders be pushed into
the tank as atmospheric pressure filled the annular void.
This procedure was much quicker and easier than trying to
fill the insulation space by hand. It was also found that
better packing and distribution of the insulation material
was obtained since no hot spots were noticeable on the
exterior of the outer tank.

The storage tank had thermocouples attached at various
points to the exterior of the inner tank, as shown in

Figure 18, and they were also placed in the powder insulation so that a temperature profile through the powder could be observed. Surface temperatures of the outer tank were taken externally.

The thermocouple port was part of the forward vacuum port. The thermocouples were fed through a u-shaped tube and the u-shaped tube was then filled with a high temperature wax. This formed an effective seal since the thermocouple port was far enough away from the heated tank so that the thermocouples were not affected by heat conduction through the wires. That is, heat did not cause the wires to expand and contract. As a result, no leaks were detected between the wire and wax seal. The thermocouples were stripped of insulation prior to emerging from the wax to prevent leaks from developing under the wire insulation.

The cylindrical portion of the inside of the outer tank was lined with a blanket of fine steel wool, grade (000). This provided the path of least flow resistance for evacuating gases from the powder insulation. It appears that the steel wool made it possible for air to flow essentially in a radial path out of the powders so that an air molecule traveled approximately 6.75 inches through the powder instead of through all of the powder from the bottom to top of the tank. It also filtered powder entrained in the evacuation flow so that only minimum filtration was needed at the
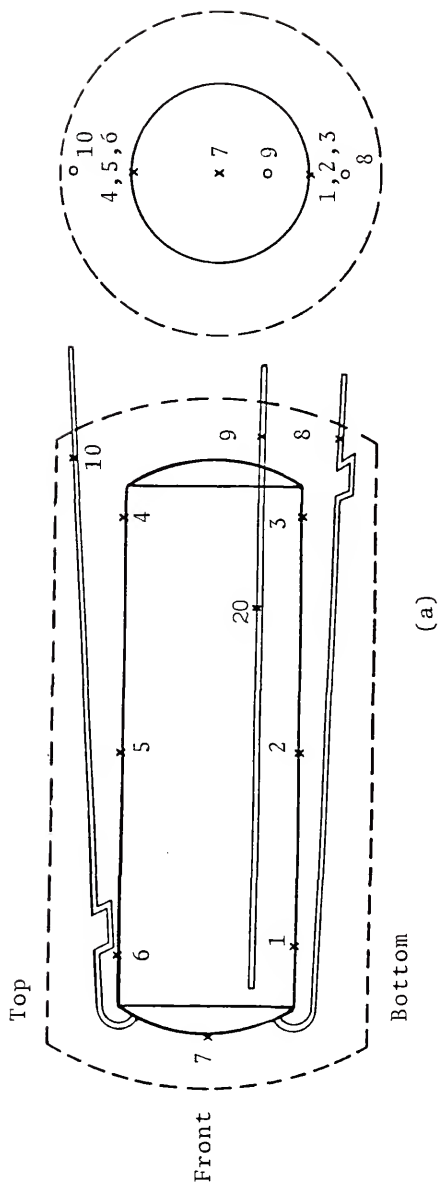
Inner Tank and Outlet Ports

Figure 18

(a)

Thermocouple Location for Prototype
High Temperature Thermal Energy Storage Vessel

104



In Evacuated Powder
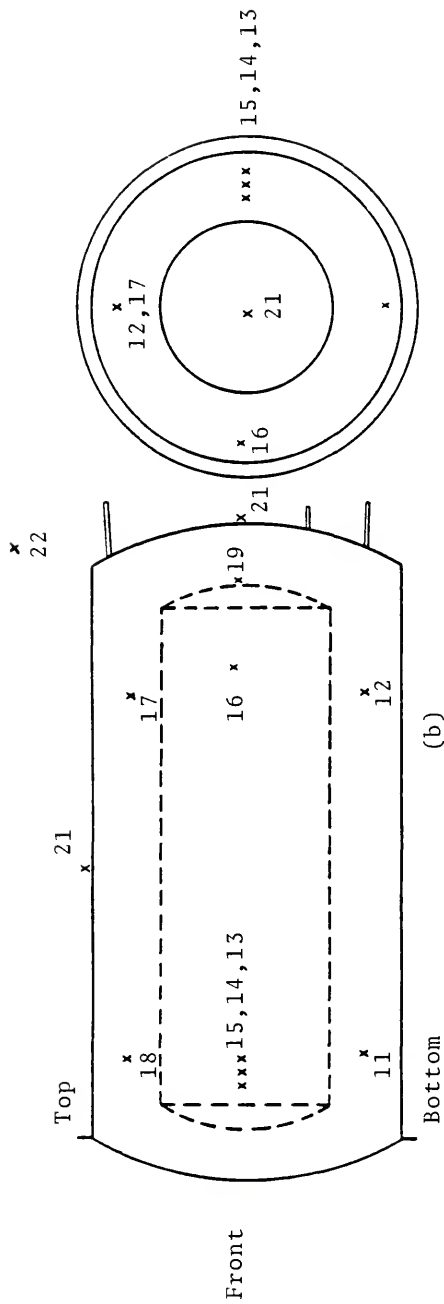
Figure 18 (Cont'd.)

Thermocouple Location for Prototype
High Temperature Thermal Energy Storage Vessel

inlet to the vacuum pump.  The steel wool worked well because it slowed the flow of air sufficiently so that entrained particles could not be carried any great distance.  This was observed in a glass cylinder that was closed at its bottom and evacuated at its top.

The steel wool blanket was fabricated by weaving the 4" wide wool strands through wire fencing.  The fencing was rolled up and inserted into the outer tank where the fencing expanded, holding the steel wool against the tank surface.

The inner tank was charged with 180 pounds of vegetable oil (soybean).  The powders were evacuated and the tank heater was turned on and heating of the oil was initiated. At intervals the tank was allowed to reach steady-state, so that the effectiveness of the insulation could be determined. When the oil reached a temperature near its boiling point, the power was disconnected and the tank was allowed to cool.

## Results of Prototype Thermal Energy Storage System Test

A typical result of the cool down process is shown in Figure 19 for a test with the powder evacuated and a test in which the vacuum on the powder was released after the tank of oil was heated close to its boiling point ($T_{boiling}$ = 700°F @ 1 atm. for new oil) [3].

Figure 20 shows typical temperature profiles through the evacuated powder insulation for several insulation hot face
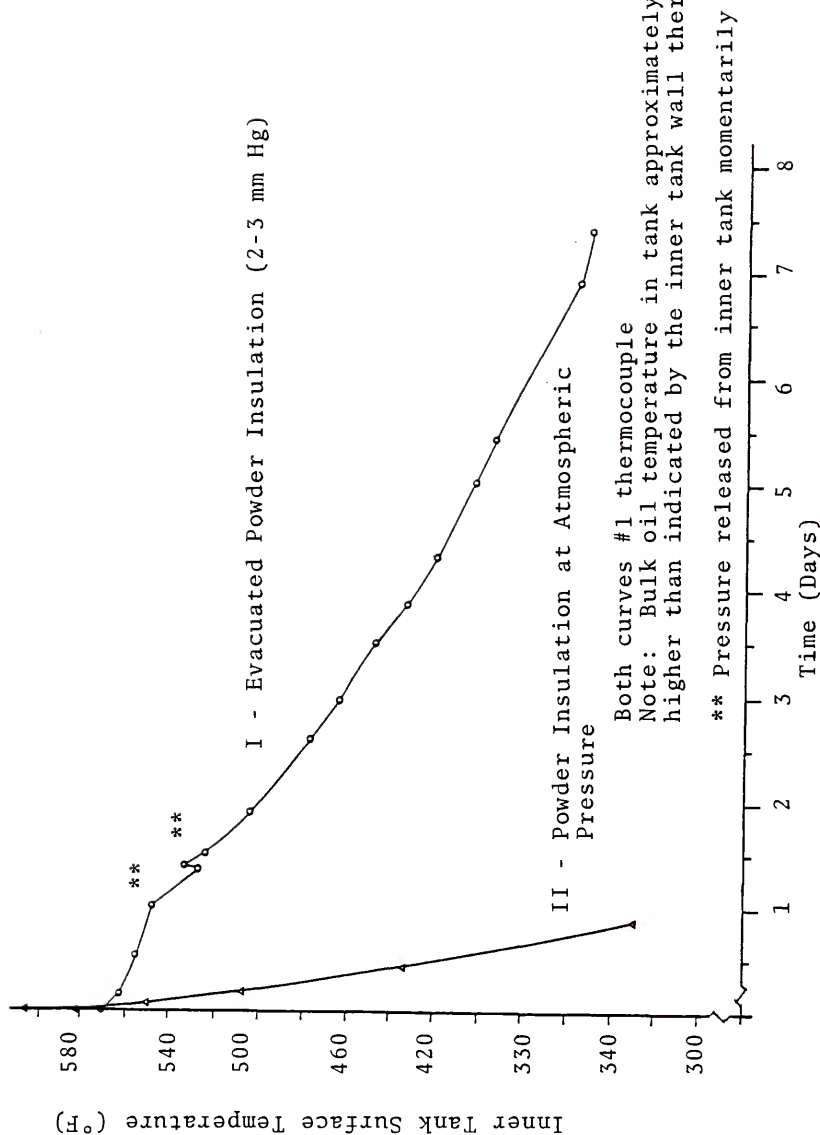
Figure 19

Cool-Down of Prototype High Temperature Thermal Energy Storage System
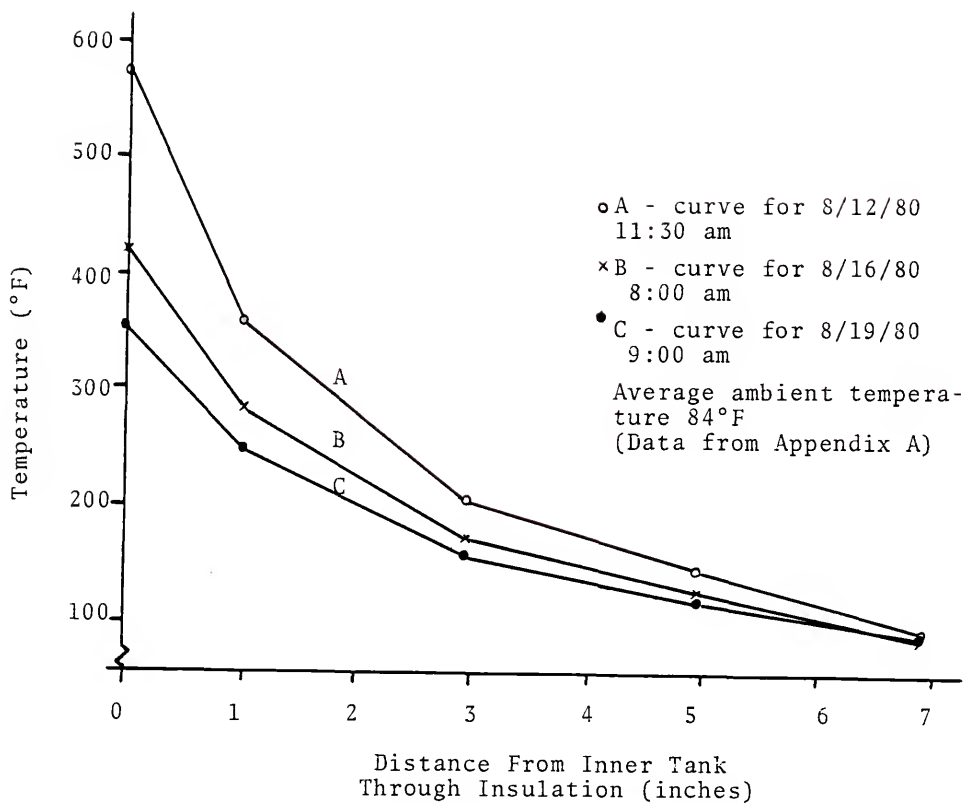
Figure 20

Temperature Profile Through
Powder Insulation Under Vacuum
(2-3 mm Hg)

temperatures. The data for Figures 19 and 20 were taken
from the data presented in Appendix A.

All thermocouples were calibrated to read within
1/2°F of each other when immersed at 212°F and at 70°F.
When all thermocouples were fixed in place, they were
checked again at room temperature to insure uniformity.

An electric resistance heater was built into the
storage tank as shown in Figure 7(a). It consisted of
a glass rod with a resistance heating coil wound around
it and the wire was covered with a thin asbestos cover,
for electrical insulation. The heater was placed in the
heater port. A rheostat was used to regulate AC power
to the heating element. An ammeter and a voltmeter were
connected to the heating element leads to measure the
power delivered to the tank. See Figure 21.

## Discussion of Results for the Thermal Energy Storage System Test

Insulation performance. Figure 19 indicates that
powder insulation under vacuum performed as expected as a
high temperature thermal insulation. Using 70°F as the
reference for the sensible energy obtainable from the
storage tank, Figure 19 shows a 4.0% loss of the stored
energy the first day. After one week, over 50% of the
original stored energy was still available.

In contrast to the evacuated insulation, atmospheric insulation (curve II in Figure 19) lost approximately 60% of its energy in less than one day, once the vacuum was released. Specifically, in less than 18 hours, its temperature dropped to a level that took the evacuated powder insulation 168 hours (7 days) to reach.
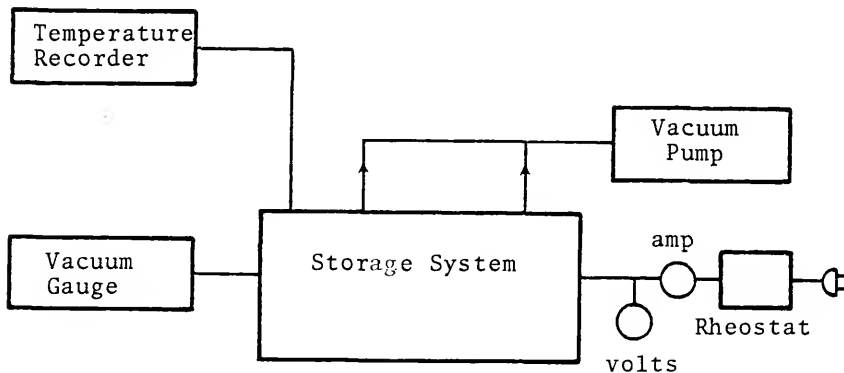


Figure 21

Storage System Test Equipment Arrangement

Figure 20 shows typical temperature profiles through the powder insulation under vacuum. The data points indicated on the graph were taken by placing thermocouples in the powder at 1, 3 and 5 inches from the hot surface boundary.

The cold face temperature was measured on the surface of the external tank. The thermocouple locations of the data points of Figure 20 are shown in Figure 18 and a reference list is shown in Appendix A.

The temperature profiles of Figure 20 raise some interesting questions concerning the reasons for the rapid increase in the slope of the curve as the hot surface temperature increases and as the hot surface boundary is approached. Several causes for this are

1. for cylinderical geometry where energy transport is radial, a decreasing temperature profile is expected since the amount of insulating material increases with an increasing radius,

2. the particle thermal conductivity may decrease with a rise in temperature,

3. the powder next to the hot surface boundary may impede radiative transfer,

4. the local effect of temperature on lowering gaseous molecular energy transfer is more pronounced near the hot surface boundary than near the cold surface boundary, and

5. an interaction between the above mechanisms may be occurring with a consequential local rise in temperature as the hot surface is approached.

The shape of Curve A in Figure 20 suggest that radiant and gaseous molecular energy transfer may be responsible for the temperature gradient next to the hot surface boundary. This is evidenced by the sudden rise in temperature of Curve A between a point three inches from the hot surface and the hot surface. Hence, although the net

effect of radiant transport through the powders may be
negligible its local effect, in combination with the other
modes of energy transport near the hot surface boundary
is significant. The shape of the right-hand portion of
Curve A, as well as Curve B and Curve C, suggest that
linear heat transfer mechanisms control energy transfer
in that region. Also that portion of the curves are more
consistent with constant heat flux distribution through
cylindrical geometry according to the term $\ln (r_o/r_i)$ in
Equation 41.

The temperature profiles shown in Figure 20 indicate
that powder insulation under vacuum is effective since
the outer boundary temperature was only a few degrees
higher than ambient.

Heating of organic oil. Curve I of Figure 19, page 106,
begins at a temperature well below the normal boiling point
of soybean oil, that is 700°F at atmospheric pressure. In
the first run of the high temperature storage system, the
oil was heated to the vicinity of its boiling point. The
consequent rise in tank pressure caused tank failure.
This was not anticipated as the storage system had been
pressure tested to 250 psig and the air and oil vapor
pressure, at an oil temperature of 700°F, was expected to
be less than 75 psig. Analysis of the tank failure showed
that the heater area was undersized. Since the expected
natural convection coefficient of heat transfer of organic
oil is small, about 7.5 Btu/hrft²°F at 670°F, the tempera-

ture of the oil next to the heater surface can reach or
exceed its boiling point.  This indicates that if organic
oil is used for heat transfer purposes, then the heat
transfer surface must be large or the temperature differences
between it and the oil must be small, if the oil is to be
used near its boiling temperature.  This also implies that
for forced convection systems, high flow rates will be
required [3].  Also, if the oil is to be used near its
boiling point, then safety precautions must be taken in
view of the high pressures that may be encountered.

Steel wool blanket.  The steel wool blanket (grade 000)
performed well in suppressing powder entrainment during
the evacuation of air from the powder insulating material.
The operating principle of the steel wool blanket was
observed by evacuating powder in a glass cylinder.  As
the air was evacuated, small holes formed in the powder
permitting air to escape.  As the air exists through the
small holes, its velocity in the cavity was sufficient to
entrain powder particles.  When steel wool was placed
over the powder surface, the air jets coming out of the
powder surface were diffused by the steel wool, thus mini-
mizing entrainment.

Overall storage vessel performance.  During the
heating phase of the storage vessel performance test the
system was periodically allowed to attain a steady state
condition.  At that point the current and voltage to the

heater element were monitored and the apparent conductivity
of the insulation material was approximated by the following,

$$Q_{loss} = K_a \ \pi \ \Delta T \ (\frac{2 \ L}{\ln(r_o/r_i)} + \frac{D^2}{2\Delta x}) \tag{50}$$

The first part of Equation 50 represents the heat loss
form the cylindrical portion of the tank and the second
part represents the heat loss through the ends of the tank.
The diameter of the end of the tank was approximated
by taking the arithmetic mean of the inner and outer tank
diameters to compensate for edge losses.  Solving Equation
50 for the apparent conductivity, $K_a$, and evaluating with
the following conditions,

$Q_{loss}$ = 200 Btu/hr

$r_o$     = 1.25 ft (outer tank radius)

$r_i$     = 0.67 ft (inner tank radius)

L      = 4.17 ft (inner tank length)

$\Delta T$     = (530 - 93)°F

$\Delta X$     = 0.58 ft (insulation thickness)

D      = 1.92 ft

gives,

$K_a$ ~ 0.0097 Btu/hrft°F

This value is consistent with apparent conductivity values
obtained in the conductivity test cell.  It should be

recalled that the density of the powder in the storage vessel was about 32 lbm/ft$^3$. With this density, the vacuum level was allowed to operate between 2-3 mm Hg.

Heat losses through the inlet and outlet pipes, the thermocouple wires, and the tank support cables were found to be negligible as explained in Chapter V. The heater port was found to carry about 5% of the total heat loss. If a larger heater port should be needed, as indicated earlier, then heat loss through it could become significant, and care should be taken in its design.

Tank support. The small stainless steel cable used in the high temperature thermal energy storage vessel was found to be sufficient for its intended purpose. Heat loss through the calbes was found to be negligible as indicated in Chapter V.

The test data for the Tyler Sieve #500 compressed powder, Figure 16, indicates that it may be possible to let the insulating powder support the inner tank. This could be accomplished by using compressed powders under the tank and then filling the remaining volume with loose fill or uncompressed powders. The benefit of this design would be the elimination of a heat loss path and the elimination of external supports needed to support the weight of the inner tank and its heat storage medium.

Cost of high temperature storage. Inevitably, cost will be a primary factor in governing the use of the high

temperature thermal energy storage systems. Assume a self-sufficient residential system requires a storage capacity of $10^6$ Btu. The required storage volume is then approximated as follows

| Heat Storage Material | Volume (ft$^3$) | Sphere Radius (ft) |
|---|---|---|
| Soybean Oil (600°F) | 65 | 2.5 |

The oil storage tank will require two tanks. The outer tank radius is assumed to be 0.5 feet larger than the inner tank radius. Table 8 gives an estimated cost of this storage system.

The economics of the high temperature storage vessel are greatly enhanced if the latent heat of fusion of a heat storage medium is used along with sensible heat storage. For example, if $NaNO_3$ [35] were used instead of organic oil, then the high temperature storage vessel would contain approximately $2.13 \times 10^6$ Btu. This gives a storage cost of $493 - 1221 per $10^6$ Btu. This phase change material requires a rather elaborate heat exchanger and it will displace some of the heat storage material. This will make the above cost higher but the cost is competitive with that of low temperature thermal energy storage vessels such as hot water storage.

Table 8

Estimated Manufacture's Cost for Storage Vessels

<u>System Specifications</u>

Tank volume (ft$^3$)
    (a) inner                              65
    (b) outer                              113

Insulation volume (ft$^3$)                 48

Tank material - carbon steel               -

            Cost Range of Fabrication [36]

Spherical tanks
    (two required)                 $500 - 2000[†]

Insulation powder                  $ 50 -  100[*]
    (diatomaceous earth)

Labor - 40 hrs                         $400
    @ $10.00/hr

Tank testing - 5 hrs                   $100
    @ $20/hr
                                   _____
Cost for storing 10$^6$ Btu        $1050 - 2600
(Storage medium - soybean
   oil @ 600°F)

_____

[†]Cost depends upon quantity, source of purchase and wall
 thickness of tanks.

[*]Cost depends upon quantity, grade of material, particle
 size and source of purchase.

## Uncertainty in the Measurement of $K_a$

The uncertainty analysis is presented in Appendix C concludes that a maximum uncertainty in the physical measurements of the apparent thermal conductivity coefficient to be approximately 4.1% at a specified pressure. This value is within acceptable engineering limits for experimental work. Included in Appendix C is also a discussion concerning the methodology in the use of thermocouples for temperature measurement.

# CHAPTER VI

## CONCLUSIONS AND RECOMMENDATIONS

### Conclusions

Based on the work described in this dissertation, the following conclusions are given.

1. The overall use of powder insulation under vacuum for high temperature thermal energy storage is technically and economically feasible.

2. Thermal conductivity values of 0.0029 - 0.110 Btu/hrft°F were achieved experimentally for vacuum levels ranging from 0.5 - 3.0 mm Hg and hot surface temperatures ranging from 340 - 711°F.

3. A vacuum level of 0.5 mm Hg to 10 mm Hg is the recommended pressure range for operating powder insulation. The choice of vacuum level will depend upon particle size, particle material, type of gas present, temperature level, and system costs.

4. Small particles of diatomaceous earth suppress gaseous conductivity more effectively than large particles when compared using the same residual gas of the same pressure.

5. From the theoretical considerations the apparent thermal conductivity of powder under vacuum can be improved by selecting residual gases that inhibit molecular energy transport, such as gases with high molecular weight and specific heat ratios.

6. An evacuated powder can be used to support a load and still maintain a relatively low thermal conductivity.

7. The desirable characteristics of an insulating
   powder particle are small particle size, spheri-
   cal geometry, low thermal conductivity, non-con-
   ducting electrically, non-corroding, stable at
   elevated temperatures, universally available, and
   inexpensive.

8. Particle size and distribution, as measured by
   mechanical spearators, of the materials used in
   this study did not appear to be consistent with
   electron microscope photographs of the material.
   The particles as viewed by the electron micro-
   scope appear to be much smaller and of various
   sizes.

9. The use of a fine steel wool blanket permitted
   evacuation of air from the storage vessel with
   minimal entrainment of the powder insulation.


## Recommendations

Based on the work carried out in developing this

dissertation, the following recommendations are made.

1. There is need for quantitative data and correla-
   tion techniques for predicting actual particle
   size, shape, and distribution.

2. Methods can be explored for fabricating porous
   powders that will minimize heat transfer by
   particle-to-particle conductivity while at the
   same time suppressing gaseous and radiative
   conductivity.

3. Experimental data at low pressure and high
   temperature for apparent thermal conductivity
   of porous powders, with various interstitial
   gases, would be very useful.

4. The evaluation of the temperature-pressure
   relationship of organic oils along with an
   evaluation of the corrosion potential of the
   oils at elevated temperatures would be useful
   in designing high temperature thermal energy
   storage vessels.

5.  There is a need for an investigation into the
    design of high temperature storage vessels for
    use with phase change material.  The primary
    area of investigation would be to identify and
    develop suitable heat exchangers or other means
    of extracting energy from the solidifying phase
    change material.

APPENDIX A

STORAGE VESSEL TEST DATA

## Thermocouple Number and Location
## For Prototype Thermal Energy Storage Vessel Test

| Thermocouple No.* | Location (See Figure 18) |
|---|---|
| 1 | Bottom, front |
| 2 | Bottom middle |
| 3 | Bottom, back        Positions on |
| 4 | Top, back               inner tank |
| 5 | Top, middle             1 - 7 |
| 6 | Top, front |
| 7 | Center, front |
| 8 | Bottom Inlet Pipe 4-1/2" from inner tank |
| 9 | Heater Port 4-1/2" from inner tank |
| 10 | Top Inlet 4-1/4" from inner tank |
| 11 | Bottom, front 4" from inner tank |
| 12 | Bottom, back 4" from inner tank |
| 13 | Side, front 5" from inner tank |
| 14 | Side, front 3" from inner tank |
| 15 | Side, front 1" from inner tank |
| 16 | Side, back 4" from inner tank |
| 17 | Top, back 4" from inner tank |
| 18 | Top, front 4" from inner tank |
| 19 | Center, back 4" from inner tank |
| 20 | Heater Port - on outside of heater rod in heater port |
| 21 | Outer tank surface (moveable probe) |
| 22 | Ambient |

---

*Chromel-Alumel thermocouples, referenced to ice bath.

—

123

TEST A

Prototype Thermal Energy Storage Vessel Test Data
Cool Down Time for Evacuated Powder Insulation

| Date | Time | 1 | 2 | 3 | 4 | 5 | 6 | 7 | 8 | 9 | 10 | 11 | 12 | 13 | 14 | 15 | 16 | 17 | 18 | 19 | 20 | 21 | 22 | Comments |
|---|---|---|---|---|---|---|---|---|---|---|---|---|---|---|---|---|---|---|---|---|---|---|---|---|
| 7/29 | 8:45 pm | 85 F all points | | | | | | | | | | | | | | | | | | | | | | |
| 7/30 | 11:30 am | 197 | 195 | 197 | 198 | 198 | 195 | 197 | 174 | 287 | 128 | 140 | 115 | 100 | 117 | 176 | 105 | 130 | 116 | 115 | 294 | 85 | | vacuum level in powder 1-3 mm Hg throughout test |
| 7/30 | 9:30 pm | 225 | 252 | 255 | 258 | 238 | 253 | 255 | 207 | 393 | 141 | 197 | 110 | 118 | 152 | 211 | 129 | 142 | 116 | 140 | 547 | 87 | | |
| 7/31 | 11:30 am | 322 | 322 | 325 | 329 | 329 | 322 | 324 | 241 | 447 | 171 | 271 | 125 | 145 | 207 | 322 | 100 | 156 | 140 | 129 | 509 | 97 | | |
| 7/31 | 12:00 pm | 263 | 282 | 277 | 278 | 278 | 271 | 278 | 197 | 261 | 162 | 285 | 104 | 162 | 230 | 201 | 187 | 165 | 187 | 170 | 339 | – | | |
| 8/1 | 9:30 am | 328 | 342 | 348 | 352 | 359 | 348 | 344 | 234 | 450 | 163 | 297 | 183 | 159 | 230 | 269 | 183 | 165 | 134 | 172 | 638 | 113 | | |
| 8/2 | 3:30 pm | 338 | 345 | 349 | 365 | 362 | 340 | 347 | 237 | 312 | 267 | 359 | 174 | 194 | 282 | 239 | 231 | 220 | 162 | 189 | 515 | 152 | | tank insulated on outside |
| 8/3 | 10:30 am | 349 | 350 | 353 | 360 | 360 | 352 | 352 | 239 | 315 | 273 | 369 | 175 | 204 | 290 | 236 | 241 | 223 | 162 | 190 | 531 | 170 | | |
| 8/3 | 11:45 pm | 411 | 420 | 433 | 429 | 437 | 418 | 433 | | 344 | 282 | 389 | 179 | 213 | 305 | 290 | 250 | 235 | 168 | 202 | 573 | 175 | | |
| 8/4 | 8:30 pm | 414 | 431 | 451 | 429 | 436 | 424 | 442 | 267 | 364 | 304 | 422 | 200 | 226 | 326 | 290 | 267 | 263 | 180 | 212 | 660 | 178 | | |
| 8/4 | 10:30 pm | 488 | 502 | 514 | 497 | 514 | 482 | 504 | 335 | 435 | 292 | 434 | 189 | 210 | 333 | 335 | 262 | 250 | 237 | 215 | 609 | 100 | | tank insulation off |
| 8/5 | 9:30 am | 421 | 437 | 431 | 436 | 436 | 426 | 439 | 301 | 365 | 252 | 347 | 178 | 197 | 305 | 296 | 235 | 204 | 180 | 199 | 409 | 101 | | |
| 8/6 | 9:00 am | 319 | 328 | 340 | 332 | 332 | 325 | 330 | 244 | 293 | 207 | 302 | 150 | 162 | 237 | 240 | 167 | 162 | 132 | 163 | 380 | 95 | | |
| 8/7 | 3:30 pm | 339 | 348 | 360 | 352 | 352 | 347 | 349 | 255 | 310 | 147 | 227 | 109 | 140 | 189 | 253 | 140 | 117 | 124 | 120 | 404 | 97 | | |
| 8/7 | 8:45 am | 358 | 368 | 380 | 372 | 372 | 366 | 369 | 263 | 319 | 134 | 216 | 102 | 131 | 178 | 259 | 130 | 107 | 126 | 120 | 406 | 45 | | |
| 8/7 | 4:00 am | 402 | 407 | 418 | 417 | 372 | 409 | 409 | 286 | 386 | 134 | 223 | 104 | 134 | 181 | 284 | 132 | 112 | 126 | 126 | 368 | – | | |
| 8/7 | 9:00 pm | 431 | 435 | 447 | 450 | 448 | 441 | 447 | 300 | 347 | 140 | 241 | 107 | 138 | 189 | 299 | 135 | 124 | 130 | 127 | 376 | 98 | | |
| | 11:45 pm | 421 | 418 | 443 | 419 | 421 | 418 | 417 | – | 330 | 170 | 286 | 131 | 154 | 224 | 288 | 164 | 167 | 163 | 142 | 351 | – | | |

TEST A, Continued

| Date | Time | 1 | 2 | 3 | 4 | 5 | 6 | 7 | 8 | 9 | 10 | 11 | 12 | 13 | 14 | 15 | 16 | 17 | 18 | 19 | 20 | 21 | 22 | Comments |
|---|---|---|---|---|---|---|---|---|---|---|---|---|---|---|---|---|---|---|---|---|---|---|---|---|
| 8/8 | 8:45 am | 459 | 455 | 491 | 456 | 458 | 457 | 454 | - | 371 | 141 | 234 | 106 | 137 | 191 | 303 | 132 | 126 | 131 | 123 | - | 93 | - | |
| | 11:30 am | 497 | 490 | 496 | 493 | 496 | 494 | 488 | - | 440 | 140 | 237 | 197 | 137 | 191 | 330 | 133 | 136 | 131 | 127 | 604 | 95 | - | |
| | 3:30 | 533 | 535 | 535 | 528 | 530 | 529 | 531 | - | 413 | 145 | 245 | 113 | 141 | 195 | 370 | 137 | 274 | 137 | 130 | - | - | - | |
| | 6:45 | 535 | 536 | 537 | 530 | 533 | 530 | 534 | - | 412 | 149 | 249 | 113 | 141 | 196 | 372 | 137 | 302 | 137 | 128 | - | 89 | - | |
| | 9:45 | 532 | 533 | 533 | 528 | 531 | 530 | 532 | - | 409 | 149 | 248 | 109 | 138 | 194 | 370 | 133 | 304 | 133 | 123 | - | 98 | - | |
| | 11:40 | 532 | 535 | 535 | 528 | 531 | 530 | 532 | - | 408 | 149 | 247 | 107 | 137 | 193 | 375 | 131 | 250 | 132 | 120 | - | 93 | - | |
| 8/9 | 12:30 pm | 527 | 528 | 528 | 524 | 526 | 525 | 527 | - | 403 | 147 | 245 | 104 | 134 | 192 | 340 | 129 | 182 | 128 | 119 | - | 93 | - | |
| | 7:30 am | 508 | 510 | 508 | 506 | 506 | 507 | 507 | - | 381 | 147 | 238 | 102 | 132 | 186 | 329 | 126 | 153 | 124 | 114 | - | 89 | - | |
| | 9:00 am | 503 | 503 | 502 | 502 | 502 | 502 | 502 | - | 377 | 145 | 235 | 99 | 130 | 185 | 323 | 124 | 137 | 122 | 112 | - | 89 | - | |
| | 12:30 am | 506 | 506 | 505 | 505 | 506 | 506 | 504 | - | 390 | 150 | 239 | 105 | 136 | 189 | 328 | 130 | 144 | 127 | 121 | - | 95 | - | |
| | 6:30 pm | 503 | 503 | 502 | 501 | 503 | 502 | 500 | - | 389 | 152 | 240 | 109 | 139 | 191 | 329 | 133 | 150 | 130 | 126 | - | 102 | - | |
| | 8:45 pm | 500 | 500 | 499 | 499 | 501 | 500 | 500 | - | 387 | 152 | 239 | 107 | 137 | 190 | 325 | 132 | 137 | 129 | 122 | - | 95 | - | |
| | 11:40 pm | 499 | 499 | 498 | 498 | 499 | 499 | 496 | - | 386 | 150 | 236 | 113 | 135 | 189 | 323 | 128 | 125 | 127 | 120 | - | 91 | - | |

TEST A

| Date | Time | 1 | 2 | 3 | 4 | 5 | 6 | 7 | 8 | 9 | 10 | 11 | 12 | 13 | 14 | 15 | 16 | 17 | 18 | 19 | 20 | 21 | 22 | Comments |
|---|---|---|---|---|---|---|---|---|---|---|---|---|---|---|---|---|---|---|---|---|---|---|---|---|
| 8/10 | 7:30 am | 498 | 497 | 497 | 497 | 498 | 498 | 495 | - | 385 | 143 | 230 | 109 | 133 | 185 | 322 | 126 | 129 | 125 | 117 | - | 89 | - | power 487.5 watts |
|  | 11:30 am | 509 | 506 | 506 | 508 | 508 | 508 | 503 | - | 405 | 142 | 230 | 110 | 134 | 185 | 327 | 127 | 120 | 125 | 120 | - | 93 | - |  |
|  | 3:30 pm | 519 | 516 | 516 | 518 | 519 | 519 | 514 | - | 413 | 144 | 233 | 115 | 138 | 187 | 335 | 131 | 139 | 128 | 120 | - | 102 | - |  |
|  | 8:00 pm | 550 | 543 | 543 | 549 | 550 | 549 | 540 | - | 455 | 141 | 235 | 112 | 134 | 187 | 347 | 128 | 140 | 126 | 124 | 574 | 93 | 88 |  |
|  | 11:30 pm | 513 | 572 | 573 | 585 | 583 | 582 | 572 | - | 482 | 139 | 239 | 110 | 132 | 188 | 359 | 126 | 139 | 125 | 122 | 624 | 85 | 80 | power 53 watts |
| 8/11 | 1:00 am | 594 | 585 | 585 | 585 | 592 | 592 | 584 | - | 479 | 139 | 240 | 111 | 133 | 189 | 364 | 127 | 144 | 126 | 123 | 598 | 88 | 81 |  |
|  | 2:00 am | 592 | 587 | 586 | 591 | 592 | 591 | 586 | - | 431 | 140 | 243 | 113 | 135 | 191 | 361 | 128 | 140 | 127 | 122 | - | 89 | 85 |  |
|  | 3:30 am | 589 | 600 | 599 | 599 | 598 | 597 | 597 | - | 439 | 144 | 114 | 135 | 192 | 599 | 410 | 129 | 272 | 131 | 120 | - | 89 | 85 | pressure of inner cell tank vented |
|  | 1:00 pm | 586 | 586 | 586 | 585 | 585 | 586 | 585 | - | 410 | 150 | 257 | 119 | 140 | 198 | 380 | 134 | 228 | 133 | 128 | - | 96 | 91 |  |
|  | 3:45 pm | 582 | 583 | 582 | 580 | 582 | 582 | 581 | - | 438 | 152 | 258 | 121 | 143 | 200 | 375 | 136 | 220 | 134 | 131 | - | 98 | 95 |  |
|  | 8:30 pm | 573 | 573 | 573 | 573 | 573 | 573 | 571 | - | 432 | 153 | 259 | 120 | 142 | 201 | 355 | 135 | 143 | 133 | 124 | - | 91 | 87 | power 780 watts |
| 8/12 | 1:30 am | 574 | 573 | 573 | 573 | 574 | 573 | 572 | - | 433 | 152 | 259 | 119 | 142 | 201 | 358 | 134 | 143 | 133 | 124 | - | 88 | 83 |  |
|  | 5:30 am | 572 | 572 | 571 | 572 | 573 | 572 | 570 | - | 433 | 150 | 258 | 118 | 141 | 201 | 357 | 133 | 164 | 133 | 124 | - | 91 | 85 |  |
|  | 8:30 am | 571 | 509 | 569 | 569 | 570 | 571 | 567 | - | 430 | 148 | 258 | 117 | 141 | 201 | 353 | 133 | 153 | 133 | 123 | - | 89 | 83 | power 96.3 watts |
|  | *11:30 am | 573 | 571 | 571 | 572 | 573 | 572 | 569 | - | 432 | 147 | 258 | 117 | 142 | 202 | 355 | 134 | 150 | 133 | 124 | - | 92 | 89 | *power off - cool off begins |
|  | 3:00 pm | 565 | 564 | 563 | 565 | 565 | 564 | 562 | - | 418 | 148 | 259 | 121 | 144 | 203 | 354 | 137 | 153 | 137 | 128 | - | 98 | 95 |  |
|  | 6:30 pm | 557 | 557 | 556 | 557 | 557 | 557 | 555 | - | 413 | 147 | 259 | 120 | 143 | 203 | 349 | 137 | 150 | 136 | 126 | - | 95 | 91 |  |

*Cool down begins.

TEST A, Continued

| Date | Time | 1 | 2 | 3 | 4 | 5 | 6 | 7 | 8 | 9 | 10 | 11 | 12 | 13 | 14 | 15 | 16 | 17 | 18 | 19 | 20 | 21 | 22 | Comments |
|---|---|---|---|---|---|---|---|---|---|---|---|---|---|---|---|---|---|---|---|---|---|---|---|---|
| 8/13 | 11:00 pm | 548 | 547 | 548 | 549 | 548 | 548 | 546 | - | 407 | 144 | 257 | 118 | 142 | 202 | 344 | 134 | 146 | 134 | 124 | 608 | 91 | 84 | |
| | 8:00 am | 528 | 528 | 528 | 528 | 528 | 528 | 527 | - | 394 | 139 | 255 | 115 | 139 | 201 | 334 | 132 | 139 | 133 | 122 | 589 | 88 | 80 | |
| | 9:30 am | 534 | 535 | 534 | 535 | 535 | 534 | 534 | - | 402 | 138 | 256 | 160 | 139 | 201 | 342 | 133 | 139 | 133 | 124 | 587 | - | - | |
| | 11:15 am | 524 | 524 | 524 | 524 | 524 | 524 | 524 | - | 393 | 138 | 250 | 139 | 141 | 202 | 334 | 134 | 141 | 134 | 126 | 583 | 91 | 8? | |
| | 10:00 pm | 503 | 503 | 502 | 502 | 503 | 503 | 503 | - | 374 | 137 | 240 | 116 | 137 | 196 | 322 | 130 | 114 | 130 | 120 | 550 | 88 | 82 | |
| 8/14 | 2:30 pm | 478 | 477 | 477 | 477 | 477 | 477 | 477 | - | 366 | 137 | 233 | 117 | 136 | 189 | 302 | 130 | 116 | 129 | 120 | 531 | 91 | 87 | |
| | 11:00 pm | 464 | 464 | 464 | 464 | 464 | 464 | 464 | - | 357 | 134 | 326 | 119 | 132 | 184 | 305 | 127 | 114 | 124 | 118 | 516 | 86 | 74 | |
| 8/15 | 1:15 am | 463 | 462 | 462 | 462 | 462 | 462 | 462 | - | 355 | 134 | 225 | 115 | 132 | 184 | 303 | 127 | 113 | 124 | 117 | 516 | 87 | 84 | |
| | 12:30 pm | 440 | 446 | 446 | 446 | 446 | 440 | 446 | - | 345 | 130 | 216 | 111 | 130 | 177 | 296 | 125 | 110 | 121 | 117 | 497 | 89 | 88 | |
| | 9:45 pm | 434 | 434 | 439 | 434 | 435 | 434 | 433 | - | 338 | 131 | 212 | 111 | 130 | 176 | 291 | 125 | 111 | 121 | 116 | 483 | 91 | 82 | |
| 8/16 | 8:00 am | 421 | 421 | 420 | 420 | 421 | 420 | 420 | - | 329 | 127 | 204 | 105 | 124 | 169 | 283 | 120 | 103 | 116 | 111 | 470 | 84 | 80 | |
| 8/17 | 12:25 am | 403 | 403 | 402 | 403 | 404 | 402 | 405 | - | 319 | 128 | 198 | 108 | 126 | 167 | 276 | 122 | 106 | 117 | 115 | 450 | 90 | 88 | |
| | 10:25 am | 395 | 395 | 395 | 395 | 396 | 395 | 395 | - | 315 | 127 | 195 | 107 | 125 | 165 | 274 | 121 | 105 | 117 | 115 | 441 | 90 | 87 | |
| 8/18 | 10:15 pm | 359 | 359 | 359 | 360 | 359 | 359 | 359 | - | 290 | 123 | 181 | 103 | 121 | 155 | 254 | 117 | 102 | 112 | 109 | 401 | 88 | 81 | |
| 8/19 | 9:00 am | 351 | 351 | 350 | 351 | 351 | 351 | 351 | - | 285 | 118 | 175 | 100 | 117 | 151 | 250 | 114 | 99 | 109 | 108 | 392 | 86 | 84 | |
| 8/20 | 10:25 am | 332 | 332 | 331 | 331 | 332 | 332 | 332 | - | 274 | 119 | 169 | 100 | 117 | 147 | 242 | 114 | 100 | 108 | 108 | 371 | 90 | 88 | |

TEST B

Prototype Thermal Energy Storage Vessel Test Data
Cool Down Time for Non-Evacuated Powder Insulation

| Date | Time | 1 | 2 | 3 | 4 | 5 | 6 | 7 | 8 | 9 | 10 | 11 | 12 | 13 | 14 | 15 | 16 | 17 | 18 | 19 | 20 | 21 | 22 | Comments |
|---|---|---|---|---|---|---|---|---|---|---|---|---|---|---|---|---|---|---|---|---|---|---|---|---|
| 8/22 | 10:30 pm | 110 | 110 | 110 | 110 | 110 | 110 | 110 | 110 | – | 114 | 102 | 108 | 97 | 100 | 106 | 105 | 102 | 98 | 98 | 101 | 193 | 90 | 83 | powder evacuated |
| 8/23 | 5:45 am | 102 | 102 | 102 | 102 | 102 | 102 | 102 | 102 | – | 104 | 81 | 86 | 81 | 85 | 95 | 82 | 77 | 78 | 78 | 78 | 168 | 72 | 74 | 1-3 mm Hg |
| | 9:30 am | 136 | 134 | 134 | 134 | 134 | 134 | 134 | 134 | – | 140 | 93 | 100 | 94 | 98 | 121 | 95 | 89 | 90 | 92 | 92 | 305 | 87 | 84 | |
| | 12:30 pm | 146 | 145 | 145 | 145 | 145 | 145 | 145 | 145 | – | 148 | 92 | 100 | 94 | 98 | 129 | 95 | 90 | 90 | 94 | 94 | 317 | 90 | 88 | |
| | 3:30 pm | 156 | 156 | 155 | 155 | 155 | 155 | 155 | 155 | – | 157 | 93 | 101 | 96 | 93 | 137 | 95 | 94 | 90 | 95 | 95 | 324 | 93 | 92 | |
| | 9:00 pm | 179 | 177 | 177 | 177 | 177 | 177 | 177 | 177 | – | 186 | 93 | 101 | 89 | 98 | 152 | 94 | 92 | 90 | 95 | 95 | 427 | 92 | 89 | |
| | 11:00 pm | 194 | 194 | 192 | 192 | 194 | 194 | 192 | 192 | – | 190 | 92 | 101 | 89 | 98 | 181 | 94 | 90 | 90 | 95 | 95 | 436 | – | – | |
| 8/24 | 10:00 am | 244 | 242 | 243 | 244 | 244 | 277 | 241 | 241 | – | 215 | 91 | 103 | 93 | 98 | 191 | 91 | 89 | 87 | 93 | 93 | 480 | 86 | 85 | |
| | 4:30 pm | 285 | 281 | 282 | 284 | 284 | 284 | 280 | 280 | – | 267 | 95 | 108 | 92 | 97 | 161 | 95 | 89 | 90 | 100 | 100 | 550 | 95 | 94 | |
| | 11:20 pm | 326 | 321 | 322 | 325 | 325 | 325 | 320 | 320 | – | 297 | 99 | 112 | 100 | 98 | 218 | 96 | 99 | 90 | 99 | 99 | 589 | 93 | 88 | |
| 8/25 | 9:00 am | 318 | 314 | 314 | 314 | 314 | 314 | 309 | 309 | – | 273 | 97 | 115 | 91 | 104 | 239 | 93 | 94 | 88 | 90 | 90 | 613 | 83 | 80 | |
| | 10:30 pm | 407 | 402 | 403 | 406 | 406 | 405 | 400 | 400 | – | 419 | 104 | 126 | 97 | 100 | 231 | 97 | 101 | 93 | 104 | 104 | 660 | 90 | 86 | powder in – 281.1 watts |
| | 11:45 pm | 416 | 410 | 411 | 414 | 414 | 413 | 409 | 409 | – | 425 | 105 | 130 | 98 | 113 | 281 | 98 | 102 | 94 | 105 | 105 | 668 | 89 | 86 | |
| 8/26 | 9:00 am | 411 | 408 | 409 | 409 | 409 | 409 | 408 | 408 | – | 342 | 106 | 137 | 96 | 116 | 285 | 96 | 100 | 94 | 97 | 97 | 673 | 85 | 83 | |
| | 2:30 pm | 432 | 426 | 428 | 430 | 430 | 429 | 428 | 428 | – | 432 | 107 | 140 | 100 | 118 | 293 | 97 | 104 | 95 | 106 | 106 | 677 | 94 | 90 | powder in – 59.12 watts |
| | 10:30 pm | 465 | 460 | 462 | 463 | 464 | 463 | 459 | 459 | – | 224 | 110 | 146 | 101 | 122 | 307 | 105 | 105 | 95 | 105 | 105 | 691 | 88 | 83 | |

| Date | Time | 1 | 2 | 3 | 4 | 5 | 6 | 7 | 8 | 9 | 10 | 11 | 12 | 13 | 14 | 15 | 16 | 17 | 18 | 19 | 20 | 21 | 22 | Comments |
|---|---|---|---|---|---|---|---|---|---|---|---|---|---|---|---|---|---|---|---|---|---|---|---|---|
| 8/27 | 8 00 am | 502 | 501 | 502 | 499 | 500 | 499 | 560 | - | 424 | 111 | 154 | 101 | 104 | 125 | 320 | 90 | 102 | 96 | 99 | 652 | 85 | 82 | pressure of inner tank - 20 psig |
| | 10 50 am | 530 | 528 | 528 | 525 | 536 | 525 | 527 | - | 441 | 112 | 161 | 108 | 106 | 120 | 383 | 99 | 106 | 98 | 101 | 681 | 87 | 83 | pressure of inner tank - 60 psig |
| | *1 30 pm | 604 | 601 | 601 | 601 | 595 | 597 | 602 | - | 450 | 129 | 176 | 121 | 108 | 137 | - | 104 | 354 | 109 | 111 | 644 | - | 87 | vacuum on insulation released |
| | 2 10 pm | 583 | 582 | 583 | 569 | 563 | 565 | 579 | - | 431 | 165 | 295 | 133 | 115 | 172 | 459 | 134 | - | - | - | - | - | 92 | |
| | 3 10 pm | 551 | 555 | 557 | 541 | 542 | 541 | 551 | - | 413 | 217 | 335 | 146 | 133 | 208 | 393 | 162 | 351 | 173 | 148 | 608 | 114 | 93 | |
| | 6 00 pm | 507 | 504 | 506 | 506 | 503 | 500 | 504 | - | 386 | 254 | 365 | 173 | 168 | 256 | 349 | 202 | 239 | 212 | 178 | 560 | 114 | 94 | top outlet pipe - 140°F, heater |
| | 8 20 pm | 473 | 466 | 468 | 468 | 469 | 460 | 461 | - | 364 | 250 | 368 | 187 | 181 | 273 | 321 | 214 | 227 | 224 | 190 | 522 | 100 | 91 | outlet pipe - 118°F |
| | 10 20 pm | 451 | 448 | 448 | 448 | 448 | 446 | 446 | - | 352 | 243 | 365 | 182 | 187 | 278 | 308 | 217 | 209 | 226 | 104 | 490 | 105 | 90 | hot spot on back end of tank - 110°F |
| | 11 40 pm | 434 | 429 | 429 | 432 | 431 | 429 | 429 | - | 341 | 238 | 360 | 187 | 186 | 279 | 300 | 217 | 204 | 255 | 194 | 481 | 112 | 88 | |
| 8/28 | 8 45 am | 352 | 348 | 360 | 342 | 348 | 347 | 349 | - | 288 | 205 | 311 | 167 | 178 | 252 | 295 | 195 | 175 | 201 | 174 | 391 | 103 | 87 | pressure of inner tank - 44 psig |
| | 12 00 am | 330 | 328 | 328 | 330 | 327 | 326 | 328 | - | 275 | 196 | 294 | 103 | 171 | 239 | 245 | 187 | 170 | 192 | 168 | 366 | 106 | 82 | pressure of inner tank - 32 psig |
| | 11 00 pm | 263 | 263 | 264 | 258 | 262 | 261 | 263 | - | 229 | 239 | 239 | 214 | 152 | 201 | 208 | 163 | 150 | 105 | 148 | 292 | 102 | 85 | |

*Vacuum on insulating powders released at this time. Cooling process.

APPENDIX B

CONVECTION HEAT TRANSFER ANALYSIS
FOR A POROUS POWDER

In powder with particle dimensions less than 0.2 inches in diameter, investigators, such as Hill and Wilhelm [20], found no evidence of convective heat transfer in quiescent gas-solid beds. The condition encountered in their study was similar to those of this work.

The above investigation applied particularly to a gas-solid bed at atmospheric pressure. This study was primarily interested in heat transfer through powders under vacuum conditions. Hence, for the conditions mentioned above, it was concluded that convective heat transfer would be eliminated. Justification for this conclusion follows.

Convective heat transfer in the laminar region can be expressed in the following form,

$$Nu = (\frac{hb}{k_f}) = G(Ra)^{\frac{1}{4}} \tag{51}$$

where b is a characteristic dimension of a given geometry, G is a constant of the order of unity and Ra is the Rayleigh number. In expanded form Equation 51 can be written as,

$$Nu = G(g\beta C_p \rho^2 b^3 \Delta T/\mu k_f)^{\frac{1}{4}} \tag{52}$$

The term $\beta$ for a perfect gas is $\beta = 1/T$. The task now is to show that convective heat transfer is negligible for conditions encountered in this study. Specifically, one

must show that convective heat transfer is negligible over the temperature and pressure range encountered. These values are 250-1000°F and 0.5-760 mm Hg.

If Equation 52 is evaluated at the 250°F and 1000°F at a pressure of one atmosphere, for b = 0.015 ft, $\Delta T$ = 10°F[+], the Nusselt number is found to be of the order of unity for both temperatures. Since the Nusselt number is given by Equation 2, then

$$Nu = \frac{hb}{k} \sim 1 \qquad (2)$$

and the convective heat transfer coefficient is seen to be of the same order of magnitude as the thermal conductance of the fluid. That is,

$$h \sim k/b \qquad (53)$$

A decrease in the heat transfer coefficient with a decrease in pressure, as calculated by Equation 52, is illustrated by substituting for the density term,

$$\rho = P/RT \qquad (7)$$

_____

[+] Assumed maximum temperature difference between particles or between particles and a container boundary.

This substitution, along with setting $\beta = 1/T$, gives

$$Nu = G(gC_p P^2 b^3 \Delta T / \mu_f k_f R^2 T^2)^{\frac{1}{4}} \qquad (52)$$

Restricting the above equation to a continuum, it is clear that the Nusselt number and, hence, the convective heat transfer coefficient decreases as the pressure decreases. The decrease is proportional to $P^{\frac{1}{2}}$. More importantly, the above equation shows that the Nusselt number is proportional to $(P/T)^{\frac{1}{2}}$. Typically, the operating conditions encountered in this study were that pressure, P, would be decreased and temperature, T, would increase. Assuming a continuum exists in a gas-solid bed for a fluid at 1 mm Hg, and temerature increased from 250°F (710°R) to 1000°F (1460°R), the Nusselt number, and hence the convective heat transfer coefficient, would decrease by approximately two orders of magnitude, as compared to values obtained at atmospheric conditions. The above factors indicate that convective heat transfer is no longer significant at reduced pressures and high temperatures.

The above paragraph illustrates that convective heat transfer becomes negligible as the pressure changes from 760 mm Hg to 1 mm Hg. In the region of 1 mm Hg and where the gas molecules are confined such that Kn > 1, the assumption of a continuum no longer applies. In this case, convec-

tion heat transfer is negligible and molecular thermal conductivity of the fluid is proportional to pressure. This situation has been explored in Chapter III.

APPENDIX C

UNCERTAINTY IN THE MEASUREMENT OF $K_a$

The uncertainty analysis presented here deals with the uncertainty in the physical measurement of the apparent thermal conductivity coefficient, $K_a$. The apparent thermal conductivity coefficient, as given by Equation 42, is a function of

$$K_a = K_a(E, I, \theta, r_o, r_i, L, T_H, T_c) \tag{54}$$

Equation 54 does not explicitly contain the variable pressure, P, under which the insulating material was tested. Hence, the uncertainty in the measurement of $K_a$ will be given with $K_a$ as the dependent variable and pressure, P, as the independent variable.

Before proceeding to calculate uncertainty in the measurement of $K_a$, an explanation of the difficulty of including pressure as an explicit variable in the analysis is in order. If $K_a$ in Equation 41 is replaced with the sum of Equations 19 and 37

$$K_a = \frac{9\gamma - 5}{4(\gamma - 1)} \left(\frac{2R_u}{\pi MT}\right)^{\frac{1}{2}} (1/P\overline{d} + 1/B)^{-1}$$

$$+ \frac{C \, n \, \pi \, K_s \, D_c N_A}{2 \, N_h \, \ln \, (D_c/y^*)} \tag{55}$$

then variables are introduced whose values are not readily available, such as $k_s$, $\overline{d}$, n, $N_A$, $N_h$, $D_c$. Using this approach would require assuming values for these parameters and this would negate the purpose of calculating uncertainty.

135

The standard deviation, $\Delta K_a$, in the measurement of $K_a$ is calculated with [37]

$$\Delta K_a = (\sum_{i}^{j} (\frac{\partial K_a}{\partial z_i})_{z_j}^2 \, u^2_{zi})^2 \tag{56}$$

where

$z$ = independent variable

$u_{zi}$ = instrument deviation in measuring $z$.

Equation 55 is based on the assumption that the standard deviation of the input parameter, $z$, is Gaussian in nature.

Applying Equation 56 to Equation 42,

$$K_a = \frac{EI \ln (r_o/r_i)}{2\pi L (T_H - T_c)} \tag{42}$$

and dividing the result by $K_a$ yields

$$\frac{\Delta K_a}{K_a} = [(\frac{u_E}{E})^2 + (\frac{u_I}{I})^2 + (\frac{-u_{r_o}}{r_o \ln(r_o/r_i)})^2$$

$$+ (\frac{u_{r_i}}{r_i \ln(r_o/r_i)}) + 2(\frac{u_{T_H}}{T_H - T_L})^2 + (\frac{-u_L}{L})^2]^{\frac{1}{2}} \tag{57}$$

The maximum deviation of each of the instruments used in the measurement of the parameters in Equation 54 and for the pressure measurement is given below.

| Parameter | Instrument | Maximum Division |
|---|---|---|
| Temperature | Chromel-Alumel thermocouple | $\pm$ 0.75% |
| Current | Ammeter-Westinghouse Type PA-4 | $\pm$ 2.5% |
| Potential | Weston-Schlumberger Digital VOM | $\pm$ 1.0% |
| Length | Stainless Steel Scale | $\pm$ 1.3x10$^{-3}$ ft. |
| Pressure | McLeod Vacuum Gauge | $\pm$ 3.0% |

Two sample problems to illustrate the range of uncertainty will be calculated for typical conditions, at both high and low temperatures, encountered in the measurement of the apparent thermal conductivity coefficient

Sample 1.

$K_a$ = 0.0072 Btu/hrft°F (Table 5, line 5)

$T_H$ = 730°F (Table 5, line 5)

$T_C$ = 104°F (Table 5, line 5)

E = 25.0V

I = 0.55 amperes

L = 1.0 ft

$r_o$ = 0.163 ft

$r_i$ = 0.089 ft

Applying these parameters and the instrument deviations from the above list into Equation 57 yields

$$\frac{\Delta K_a}{K_a} = [(\frac{0.01 \times 25.0}{25.0})^2 + (\frac{0.025 \times 0.55}{0.55})^2 + (\frac{0.0013}{0.163 \times 0.605})^2$$

$$+ (\frac{0.0013}{0.089 \times 0.605})^2 + 2 (\frac{0.0075 \times 730}{730 - 104})^2$$

$$+ (\frac{0.0013}{1})^2]^{\frac{1}{2}}$$

$$\frac{\Delta K_a}{K_a} = 0.041$$

That is $\Delta K_a = \pm 4.1\%$ of $K_a$ @ P = 1000 mm Hg $\pm$ 3%. Note that in the numerator of the first three terms in the above sample calculation that the instrument deviation, given as a percentage of the scale reading, was multiplied by the scaled value to obtain the instrument deviation.

Sample 2

$K_a$ = 0.00407 Btu/hrft°F (Table 5, line 8)

$T_H$ = 452°F (Table 5, line 8)

$T_C$ = 87°F (Table 5, line 8)

E = 11.3 V

I = 0.4 amperes

L, $r_o$, $r_i$ - same as above

Calculating as before, one obtains

$$\frac{\Delta K}{K_a} = 0.041$$

or, $\Delta K_a = \pm 4.1\% @ K_a @ P = 1000 \mu m Hg \pm 3\%$.

From the above calculations it is apparent that deviations in the measurement of $K_a$ fall within an acceptable range.

Of the variables measured for calculating $K_a$, the variable temperature requires additional comments concerning methodology in the use of the temperature transducers or thermocouples. All thermocouples junctions were welded together to form a small bead. The thermocouples used to measure $T_H$ were brazed to a copper surface and all excess brazing material was removed. The asbestos-covered lead wires from the junction were placed adjacent to the copper surface to minimize conduction losses from the thermocouple junction. The thermocouple used to measure $T_C$ was welded together and the resulting beaded junction was ground away until a thin, flat junction was obtained. This junction was covered with a small piece of ceramic insulation and then held against a surface for temperature measurement. Efforts were made to maintain constant pressure on the temperature probe when a surface temperature was taken. This procedure yields more consistent data [38].

The cold junction of the thermocouple was an ice bath. Even though ordinary tap water was used in the bath, a high quality mercury-in-glass thermometer showed negligible deviation from 32°F.

BIBLIOGRAPHY

1.  Farber, E. A., Morrison, C. A., Ingley, H. A., "A
    a Residential Solar Cooking System," 11th Annual
    Intersociety Energy Conservation Conference, September,
    1976.

2.  Cope, N. A., Ingley, H. A., Farber, E. A., Morrison,
    C. A., "Dynamic Response Analysis of a Solar Powered
    Heliotropic Fluid-Mechanical Drive System," 2nd Miami
    International Conference on Alternative Energy Sources,
    December 10-13, 1979.

3.  Ingley, Herbert A., Vegetable Oils:  Liquid Coolants for
    Solar Heating and Cooling Applications, prepared by the
    Solar Energy and Energy Conversion Laboratory, University
    of Florida, Gainesville, Florida for the Department of
    Energy, Contract No. EM-78-C-04-4298, 1980

4.  Wark, Kenneth, Thermodynamics, 2nd Edition, McGraw-
    Hill, New York, 1971.

5.  Angrist, Stanley W., Direct Energy Conversion, 3rd
    Edition, Allyn and Bacon, Incorporated, Boston,
    Massachusetts, 1976, p. 50.

6.  Jakob, Max, Heat Transfer, John Wiley & Sons, Incorpora-
    ted, New York, 1950, pp. 83-91.

7.  Strong, H. M., Bundy, F. P., Bovenkerk, H. P., "Flat
    Panel Vacuum Thermal Insulation," Journal of Applied
    Physics, Vol. 31, No. 1, January 1969, p. 41.

8.  Smoluchowski, M., Proceedings of the 2nd Refrigeration
    Congress, Vol. 2, 1910, pp. 187-193.

9.  Kistler, S. S., and Caldwell, A. G., Industrial Engineer-
    ing Chemistry, Vol. 26, 1934, p. 658.

10. Wilkes, Gordon B. Heat Insulation, John Wiley & Sons,
    Incorporated, New York, 1950, p. 95.

11. Peterson, P., The Heat-Tight Vessel, University of Lund,
    Sweden (1951), Office of Naval Intelligence, Translation
    No. 1147, 1953.

12. Klett, Robert D., Analytical Thermal Design of Cellular Insulation and Laminated Composites, Sandia Laboratories, Albuquerque, New Mexico, SAND 74-0232.

13. Delil, A. A. M., and Heemskerk, J. F., "A Theoretical Investigation of Gas Conduction Effects on Multi-Layer Insulation Performance," Netherlands Agency for Aerospace Programs, NIVR Nr 1766, 1976.

14. Niendorf, L. R., The Design, Development and Delivery of High Temperature Insulation Systems for SNAP-21 Thermoelectric Power Systems, Union Carbide Corporation, Linde Division, Tonawanda, New York, June 1970.

15. Black, A., Fowle, A. A., Glaser, P.E., Development of High Efficiency Insulation, Author D. Little, Incorporated, Cambridge, Massachusetts.

16. Sparrow, E. M., Gupta, B. P., Wehner, G. K., Research Applied to Solar-Thermal Power Systems, NTIS Report: NSF/RANN/SE/GI 34871/PR/75/2.

17. Chubb, Talbot A., "Energy Storage Tank," E. O. Hulburt Center for Space Research, Naval Research Laboratory, Washington, D.C., June 1976.

18. Baumeister, Theodore, and Marks, Lionel S., Editors, Standard Handbook for Mechanical Engineers, 7th Edition, McGraw-Hill, New York, 1967, pp. 4-94.

19. Johns-Manville, Insulation Product Information, A.I.A. File No. 37-D.

20. Hill-F. B., and Wilhelm, R. H., "Radiative and Conductive Heat Transfer in a Quiescent Gas-Solid Bed of Particles: Theory and Experiment," American Institute of Chemical Engineers, Vol. 5, December 1959, p. 486.

21. Kennard, E. H., Kinetic Theory of Gases, McGraw-Hill, Inc., New York, 1938.

22. Klett, Robert D., Analytical Thermal Design of Cellular Insulation and Laminated Composites, Saudia Laboratories, Albuquerque, New Mexico, SAND 74-0232, p. 12.

23. Haung, Francis F., Engineering Thermodynamics, Macmillan Publishing Company, Incorporated, New York, 1976, p. 138.

24. Dushman, S., Scientific Foundations of Vacuum Technique, John Wiley, & Sons, Incorporated, New York, 1949, p. 32.

25. Knudsen, Martin, Kinetic Theory of Gases, John Wiley
    & Sons, Incorporated, New York, 1950, pp. 46-51.

26. Dushman, S., Scientific Foundations of Vacuum Technique,
    John Wiley & Sons, Incorporated, New York, 1949, p. 49.

27. Arpaci, Vedat S., Conduction Heat Transfer, Addison-
    Wesley Publishing Company, Reading, Massachusetts,
    1966, p. 104.

28. Shigley, Joseph E., Mechanical Engineering Design,
    McGraw-Hill, New York, 1977, p. 75.

29. Argo, W.B., and Smith, J.M., "Heat Transfer in
    Packed Beds," Chemical Engineering Progress, Vol. 49,
    No. 8, August 1953, pp. 443-451.

30. Schotte, William, "Thermal Conductivity of Packed Beds,"
    American Institute of Chemical Engineers, Vol. 6, No. 1,
    March 1980, pp. 63-67.

31. Damkoehler, G., "Der Chemie Ingenieu," Euken Jocob,
    Vol. 3, Part 1, Adndemische Verlagegesellschaft
    M.B.H., Leipzig, 1937.

32. Brownell, Lloyd E., and Young, Edwin H.  Process
    Equipment Design, John Wiley & Sons, Incorporated,
    New York, 1959, pp. 141-154.

33. Baumeister, Theodore, Editor, Standard Handbook for
    Mechanical Engineers, McGraw-Hill, New York, 7th
    Edition, 1967, pp. 4-94.

34. American Society of Heating, Refrigerating and
    Air Conditioning Engineers, Incorporated, Handbook of
    Fundamentals, George Banta Co. Inc., Menasha, Wisconsin,
    1972, p. 273.

35. Masayuki Kamimoto, Tadayoshi Tanaka, Tatsuo Tani, and
    Takashi Horigome, "Investigation of Nitrate Salts for
    Solar Latent Heat Storage," Solar Energy Journal,
    Vol. 24, No. 6, 1980, pp. 581-587.

36. Private Communication with Mr. Jack Nilsson, Seige
    Corporation, Easley, S.C., September, 1981.

37. Holman, Jack Phillip, Experimental Methods for
    Engineers, 3rd Edition, McGraw-Hill, New York, 1978.

38. Honig, Daniel A., Requirements of a Thermocouple Probe
    Which Gives a Reproductile Means of Determining Surface
    Temperature, High Honors Project, University of
    Florida, 1957.

# EXTENDED BIBLIOGRAPHY

Chen, John C., and Churchill, Stuart W., "Radiant Heat Transfer in Packed Beds," American Institute of Chemical Engineers Journal, Vol. 9, No. 1, 1963, p. 35-41.

Ho, C. Y., and Taylor, R. E. (editors), Thermal Conductivity, Proceedings of the Eighth Conference, Plenum Press, New York, 1969, pp. 897-911.

Larkin, Bert K., and Churchill, Stuart W., "Heat Transfer by Radiation through Porous Insulation," American Institute of Chemical Engineers Journal, Vol. 5, No. 4, 1959, pp. 467-474.

Masamune, Shinobu, and Smith, J. M., "Thermal Conductivity of Porous Catalyst Pellets," Journal of Chemical and Engineering Data, Vol. 8, No. 1, 1963, pp. 54-58.

Smith, W. R., and Wilkes, G. B., "Thermal Conductivity of Carbon Black," Industrial and Engineering Chemistry, Vol. 36, No. 12, pp. 1111-1112.

Reynolds, C. D., and Ardany, Z. L., Palarite Thermal Insulation, Union Carbide Corporation, Oak Ridge Y-12 Plant, Oak Ridge, Tennessee, TID-4500, April, 1970.

Touloukian, Y. S., Thermophysical Properties of Matter, Vol. 2, IFI/Plenum, New York, 1970.

Whetley, S. J., and Mallett, A. J., Foam Plastic Insulation for High Temperature and Shock Protection, Union Carbide Corporation, Nuclear Division, Oak Ridge Gaseous Diffusion Plant, Oak Ridge, Tennessee, 1968.

Yagi, Sakoe and Kunnii, Daizo, "Studies on Effective Thermal Conductivities in Packed Beds," American Institute of Chemical Engineers Journal, Vol. 3, No. 3, pp. 373-380.

BIOGRAPHICAL SKETCH

Norman Alan Cope was born May 11, 1947, in Gaston County, North Carolina. He graduated from Stanley High School in June, 1965. He attended Gaston Community College from 1965 to 1967 and the University of North Carolina at Chapel Hill from 1967 to 1969. From the latter he received a degree in American history. After graduation from the University of North Carolina at Chapel Hill, he received basic training in the North Carolina Army National Guard. Work on a bachelor's degree in mechanical engineering was begun at the University of North Carolina at Charlotte in 1971 and completed in 1975. In 1972 he married Elizabeth Ann Brown. Two sons, Christopher Alan and Eric Keith, were born in November 1973, and November 1977, respectively. Work on his Master of Engineering degree in mechanical engineering began in 1975 and was completed in 1977. Work on the degree of Doctor of Philosophy was begun in 1977.

Norman Alan Cope is a member of American Society of Mechanical Engineers, the American Society of Heating, Refrigerating and Air Conditioning Engineers and the American Section of the International Society of Solar Engineering.
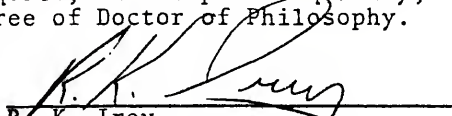
I certify that I have read this study and that in my opinion it conforms to acceptable standards of scholarly presentation and is fully adequate, in scope and quality, as a dissertation for the degree of Doctor of Philosophy.

Erich A. Farber, Chairman
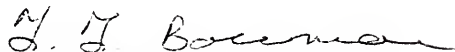Professor of Mechanical
    Engineering

I certify that I have read this study and that in my opinion it conforms to acceptable standards of scholarly presentation and is fully adequate, in scope and quality, as a dissertation for the degree of Doctor of Philosophy.

H. A. Ingley
Associate Professor of
    Mechanical Engineering

I certify that I have read this study and that in my opinion it conforms to acceptable standards of scholarly presentation and is fully adequate, in scope and quality, as a dissertation for the degree of Doctor of Philosophy.

R. K. Irey
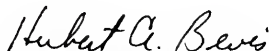Professor of Mechanical
    Engineering

I certify that I have read this study and that in my opinion it conforms to acceptable standards of scholarly presentation and is fully adequate, in scope and quality, as a dissertation for the degree of Doctor of Philosophy.

V. P. Roan
Professor of Mechanical
    Engineering

I certify that I have read this study and that in my opinion it conforms to acceptable standards of scholarly presentation and is fully adequate, in scope and quality, as a dissertation for the degree of Doctor of Philosophy.

T. T. Bowman
Associate Professor of
  Mathematics

This dissertation was submitted to the Graduate Faculty of the College of Engineering and to the Graduate Council, and was accepted as partial fulfillment of the requirements for the degree of Doctor of Philosophy.

December 1981

Dean, College of Engineering

Dean for Graduate Studies and
Research